NAVAL POSTGRADUATE SCHOOL

MONTEREY, CALIFORNIA

THESIS

STUDIES IN FORECASTING UPPER-LEVEL TURBULENCE

by

Christopher T. Kuhl

September 2006

Thesis Advisor:	Carlyle H. Wash
Co-Advisor:	Karl Pfeiffer

Approved for public release; distribution is unlimited

THIS PAGE INTENTIONALLY LEFT BLANK

REPORT DOCUMENTATION PAGE			Form Approved OMB No. 0704-0188

1. AGENCY USE ONLY *(Leave blank)*	2. REPORT DATE September 2006	3. REPORT TYPE AND DATES COVERED Master's Thesis

4. TITLE AND SUBTITLE Studies In Forecasting Upper-Level Turbulence	5. FUNDING NUMBERS
6. AUTHOR(S) Christopher T. Kuhl	
7. PERFORMING ORGANIZATION NAME(S) AND ADDRESS(ES) Naval Postgraduate School Monterey, CA 93943-5000	8. PERFORMING ORGANIZATION REPORT NUMBER
9. SPONSORING /MONITORING AGENCY NAME(S) AND ADDRESS(ES) N/A	10. SPONSORING/MONITORING AGENCY REPORT NUMBER

11. SUPPLEMENTARY NOTES The views expressed in this thesis are those of the author and do not reflect the official policy or position of the Department of Defense or the U.S. Government.

12a. DISTRIBUTION / AVAILABILITY STATEMENT Approved for public release; distribution is unlimited	12b. DISTRIBUTION CODE

13. ABSTRACT (maximum 200 words)

Encounters with turbulence generated by complex topography, convection, or mechanical forcing present a significant threat to military aircraft operations. Properly forecasting the initiation, duration, and intensity of such encounters is a tremendous challenge to forecasters often resulting in the over-forecasting of turbulence. Over-forecasting the presence or intensity of turbulence can result in unnecessary mission delays, cancellations, and re-routing. The lack of observations and the fact that turbulence is a microscale phenomenon which Numerical Weather Prediction (NWP) models currently can not resolve are what make forecasting turbulence so difficult.

Progress has been made in the last several decades in both the observation of turbulence and the resolution of NWP models. A new turbulence forecast approach has been created based on recent developments in observing turbulence and using automated turbulence diagnostics. The development of an in-situ observation platform, using the Eddy Dissipation Rate (EDR), and the Graphical Turbulence Guidance (GTG) model are discussed. A turbulence forecast approach is derived that includes the synoptic patterns which create or allow the turbulent environment to exist, the use of current tools to observe turbulence, and the use of models to help form the turbulence forecast. A turbulence forecasting manual has been created to give the new forecaster improved guidance to effectively forecast turbulence.

14. SUBJECT TERMS Turbulence, Clear-air turbulence, Mountain Wave, thermal turbulence, mechanical turbulence, PIREPs, Eddy Dissipation Rate, Integrated Turbulence Forecasting Algorithm, Graphical Turbulence Guidance, forecasting turbulence, diagnostics, Richardson number	15. NUMBER OF PAGES 191
	16. PRICE CODE

17. SECURITY CLASSIFICATION OF REPORT	18. SECURITY CLASSIFICATION OF THIS PAGE	17. SECURITY CLASSIFICATION OF REPORT	18. SECURITY CLASSIFICATION OF THIS PAGE
Unclassified	Unclassified	Unclassified	Unclassified

NSN 7540-01-280-5500 Standard Form 298 (Rev. 2-89)
Prescribed by ANSI Std. 239-18

THIS PAGE INTENTIONALLY LEFT BLANK

Approved for public release; distribution is unlimited

STUDIES IN FORECASTING UPPER-LEVEL TURBULENCE

Christopher T. Kuhl
2nd Lieutenant, United States Air Force
B.S., University of Minnesota Duluth, 2004

Submitted in partial fulfillment of the
requirements for the degree of

MASTER OF SCIENCE IN METEOROLOGY

from the

NAVAL POSTGRADUATE SCHOOL
September 2006

Author: Christopher Kuhl

Approved by: Carlyle H. Wash
Thesis Advisor

Karl Pfeiffer
Co-Advisor

Philip A. Durkee
Chairman, Department of Meteorology

THIS PAGE INTENTIONALLY LEFT BLANK

ABSTRACT

Encounters with turbulence generated by complex topography, convection, or mechanical forcing present a significant threat to military aircraft operations. Properly forecasting the initiation, duration, and intensity of such encounters is a tremendous challenge to forecasters often resulting in the over-forecasting of turbulence. Over-forecasting the presence or intensity of turbulence can result in unnecessary mission delays, cancellations, and re-routing. The lack of observations and the fact that turbulence is a microscale phenomenon which Numerical Weather Prediction (NWP) models currently can not resolve are what make forecasting turbulence so difficult.

Progress has been made in the last several decades in both the observation of turbulence and the resolution of NWP models. A new turbulence forecast approach has been created based on recent developments in observing turbulence and using automated turbulence diagnostics. The development of an in-situ observation platform, using the Eddy Dissipation Rate (EDR), and the Graphical Turbulence Guidance (GTG) model are discussed. A turbulence forecast approach is derived that includes the synoptic patterns which create or allow the turbulent environment to exist, the use of current tools to observe turbulence, and the use of models to help form the turbulence forecast. A turbulence forecasting manual has been created to give the new forecaster improved guidance to effectively forecast turbulence.

THIS PAGE INTENTIONALLY LEFT BLANK

TABLE OF CONTENTS

LIST OF FIGURES

LIST OF TABLES

THIS PAGE INTENTIONALLY LEFT BLANK

ACKNOWLEDGMENTS

I am thankful for the overwhelming technical and motivational support from the faculty in the Meteorology Department at the Naval Postgraduate School. I would like to thank my advisor, Dr. Carlyle H. Wash of the Department of Meteorology, Naval Postgraduate School, for his guidance and support during the development of this thesis. Thanks to my second reader, Lt Col Karl Pfeiffer, United States Air Force (USAF), for his wealth of knowledge and experience on the subject of turbulence and USAF weather operations. I wish to thank Capt Brad Schrumpf of the 15th Operational Weather Squadron, Scott Air Force Base, Illinois, for bringing my attention to this significant forecasting challenge and providing me further insight on Operational Weather Squadron forecasting procedures. Finally, a very special thank you to my wife and my family for being so patient, supportive, and understanding during the development and completion of this thesis.

THIS PAGE INTENTIONALLY LEFT BLANK

I. INTRODUCTION

A. MOTIVATION

Turbulence forecasting is of great importance to military operations as well as commercial aviation. There has been tremendous progress in the science of forecasting turbulence over the past several decades, especially upper-level turbulence. Yet even today, this science faces many challenges. It is of vital importance for the forecaster to have a thorough understanding of turbulence, what causes turbulence, where it's likely to be found, the difficulties of observing it, and the challenge of verifying turbulence forecasts.

Turbulence can cause significant damage to all types of aircraft, cause injury to passengers, and in extreme cases result in total destruction of aircraft, and death to those aboard. Of all weather-related commercial aircraft incidents, 65% can be attributed to turbulence encounters, and major carriers estimate that they receive hundreds of injury claims and pay out "tens of millions" per year (Sharman et. al 2006).

Within the United States Air Force (USAF) flight-level turbulence greatly impacts air-refueling operations. Specifically, it greatly affects strategic airlift missions into and out of the continental United States (CONUS) and the Operation Iraqi Freedom/Operation Enduring Freedom Areas of Responsibility (AOR). Additionally, intense flight-level turbulence severely degrades most heavy aircraft missions. Because turbulence of all intensities greatly affects USAF operations on a daily basis, it is crucial USAF leadership have accurate, precise, and reliable turbulence forecasts. Furthermore, equipping decision makers with ensemble produced probabilities instead of a simple deterministic forecast, will allow the decision makers to make more effective decisions in regards to daily operations.

B. PROBLEM STATEMENT

The guidance currently being used to forecast upper-level turbulence by USAF Operational Weather Squadron (OWS) personnel is the training manual Air Force Weather Agency Technical Note 98-002 (AFWA TN 98-002). It is a significant tool for all new forecasters in the USAF. Specifically, Chapter 2 of this manual is designated to

forecasting turbulence. Some of the techniques and guidance of the turbulence chapter are based on studies from as early as the 1960s, and as such, are somewhat outdated. The guidance in AFWA TN 98-002 originated from an assortment of local and regional rules of thumb from all around the globe. These rules were put into the manual while their regional or local context was left out leading to contradictory and misleading tools and guidance, and causing confusion for the new forecaster (Schrumpf 2006).

The USAF 15th OWS has reported current upper-level turbulence techniques compiled in AFWA TN 98-002 are resulting in over-forecasting by at least one-half an intensity category across the board, as evidenced by observations of nearly 50,000 flight missions per year at Tanker Airlift Control Center Weather Operations (Schrumpf 2006). The perceived errors in AFWA TN 98-002 propagate through the 15th OWS's training curriculums. Without a proper evaluation and correction of these techniques, an inordinate number of missions will end up being unnecessarily canceled, delayed, or diverted, and cost the USAF tens of millions of dollars in fuel, manpower, and aircraft-downtime losses (Schrumpf 2006). Figure 1 below illustrates a typical OWS upper-level turbulence forecast.

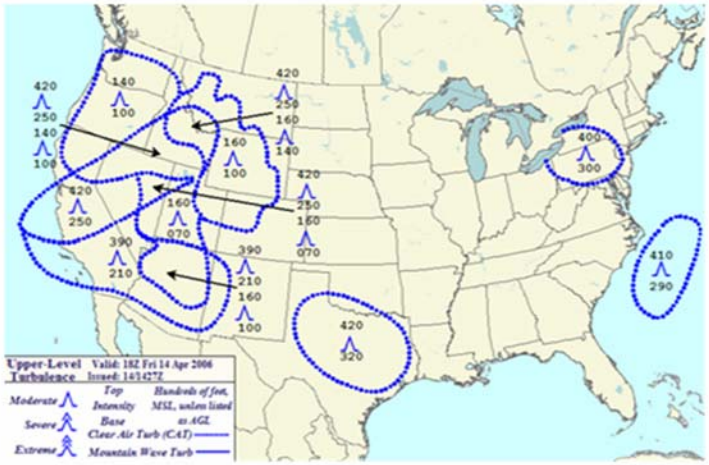

Figure 1. Upper-level turbulence forecast produced by USAF 15th OWS for 1800 GMT, 14 April 2006.

The objective of this thesis is to review, evaluate, and update the techniques for forecasting upper-level turbulence laid out in Chapter 2 of AFWA TN 98-002.

Ultimately, the thesis will strive to provide the new forecaster with the tools and guidance he/she needs to produce the best possible upper-level turbulence forecast for USAF operations.

This thesis will update and potentially improve AFWA TN 98-002, a vital training tool for all USAF forecasters, and in so doing, will hopefully result in significant savings of fuel, manpower, and mission cancellations for the USAF. An updated turbulence forecasting techniques manual based on AFWA TN 98-002 with the inclusion of the results of this research can be found in Appendix C. The new manual is the result of this thesis research and is the suggested replacement for the turbulence chapter (Chapter 2) of AFWA TN 98-002 (2005). The process of how this manual was developed will be described throughout this thesis. However, the manual itself is designed for operational use and will not include such discussions.

The guidance provided by AFWA TN 98-002 is not entirely outdated. Much of the material in the turbulence chapter of this manual is still quite accurate and true. The definition, description, categories, intensities, and aircraft dependence are described particularly well by AFWA TN 98-002 (2005). This thesis will reference AFWA TN 98-002 where appropriate, and in some cases borrow directly from this guidance where the material is still relevant. Those sections (wake turbulence, intensity categories, aircraft dependence) which are directly taken from AFWA TN 98-002 will be included for completeness and indented for clarity. The updating of this manual will mainly apply to the forecasting guidance and rules of thumb given in AFWA TN 98-002, some of which are outdated.

This thesis has been organized into five chapters. The Background chapter (Chapter II) is subdivided into six main sections which include defining turbulence, describing the forecasting problems and history, defining the categories and intensity of turbulence, describing turbulence relative to aircraft dependence, and the dynamics and associated synoptic situations favoring turbulence. The Turbulence Analysis Chapter (Chapter III) discusses the current turbulence forecasting methods. Four different current operational methods are analyzed and compared. Also in this chapter the state of the current observational system is described and analyzed. The Turbulence Forecast

Approach Chapter (Chapter IV) describes the recommended forecasting approach for upper-level turbulence and provides the new forecaster with the tools and guidance he/she needs to produce the best possible upper-level turbulence forecast for USAF operations.

II. BACKGROUND

A. DEFINITION AND DESCRIPTION

Turbulence is the gustiness superimposed on the mean wind. These rapid, turbulent fluctuations in vertical velocity, horizontal velocity, temperature, humidity, and pressure about their mean values are random. Therefore, we cannot hope to forecast clear-air turbulence (CAT) exactly. Instead, the forecaster is limited to a statistical description of CAT (Lee et al. 1984). The unexpected air movement associated with turbulence can cause serious damage to aircraft and potentially injure aircrew members and passengers.

Turbulence is created by abrupt, irregular movements of air that create sharp, quick updrafts and/or downdrafts acting to dissipate gradients of kinetic energy (AFWA TN 98-002, 2005). These updrafts and downdrafts occur in combinations and move aircraft unexpectedly. There are two basic atmospheric conditions that cause turbulence: thermal conditions (surface heating) and mechanical mixing.

1. Thermal Conditions

Surface heating can generate turbulent conditions. As solar radiation heats the surface, the air above it is warmed by contact. Warmer air is less dense, and "bubbles" of warm air rise upward as updrafts. Uneven surface heating, and the cooling of rising air, allows for areas of downdrafts as well. These vertical motions may be restricted to low levels, or may generate cumulus clouds that can grow to great heights as thunderstorms. When these vertical motions are restricted to the boundary layer and lower levels, they can create seemingly random areas of turbulence commonly referred to as boundary layer turbulence. The following are characteristics of boundary layer turbulence:

- The maximum occurrence is between late morning and late afternoon.
- The impact on flight operations is greatest during terminal approach and departure and during low-level flights.
- Moderate turbulence may occur in hot, arid regions, as the result of irregular convective currents from intense surface heating (AFWA TN 98-002, 2005).

When and if these vertical motions do break through the boundary layer they can generate cumulus clouds that can grow to great heights as thunderstorms (AFWA TN 98-002, 2005). Within these thunderstorms, intense updrafts can exist alongside intense downdrafts. This is another prime area for turbulence, appropriately referred to as convective turbulence. Convective turbulence is often found in and around thunderstorms, especially strong and severe storms where deep convection is persistent. The stronger the convection becomes, the stronger the turbulence will be. While moderate or severe turbulence can be found anywhere within the storm, including the clear air along its outer edges, the highest probability of turbulence is found in the storm core (AFWA TN 98-002, 2005).

2. Mechanical Mixing

Mechanical turbulence is caused by horizontal and vertical wind shear and is the result of pressure gradient differences, terrain obstructions, and/or frontal zone shear (AFWA TN 98-002, 2005). The jet stream and upper-level fronts are most commonly associated with this type of turbulence. In both regions, strong horizontal and vertical wind shear is likely and can lead to the generation of turbulence.

Figure 2 shows a major form of shear turbulence which develops in a flow changing speed so rapidly in a given direction that smooth flow is no longer dynamically possible.

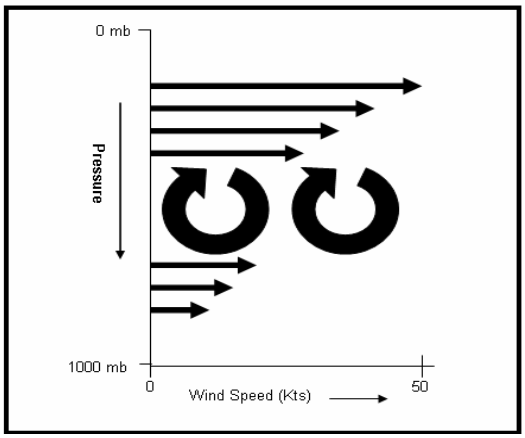

Figure 2. Example of turbulence generated by vertical wind shear. The great vertical variation in the speed of the flow turns smooth flow into turbulent eddies.

This shearing can occur in both the vertical and the horizontal, and can occur due to both directional and speed changes in the wind. In operational forecasting, vertical speed shear is predominantly the major challenge and of the most importance (Holcomb 1976). This type of turbulence is commonly referred to as clear-air turbulence (CAT), because it often occurs in the upper troposphere in the absence of any clouds, and commonly in the presence of the jet stream, or upper-level fronts. Vertical speed shear in jet-stream flow can be found both below and above the jet maximum, where wind speed decreases rapidly in the vertical away from the jet core. Most turbulence forecasts made above 10,000 feet are for areas where intense shear is present, and therefore CAT is likely.

Strong vertical wind shear within a stable layer can lead to the development of Kelvin-Helmholtz waves, a phenomenon which resembles a breaking ocean wave. The breaking of these waves can be a principal mechanism responsible for CAT. The presence of these waves is often marked by "billow" wave-cloud formations (Ludlam 1967) which can be observed in satellite imagery or radar (Ellrod and Knapp 1992).

Mountain wave turbulence is another form of mechanical turbulence caused by terrain obstructions, which force flow around the terrain and can cause wave like patterns (turbulence) to develop in the flow. Local terrain can magnify gradient winds to cause strong winds and turbulence near the surface, which creates eddy currents that can make flight operations hazardous. Strong turbulence is often associated with irregular and mountainous terrain. The greater the irregularity of the terrain and the sharper the slope of the mountains, the greater the intensity and vertical extent of the turbulence will be (AFWA TN 98-002, 2005).

Figure 3. Example of turbulence induced by terrain (from UCAR 2005a).

3. Wake Turbulence

A final form of turbulence not really associated with thermal or mechanical turbulence is wake turbulence. Wake turbulence is well described by AFWA TN 98-002 and, as such, the indented material below is taken directly from the manual.

> Although neither forecasted nor recorded in a Terminal Aerodrome Forecast (TAF), wake turbulence is a problem with the increased use of heavy aircraft. The forecaster should be aware of how wake turbulence forms and be aware of its effects.
>
> ***a. Characteristics***
>
> Every aircraft generates two counter-rotating wingtip vortices. Wake turbulence results when an aircraft encounters vortices from another aircraft. Vortex generation begins when the nose wheel lifts off the ground and ends when the nose touches back down again during landings. A vortex forms at each wingtip as air circulates outward, upward, and around the wingtip. The diameter of the vortex core varies with the size and weight of the aircraft.
>
> These vortices can be 25 to 50 feet in diameter with a much larger area of turbulence. They usually stay fairly close together (about 3/4 of the wing span) until dissipation. They sink at a rate of 400 to 500 feet per minute and stabilize about 900 feet below the flight path, where they begin

to dissipate. Vortex size is reduced by the use of winglets, smaller "wings" that curve upward from aircraft wing tips.

b. Dissipation

Atmospheric turbulence increases the dissipation of wake turbulence while ground effect and surface winds alter the low-level vortex characteristics only slightly. As the vortex sinks into the boundary layer, it begins to move laterally at about 5 knots. A crosswind will decrease the lateral movement of a vortex moving toward the wind and increase the movement of a vortex moving with the wind. This could hold one of the vortices over the runway for an extended period or allow one to drift onto a parallel runway. Vortices persist longer during inversions. Listed below are some rules for avoiding wake turbulence from the Federal Aviation Administration (FAA) Aeronautical Information Manual:

• Stable conditions combined with a crosswind of about 5 knots may keep the upwind vortex over the runway for periods of up to 15 minutes.

• Vortex generation begins with lift-off and lasts until touchdown. Therefore, aircraft should avoid flying below the flight path of a recent arrival or departure.

• If two aircraft fly in the same direction within 15 minutes of each other, the second should maintain an altitude equal to or higher than the first. If required to fly slightly below the first, the second aircraft should fly upwind of the first.

B. INTENSITIES

There is currently no standardized method of categorizing turbulence intensities. Different agencies use slightly different categorization methods. The Air Force currently uses the guidance outlined in AFWA TN 98-002 (2005) which is described below in the indented sections.

The levels of turbulence intensity are based on the impact to aircraft flying through the area of concern.

1. Light Turbulence

The aircraft experiences slight, erratic changes in attitude and/or altitude, caused by a slight variation in airspeed of 5 to 14 knots with a vertical gust velocity of 5 to 19 feet per second. Light turbulence may be found in many areas, such as:

- At low altitudes in rough terrain when winds exceed 15 knots.
- In mountainous areas, even with light winds.
- In and near cumulus clouds and near the tropopause.

2. Moderate Turbulence

The aircraft experiences moderate changes in attitude and/or altitude, but the pilot remains in positive control at all times. The aircraft encounters small variations in airspeed of 15 to 24 knots; vertical gust velocity is 20 to 35 feet per second. Moderate turbulence may be found:

- In towering cumuliform clouds and thunderstorms.
- Within 100 nm of the jet stream on the cold air side.
- At low altitudes in rough terrain when the surface winds exceed 25 knots.
- In mountain waves (up to 300 miles leeward of Ridge), winds perpendicular to the Ridge exceed 50 knots.
- In mountain waves as far as 150 miles leeward of the Ridge and 5,000 feet above the tropopause when wind perpendicular to the Ridge is 25 to 50 knots.

3. Severe Turbulence

The aircraft experiences abrupt changes in attitude and/or altitude and may be out of the pilot's control for short periods. The aircraft encounters large variations in airspeed greater than or equal to 25 knots and the vertical gust velocity is 36 to 49 feet per second. Severe turbulence occurs:

- In and near mature thunderstorms.
- Near jet stream altitude and about 50 to 100 miles on the cold-air side of the jet core.
- In mountain waves (up to 50 miles leeward of Ridge), winds perpendicular to Ridge are 25 to 50 knots.
- Up to 150 nm leeward of the Ridge and within 5,000 feet of the tropopause when a mountain wave exists and winds perpendicular to the Ridge exceed 50 knots.

4. Extreme Turbulence

The aircraft is violently tossed about and is practically impossible to control. Structural damage may occur. Rapid fluctuations in airspeed are the same as severe turbulence (greater than or equal to 25 knots) and the vertical gust velocity is greater than or equal to 50 feet per second. Though extreme turbulence is rarely encountered, it is usually found in the strongest forms of convection and wind shear. The two most frequent locations of extreme turbulence are:

- In mountain waves in or near the rotor cloud.
- In severe thunderstorms, especially in organized squall lines.

C. AIRCRAFT TURBULENCE SENSITIVITIES

Another complexity with observing and forecasting turbulence arises from the wide variation in aircraft the USAF and commercial airlines operate. With so many different aircraft, each with large differences in weight, structural design, and capabilities, it is no surprise that each type of aircraft will experience turbulence in different ways. AFWA TN 98-002 (2005) effectively describes how the Air Force handles these differences and what follows comes directly from AFWA TN 98-002:

> Different aircraft types have different sensitivities to turbulence. Table 1 lists the categories for most military fixed-wing and rotary-wing aircraft at their typical flight configurations. Turbulence forecasts in TAFs are specified for Category II aircraft. Modify the local turbulence forecast for the type of aircraft supported. Use caution, however; an aircraft's sensitivity varies considerably with its weight (amount of fuel, cargo, munitions, etc.), air density, wing surface area, wing sweep angle, airspeed, and aircraft flight "attitude."
>
> Since aircraft sensitivity to turbulence varies considerably, use caution when applying forecast turbulence (Category II) to a specific aircraft type, configuration, and mission profile. Table 2 is a guide to convert turbulence intensities for the different categories of aircraft.

Table 1. Aircraft category type from Table 2.7 in AFWA TN 98-002 (2005).

Category	Aircraft Type			
I	OH-58	UH-1	AH-1	
II	C-141	C-9	RAH-66	C-12
	C-21	F-106	C-20	C-5A
	E-4A	F-15	AH-64	B-52
	C-130	C-17	F-117	F-16
	KC-135	C-23	CH-47	U-21
	OV-1	CH-3	UH-60	CH-53
	CH-54	VC-137	T-38	
III	OV-10	KC-10	T-37	A-10
IV	A-7	F-4	B-1B	F-111*

* At 50 degree wing configuration.

Note: turbulence thresholds were developed for aircraft in Category II. Consider the synoptic situation, local terrain effects, pilot reports (PIREPS), and aircraft type and configuration before making turbulence forecasts.

Table 2. Turbulence intensities for different categories of aircraft based on Table 1 and taken from Table 2.8 in AFWA TN 98-002 (2005). For example, what a Category I aircraft might report as Moderate turbulence may only be Occasional Light turbulence for a Category IV aircraft.

	I	II	III	IV
	N	N	N	N
	(L)	N	N	N
	L	(L)	N	N
	L-(M)	L	(L)	N
Turbulence	M	L-(M)	L	(L)
Reported As	M-(S)	M	L-(M)	L
	S	M-(S)	M	L-(M)
	S-(X)	S	M-(S)	M
	X	S-(X)	S	M-(S)
	X	X	S-(X)	S
	X	X	X	S-(X)
	X	X	X	X

N = None ( ) = Occasional (less than 1/3 of the time)
L = Light M = Moderate S = Severe X = Extreme

Note: Use caution when converting extreme turbulence reports between various aircraft types. Extreme turbulence causes a range of effects from a minimum threshold (rapid airspeed fluctuations greater than 25 knots) to a maximum threshold (structural damage). Even though the table considers this, the design is more for the sake of "completeness" rather than observational or scientific evidence.

1. Fixed Wing Aircraft

Generally, the effects of turbulence for fixed-wing aircraft are increased with:

- Non-level flight.
- Increased airspeed.
- Increased wing surface area.
- Decreased weight of the aircraft.
- Decreased air density (increased altitude).
- Decreased wing sweep angle (wings more perpendicular to fuselage).

2. Rotary Wing Aircraft

Generally, the effects of turbulence for rotary-wing aircraft are increased with:

- Increased airspeed.
- Decreased weight of the aircraft.
- Decreased lift velocity (the faster the lift-off, the less the turbulence).
- Increased arc of the rotor blade (the longer the blade, the greater the turbulence).

D. FORECASTING DIFFICULTIES

Problems encountered in forecasting turbulence include the large temporal and spatial scales of the observation network, the reliability of pilot reports, and the short-lived, random nature of turbulence. Turbulence is a microscale phenomenon in an atmosphere where existing observations are made at the mesoscale at best (Lee et al. 1984). CAT forecasters are left with examining synoptic features often associated with CAT and combining those with their experience with automated computer aids to produce comprehensive CAT analyses and forecasts (Lee et al. 1984).

There are essentially two main factors which make forecasting turbulence difficult: (1) lack of observational turbulence data and (2) turbulent eddies at the scales which affect aircraft (~100m) are a microscale phenomenon and numerical weather prediction (NWP) models cannot resolve that scale (Abernethy and Sharman 2006).

Over the past half-century most of the progress made in turbulence forecasting has been in increased model resolution and improved eddy simulation and understanding. These improvements are predicated on the idea that most of the energy associated with turbulent eddies at aircraft scales cascades down from larger scales of atmospheric motion (Dutton and Panofsky 1970; Abernathy and Sharman 2006). Upon this realization, the effort was focused on linking large-scale features, easily resolvable by NWP models, to the formation of turbulent microscale eddies. In this process a vast assortment of diagnostics or empirical based rules of thumb (also referred to as algorithms, indexes, etc.) have been created to describe and predict turbulence. A brief description and analysis of the most commonly used diagnostics is presented in section C of the Chapter III. The skill of each of these diagnostics' ability to forecast upper-level turbulence is highly variable. None of the diagnostics offer a completely satisfactory method of forecasting turbulence, but rather reflect the imperfect understanding of the atmospheric processes involved.

The Turbulence Joint Safety Implementation Team (TJSIT), which is comprised of representatives from the FAA, NASA, federal laboratories, and end users, recommends a greater than 0.8 probability of moderate-or-greater (MOG) turbulence

detection and a greater than 0.85 probability of null turbulence detection[1] (Abernethy and Sharman 2006). To date, neither of these goals has been met by any automated system or human forecaster on a consistent, daily basis.

In the 1990s, and in the first few years of the new century, there has been a focused effort on developing an automated turbulence forecasting system. The first major development came in 2000 with the Integrated Turbulence Forecasting Algorithm (ITFA), developed by the Turbulence Product Development Team (TPDT) under sponsorship from the FAA/AWRP, NCAR/RAL, and NOAA's Forecast Systems Laboratory (NOAA/FSL). There were automated turbulence forecasting systems before this, but they were mainly just an automated calculation of one of the common diagnostics. For example, the Air Force Weather Agency uses the MM5 model to produce a turbulence forecast by calculating the Ellrod II diagnostic (Ellrod and Knapp 1992) using the model output data and displaying a map of where the Ellrod diagnostic predicts turbulence. The Ellrod index is simply defined as the wind shear times the sum of the horizontal deformation and convergence (discussed in detail in Section C of Chapter III). But the ITFA took into consideration several of the diagnostics. Soon after the ITFA was developed, it was implemented, and became known as the Graphical Turbulence Guidance (GTG) forecasting product. The GTG system was not the only forecasting system to use multiple diagnostics together, but was and still is the only one to combine them dynamically at forecast time (Abernethy and Sharman 2006). The diagnostics currently being used in the GTG can be found in Appendix A. The GTG will be discussed in more detail in section E (GTG Analysis) of Chapter III.

E. OBSERVATION ISSUES

Turbulence which affects flight operations most often occurs as a microscale phenomenon making it very difficult to observe. There is no current observing system with the horizontal and vertical resolution to accurately observe turbulence. Such a system would require, at the very least, less than a kilometer resolution.

[1] Probability of detection (POD) means given that a turbulence event occurred, what is the probability that it was forecasted. In other words, POD is the number of times the event was forecasted to occur and it occurred (defined as a hit), divided by the number of times the event was observed to occur, whether or not it was forecasted: POD = (hits) / (hits + misses).

1. PIREPs

"Currently, the best available real-time information concerning turbulence comes from pilot reports (PIREPs) (Takacs et al. 2006)." The reports include the date and time, latitude and longitude, altitude, and severity, as determined by the pilot, of the turbulence encounter. Unfortunately, there is no consistent objective measurement technique allowing for regular observations of turbulence. Airplanes encountering turbulence are the only source of observations available to weather personnel. Because of the irregular time and spatial distribution of airplane routes, the observations are just as irregular providing a less than reliable observation system with intense coverage over certain regions and very poor coverage over other regions.

Furthermore, the objectivity and accuracy of the observations are to be questioned. PIREPs of turbulence are made by the pilots themselves, as they are requested to log turbulence encounters and identify intensity based on their own experience or impressions. What may be a "severe" encounter with turbulence for one pilot may be a "light-moderate" turbulence encounter for another pilot (Tebaldi et al. 2002). The lack of null reports or smooth reports from pilots is unfortunate. The majority of PIREPs are made for light turbulence or greater. In areas where there are huge data gaps, the forecaster then has to guess whether there were no flights in this area to report turbulence, or whether the pilot experienced smooth, non-turbulent flying and so made no report. In either case, the forecaster cannot conclude whether there is turbulence in the area or not. The majority of pilots are trying to avoid turbulence as much as possible in order to have as smooth as flight as possible. For these reasons it is important for the forecaster to understand the distribution of PIREPs is not a true representative of the state of the atmosphere because most non-turbulent areas are not reported and many turbulent areas may go unreported. It is equally important for the forecaster to understand PIREPs can be utilized to identify regions where turbulence has been occurring and can provide a subjective assessment of how intense the turbulence was for the area.

Despite the disadvantages of using PIREPs for the verification of turbulence forecasting techniques, few other better options are currently available to researchers and operational meteorologists. Automated turbulence observations, however, from aircraft will enhance the available PIREP database (Cunningham 2006).

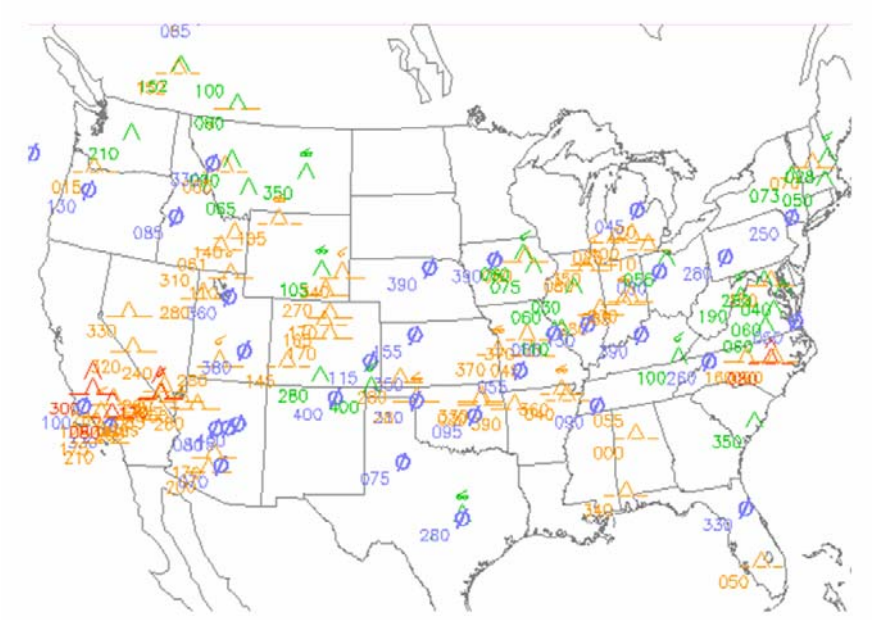

Figure 4. Example PIREPs observation display from the Aviation Weather Center (AWC) for 1800 GMT, 14 April 2006.

In the last decade a more objective form of observing turbulence has been developed in the form of automated turbulence measurements taken from aircraft every minute of their flight from take off to landing. As reported in the National Center for Atmospheric Research (NCAR) Research Application Programs (RAP) 2004 Annual Report, automated turbulence measurements from aircraft, in combination with Doppler ground-based radar, are being developed as a method for clear-air turbulence observing and nowcasting (UCAR 2005b).

2. In-situ

The automated turbulence measurements by aircraft are estimates of a form of the eddy dissipation rate, ε, which is MacCready's (1964) proposed universal turbulence standardization technique. It is quantitatively based on atmospheric turbulence, as opposed to the qualitative and aircraft-dependent turbulence a pilot may "feel."

MacCready (1964) defines the eddy dissipation rate (EDR) as "the rate at which the turbulence energy is converted into heat for steady turbulence." He stated an EDR can be measured independently of aircraft type or speed. The EDR can be measured by detecting "…the small longitudinal (or lateral) velocity turbulent fluctuation…" (MacCready 1964).

Under the sponsorship of the FAA, work began in the early 1990's at the NCAR to develop and deploy an in-situ turbulence measurement and reporting system for commercial aircraft (Cornman et al. 2004). The concept originally employed was to use existing sensors, avionics, and communication networks to produce and disseminate the EDR as measured from aircraft. The EDR is a quantitative, state-of-the-atmosphere turbulence metric unlike the subjective turbulence PIREPs. The EDR reports were intended to augment the PIREPs, and were designed to address the deficiencies of the PIREPs. Because EDR measurements provide a routine, quantitative measurement of the atmospheric turbulence, they also include much needed null reports. This allows forecasters to clearly identify regions of smooth flying and make the appropriate adjustments to their forecasts.

Two main algorithms have been developed to measure the EDR from on-board data: (1) Vertical accelerations and (2) Vertical wind component. The first algorithm uses vertical accelerations and a mathematical model of the aircraft response to turbulence in order to estimate EDR values. The second uses a calculation of the vertical wind component. A detailed description of these methods and the associated quality control methods can be found in Cornman et al. (1995, 2004).

3. EDR Reporting

With both EDR estimation methods a time series of EDR values is produced over a one-minute cruise-mode reporting interval. Two values are sent in the EDR report which can be thought of as the median value for the minute and the maximum value for the minute. This gives some indication of whether the turbulence is relatively continuous or discrete for the minute time period. For example, if the maximum value is vastly different from the median value for a given minute, it can be deducted that the turbulence event was a discrete event (Cornman et al. 2004). Both the peak and the median EDR values are binned into categories before they are downloaded from the aircraft. The

minimum EDR category is 0.05. The categories then increment by 0.10 to the maximum of 0.85. Studies have shown the 0.05 EDR category is reported over 90% of the time, while EDR categories above 0.65 are extremely rare (less than 0.01%) (Takacs et al. 2006). An EDR report of 0.05 is considered to be a null report of turbulence.

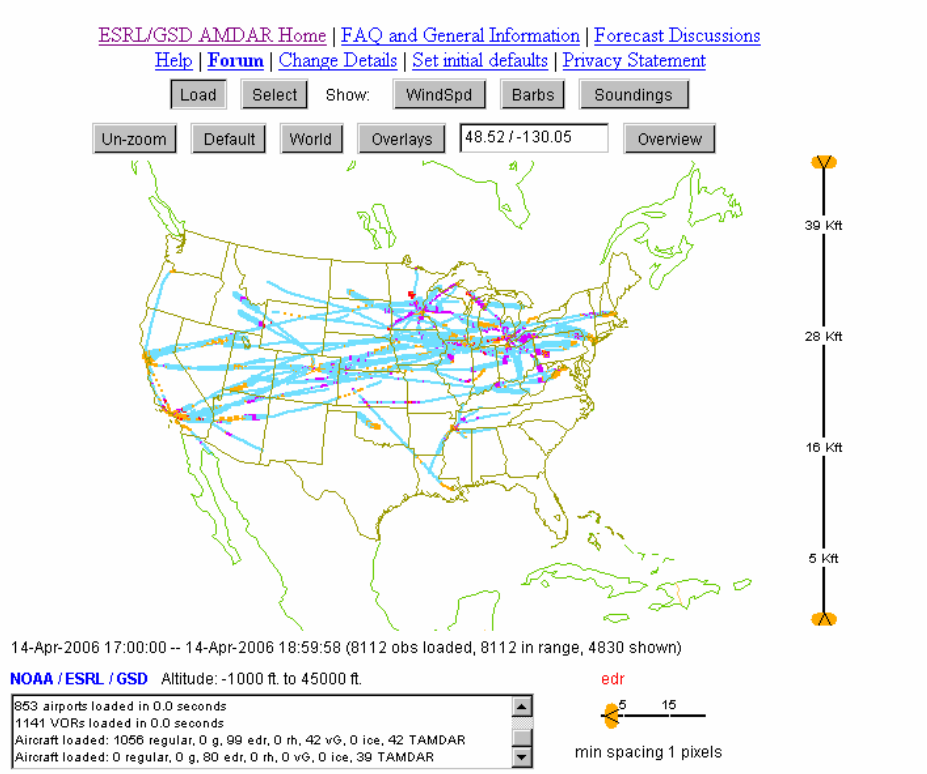

Figure 5. Example EDR observations plot from ESRL/GSD (2006) for 1700 thru 1900 GMT, 14 April 2006. Refer to section A of Chapter III for more details.

A primary advantage of the EDR reports is that they are aircraft-independent measures of turbulence (Cornman et al. 2004). Through careful testing and verification, Cornman et al. (2004) shows EDR reports can be used as a universal, aircraft-independent metric for communicating turbulence information between users and if a user desires an aircraft-dependent measure it can be estimated via a relation derived in Cornman et al. (2004).

In 1997 the implementation of the EDR reporting began on United Airlines aircraft using the vertical accelerations algorithm. Currently, 199 aircraft have EDR

reporting capability, but due to cost savings only the B737s are providing routine reports. In 2005, 160 Delta aircraft added the vertical wind component algorithm as well as 93 aircraft from Southwest Airlines.

The Global Systems Division of the Earth System Research Laboratory (ESRL/GSD), formerly Forecast Systems Laboratory (FSL), has taken a lead role in providing automated meteorological reports from commercial aircraft to atmospheric researchers and to government operational forecasters. Recently, ESRL/GSD added automated turbulence data to the other weather data on their unofficial (not operational) website http://acweb.fsl.noaa.gov/ (ESRL/GSD 2006).

It may be possible for the EDR to be directly ingested into NWP models, which suggests a future possibility of forecasting EDR directly (AMS 2003). If a pilot is provided EDR data directly he/she may be able to relate the information to an aircraft-dependent chart (particular to their aircraft flight characteristics, as well and make a determination on how to continue their flight (Cunningham 2006).

F. DYNAMICS AND ASSOCIATED SYNOPTIC CONDITIONS

With each type of turbulence there are different physical causes and conditions which are responsible for creating the turbulence. Understanding these different physical (or dynamical) causes is critical to being able to effectively forecast turbulence. A detailed discussion of these physical causes for the various types of turbulence is given in the following subsections starting with thermal turbulence, then CAT, and finishing with mountain wave turbulence.

1. Thermal Turbulence

Thermal turbulence, also called boundary layer or convective turbulence, is associated with static instability. An excellent measure of the static stability of air is the potential lapse rate, Γ: $\Gamma = \Delta\theta/\Delta Z$, where $\Delta\theta$ is the change in potential temperature over a layer of thickness ΔZ (Lee et al. 1984). For dry air, when Γ is positive the air is considered to be statically stable. When Γ is negative the air is statically unstable, and when Γ is 0 neutral stability occurs. Thermal turbulence starts in statically unstable air (Lee et al. 1984). Typically, this turbulence occurs in the boundary layer as it warms on a hot, sunny day. This leads to a negative Γ in the boundary layer or just above it, as the surface is much warmer than the air above. When the air is statically unstable it can

break down into rising/descending parcels of hot/cold turbulent air. Some of these thermals can rise far enough to cause clouds. Many other thermals are trapped below the cloud base by the temperature inversion just below the cloud base. It is important to note although thermal turbulence is most commonly found near the earth's surface, it can occur in the upper troposphere where radiative cooling or horizontal advection lowers the lapse rate, such as near cirrus clouds (Lee et al. 1984).

2. Clear-Air Turbulence

Unlike thermal turbulence, CAT is created in statically stable air. CAT occurs when the wind shear is particularly strong. When the wind shear is strong enough to create CAT the air is considered to be dynamically unstable (Lee et al. 1984). It has been shown dynamic CAT can occur only when the wind shear is strong enough to overpower the stability. The Richardson number (Kronebach 1964) is a ratio that compares the relative strength of the static stability versus the wind shear:

$$\text{Richardson number} = \text{Ri} = \frac{g\left(\frac{\Delta\theta}{\Delta z}\right)}{\left(\frac{\Delta v}{\Delta z}\right)^2}$$

where g is the acceleration due to gravity and $\Delta V/\Delta Z$ is the vector wind shear occurring over the vertical distance ΔZ (Kronebach 1964).

The Ri indicates while the wind shear tends to produce turbulent kinetic energy, stability tends to damp this energy. This means Ri must be less than one for turbulence to have a chance to occur. However, theory and experiment have shown dynamic turbulence can only occur when the Ri is less than or equal to 0.25, or when the shear is four times greater than the stability. When air has a Ri less than 0.25 it is considered to be dynamically unstable. Additionally, statically unstable air ($\Gamma<0$) is automatically dynamically unstable because the Ri is negative in that case due to the negative lapse rate. It has also been shown (Miles and Howard 1964) when Ri is near 0.25, Kelvin-Helmholtz waves often occur.

CAT often occurs near the jet stream at the tropopause as illustrated in Figures 6 and 7. These occurrences of CAT peak during winter months and reach a minimum in

the summer. The root of this CAT is often strong vertical wind shear (speed and/or direction) and strong horizontal wind shear in this region associated with the jet combined with the static stability which often exists near the tropopause. The jet is usually stronger during the winter months when strong thermal gradients are enhanced, especially over CONUS. Strong shears can first generate Kelvin-Helmholtz waves. These waves amplify, roll-up, and break similar to ocean waves (Lee et al. 1984).

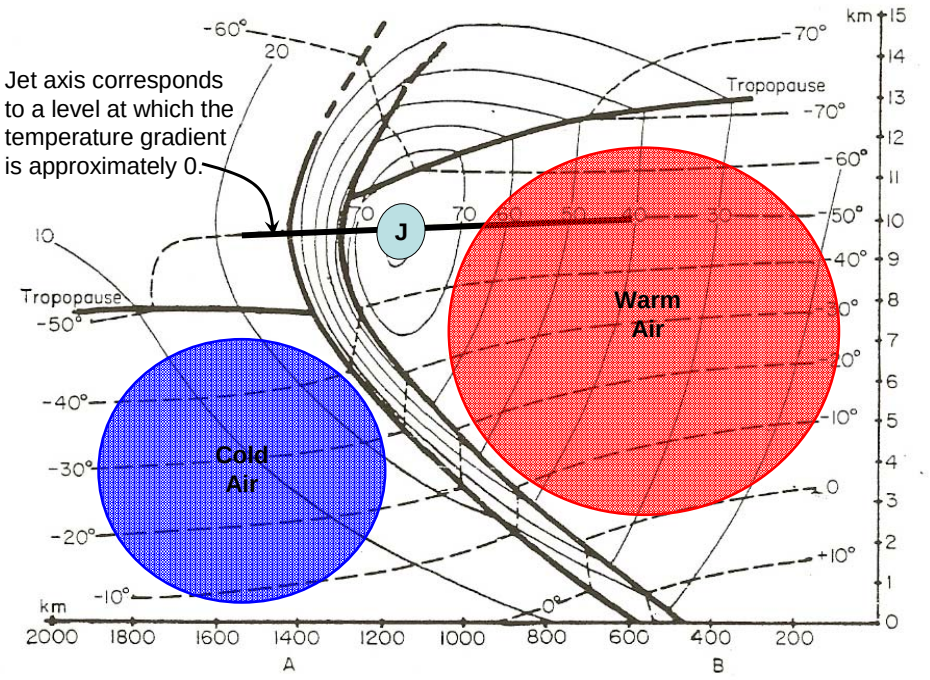

Figure 6. Typical jet stream and upper level front set up. Pale blue circle with "J" marks the jet max. Solid lines are isotachs. Dashed lines are isotherms.

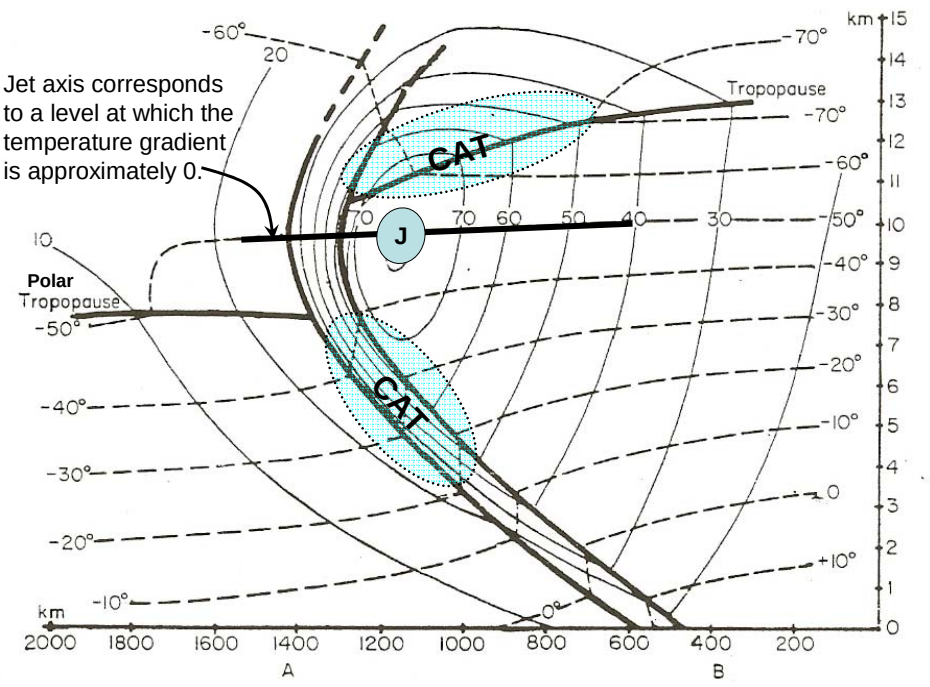

Figure 7. Same as in Figure 6 except typical location of CAT is shown in bright blue areas.

In the 1950s and 1960s early attempts to forecast CAT at the operational level involved the determination of synoptic or mesoscale conditions which are conducive to turbulence, since numerical models could not come close to resolving CAT. One of the approaches was to empirically relate forecast synoptic flow patterns to the occurrence of CAT (Rammer 1973). From these types of studies, it was shown curved segments of the jet stream associated with troughs, ridges, and closed upper lows were more likely areas to contain CAT than straight jet segments (Ellrod and Knapp 1992). Mesoscale conditions were also studied using aircraft and radiosondes. Regions favorable for significant CAT were determined to have the following characteristics:

- Strong vertical wind shear (speed and directional)
- Strong horizontal shear
- Significant convergence
- Significant horizontal deformation

- Lapse-rate discontinuities
- Strong horizontal thermal gradients

(Ellrod and Knapp 1992)

Note all of these characteristics are consistent with the characteristics of sloping upper-level frontal zones. Numerical techniques to forecast turbulence has mainly focused on predictions of vertical and horizontal wind shear, which can be relatively easily calculated from model output fields.

In a 2002 study led by NASA on characterizing the severe turbulence environments associated with commercial aviation accidents an effort was made to determine the most prevalent synoptic scale atmospheric configuration associated with severe turbulence reports (Kaplan et al. 2002). The synoptic predictor fields depicted in Appendix B represent standard derived quantities often associated with turbulence in recent studies (e.g., Keller 1990; Ellrod and Knapp 1992; Knox 1997). In the NASA study these predictor fields were calculated and the magnitudes were compared to location, elevation, and time of accident. The most useful and least useful predictor fields were then determined for when and where severe accident-producing turbulence should be occurring. Table 3 shows the most useful predictors from all 44 of the NASA case studies.

Table 3. Best Predictors for 44 Accident Case Studies (% of 44) from Kaplan et al. (2002).

1. Immediate upstream curvature	(98%)
2. Convective clouds (all bases) < 100 km away	(86%)
3. Upward vertical motion	(82%)
4. Layer-averaged absolute vorticity ≤ 10^{-4} s^{-1}	(80%)
5. Jet entrance region	(77%)
6. Higher vertical shear advection	(77%)
7. Lapse rate ≥ moist adiabatic	(77%)
8. Absolute vorticity at flight level ≤ 10^{-4} s^{-1}	(75%)
9. Convective clouds (all bases) < 30 km away	(74%)
10. Horizontal cold advection	(73%)
11. Flight level relative vorticity ≤ 0 s^{-1}	(68%)
12. Leftward-directed $v_{ageostrophic}$ flow	(64%)

It was concluded from this study the most persistent synoptic predictors of severe turbulence are a ridge or trough axis where a region of changing flow curvature is occurring, convection, upward vertical motion, low relative vorticity, and the entrance region of a jet stream (Kaplan et al. 2002). For the case studies, there was a great deal of uncertainty concerning what processes accompanying the jet entrance regions consistently organized the environment which created turbulence of greater than moderate intensity. It was found that buoyancy-based forcing, shear-based forcing, kinematics-based forcing, and complex combinations thereof can be related to characterizing the environment that organizes turbulence but may or may not be a discriminating condition for the development of severe accident-producing turbulence (Kaplan et al. 2003). Consequently, trying to discriminate when and where the environment will develop microscale severe turbulence is an unsolved problem which will continue to challenge meteorologists.

These case studies varied substantially in the intensity of the mesoscale jet streams near the accident locations, but there are many common signals among the jet streams (Kaplan et al. 2003):

> First, they represent locations of three-dimensional transition between two jet stream entrance regions and their supporting baroclinic zones. The

northern stream is curved, weaker, and lower in elevation whereas the southern stream is straighter, stronger, and higher in elevation. Second, these jet stream entrance regions indicate highly confluent ageostrophic flow with leftward-directed ageostrophy in the southern jet stream and rightward-directed ageostrophy in the northern jet stream. Third, the vertical structure depicted in Figure 8 indicates a wind maximum above and just upstream from the level of the accident with a region of stronger winds extending downward through the level of the accident; this indicates the proximity of the deep jet streams that phase above the same location in the vertical (Kaplan et al. 2003).

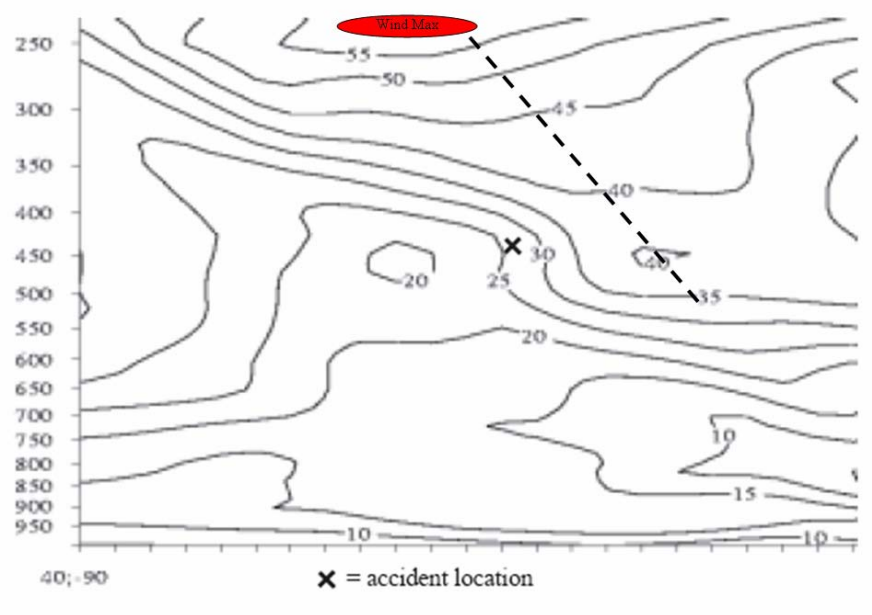

Figure 8. Simulated jet normal vertical cross sections of total wind isotachs (solid in m/s) from Kaplan et al. (2003). Wind maximum is above and upstream of accident location and dashed line indicates sloping stronger winds extending downward through the accident level. Also note the strong vertical and horizontal wind shear near the accident location.

A hypothesized mesoscale sequence of events which would maximize the potential for severe CAT and convective turbulence flow was constructed by Kaplan et al. (2002, 2003):

(1) Two jet stream entrance regions become juxtaposed resulting in proximity between curved flow in a baroclinic zone and stronger straight advective flow, which vary substantially in magnitude in the vertical.

(2) The misphasing of the along-stream and cross-stream maxima in the pressure gradient force, the centrifugal force, and the Coriolis force at the

> interface of the two jet stream entrance regions produces a local region of highly confluent ageostrophic curved flow that may be supergradient.
>
> (3) The confluence resulting from the variation of the streamwise wind component in this highly ageostrophic "stretched" state produces a mesobeta scale frontal zone and maximum in ageostrophic vertical vorticity.
>
> (4) The increasingly streamwise-oriented front becomes the locus of three-dimensional wind gradients, which are available for tilting, and vertical convergence into horizontally intensifying vortex tubes if significant buoyant lifting occurs.

This hydrostatic sequence of events results in the focusing of maxima of kinematic forcing, frontogenesis, and minima in Richardson number in the same place and the same time as the isentropic surface folds in proximity to strong two-dimensional rotation about the vertical axis. From a physical perspective, this process represents the isentropic surfaces folding over in proximity to strong gradients of ageostrophic vertical vorticity. The turbulent event will be generated by the breakdown of the flow established by the above complex sequence of dynamical processes and the resulting sequence of nonhydrostatic adjustments (Kaplan et al. 2003).

3. Mountain Wave

For his thesis in 2005, Captain Joseph D. Coughlin (USAF) fulfilled a request by US Air Forces Europe (USAFE) OWS forecasters to research and update the mountain wave turbulence guidance outlined in AFWA TN 98-002 (2005). The following description of mountain waves has been taken from his thesis, Forecasting the Onset and Intensity of Vertically Propagating Mountain Waves Over the Alps:

> Mountain waves are a form of internal gravity wave, where the wave disturbance is forced by a terrain feature. This disturbance occurs when the mean atmospheric flow encounters mountainous terrain and instead of being able to continue on its present course, it is forced vertically, transporting momentum and potential energy with it. Once displaced, this air can respond in several ways, primarily depending on the stability of the surrounding atmosphere and the general shape, height and width of the mountain range. In an unstable environment, the displaced air is warmer and less dense than its surroundings and will continue to rise until it reaches thermal equilibrium. Once thermal equilibrium is reached, this displaced air will follow the environmental flow, which has minimal vertical motion. Thus an unstable environment is not conducive to wave

> propagation. If the environment is stable, the displaced air becomes colder and denser than its surroundings. The rate of ascent then slows and ultimately reverses directions so that it may reach thermal equilibrium. As the air descends it gains kinetic energy, thus, once reaching thermal equilibrium the air is not able to stop. It continues to descend, warming dry adiabatically, becoming warmer than its surroundings. This warmer, more buoyant air, slowly stops descending and begins to ascend back to its equilibrium level. This oscillating process continues until kinetic energy dissipates, damping the amplitude of the wave (Hooke 1986).

It is critical the forecaster accurately diagnose the atmospheric conditions and understand the small variations which can change laminar flow into turbulent flow. There are two primary types of mountain induced waves to be concerned with: trapped lee waves, and vertically propagating mountain waves.

a. Trapped Lee Waves

Trapped lee waves are waves that propagate horizontally due to strong vertical wind shear or large stability changes just above ridge top level, either of which can act as a vertical propagation barrier (Coughlin 2005). This barrier interface allows wave energy to oscillate vertically below it. Typically, the scenario leading to a trapped lee wave response has an inversion just above the mountain ridge top level with less stable stratification above the inversion. A trapped lee wave response can excite an oscillation which can lead to the development of cloud bands like those shown in Figure 9 that have equidistant horizontal spacing as they oscillate and are parallel to that of the ridge axis. If the atmospheric conditions are favorable these cloud bands can extend dozens of times for hundreds of kilometers (Coughlin 2005).

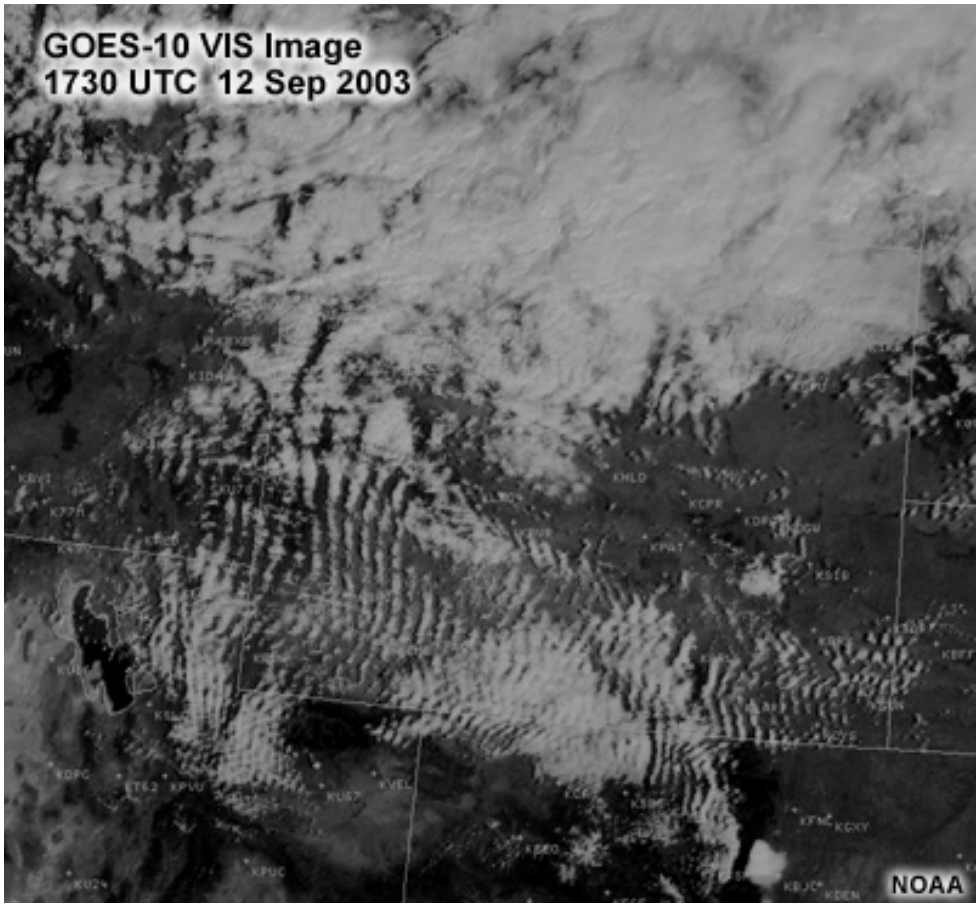

Figure 9. A trapped lee wave response formed across Wyoming on 12 September 2003. The width of the wave train exceeds 700 km. The combination of strong wind shear and an inversion located just above the ridge top created nearly ideal conditions for trapped waves (from UCAR 2005a).

Trapped lee waves are very common and significant effects to aircraft can be felt even downstream of hills with as little as 300-500m elevation gain above the background elevation (Queney et al. 1960). Turbulence associated with trapped waves can be moderate to severe, especially in a rotor zone. However, the flow associated with trapped waves is thought to be primarily laminar (especially above ridge top level) due to the stunted vertical propagation. Therefore, turbulence is relatively nominal, especially for smaller and narrow mountains (Coughlin 2005).

b. Vertically Propagating Waves (VPWs)

This section describes VPWs and is taken directly from Coughlin (2005) who accurately describes these turbulence producing waves:

> As one might expect, VPWs are waves that propagate vertically. Uniform stability and minimal background vertical wind shear allows for these waves to extend to great altitudes, thus disturbing flow in the troposphere and stratosphere. Unlike trapped lee waves, which have multiple cloud crests, VPWs almost always have one wave crest with some less severe events having a second or third wave crest of lesser vertical prominence (Durran 1986). A large cloud shield, almost always present, develops just downstream and sharply parallel to the axis of the mountain barrier. This cloud shield remains quasi-stationary (especially the leading edge) for the duration of the event and can have IR temps of -40° to -60° Celsius. Because VPWs are just a single wave, it is difficult to determine their exact wavelength; however, VPWs generally have wavelengths 30km or greater (Durran 1986). Unlike trapped wave responses, VPWs have a longer wavelength response that is easily discernable on both high resolution and low resolution imagery. Typically, it is larger mountain ranges like the Alps, Pyrenees, Rockies and Sierra Nevada that excite VPWs. Much like that of an ocean wave, the greater the amplitude of the wave the more likely the wave will break, thus causing severe to extreme turbulence. The large amplitude response of a VPW, thus, has a higher propensity to break than do trapped lee waves.

THIS PAGE INTENTIONALLY LEFT BLANK

III. TURBULENCE ANALYSIS

A. AUTOMATED IN-SITU OBSERVATIONS & PIREPS

Currently, the only USAF operational method of observing turbulence is through PIREPs. Within the commercial sector, in-situ EDR observations are becoming more available, and forecasters do have access to a limited set of current and past EDR observations via the NOAA/ESRL/GSD data website (http://acweb.fsl.noaa.gov/). Although these methods are not perfect, they are the forecaster and models' only insight into the observed turbulent atmosphere. All of the automated turbulence forecast techniques that have been developed in recent years are calibrated and verified based on these methods of observations. Until recently, all verification was done using PIREPs. With the development of the EDR observations, there is a movement within the research sector to verify using EDR observations and the GTG research team is hoping to incorporate EDR observations into the algorithm in the near future (Sharman et al. 2006). The fact remains, the algorithms and techniques which have been developed to forecast turbulence are only as good as the observations themselves. The techniques discussed in this thesis are validated only through observations and so the importance of observations and of understanding the observation system cannot be understated.

PIREPs and EDR observations are both categorized by severity but in different ways. PIREPs are translated from their verbal description (e.g., smooth, moderate, severe, or extreme) to an integer scale 0-8, where 0 is smooth or null, and 8 is extreme (Takacs et al. 2006). Recall EDR observations are binned into categories before they are downloaded from the aircraft ranging from 0.05 to 0.85 and incremented by 0.10. The FAA and AWC consider the 0.05 category to represent no-turbulence conditions and the 0.85 category represents extreme turbulence. Cornman et al. (2004) shows an EDR report in the 0.15 category correlates well with a "light" PIREP, the 0.25 category correlates with "light-moderate" turbulence and 0.35 correlates with a "moderate" PIREP turbulence report. As mentioned previously, EDR observations in the 0.05 category account for over 90% of the observations, while PIREPs in the 0 category, on average, account for only 26% of the time (Takacs et al. 2006). This great difference represents the best advantage of the EDR observations and using EDR observations for verification.

The far greater number of null reports from EDR observations (see Figure 10) more accurately represents what is thought of as the true atmosphere where turbulence is an event which occurs very infrequently, on very small scales, and for very short times. The much smaller number of smooth PIREPs proves that pilots often only make a PIREP when they encounter turbulence and do not routinely report null turbulence. PIREPs do not correctly reflect the actual distribution of turbulence intensities in the free atmosphere, where the air is predominantly nonturbulent at aircraft scales. Consequently, EDR observations are more realistic than the PIREPs (Frehlich and Sharman 2004). Results published by Takacs et al. (2006) indicate the latest version of the GTG performs better when EDR observations are used for verification rather than PIREPs. One side effect of the large distribution of EDR reports in the 0.05 category is that the false alarm ratio is going to be very poor for most cases because there will be a large number of null observations in 'yes' forecast regions. This is to be expected with the randomness and scale of an event like turbulence, and suggests a statistic like the false alarm ratio should not be used with turbulence verification.

There are far many more EDR observations made than PIREPs even though there are currently fewer than 100 aircraft reporting EDR values on a daily basis. Within the USAF there are no aircraft reporting EDR observations. EDR observations are made every minute from take-off to landing. For February 2005 there were 1.3 million EDR observations reported, but only approximately 36,000 PIREPs, a ratio of 36:1 (Takacs et al. 2006). Because only certain airlines and a limited number of aircraft have the capability to report EDR observations, the spatial coverage of the CONUS and outside of the CONUS is not optimum as can be seen in Figure 10.

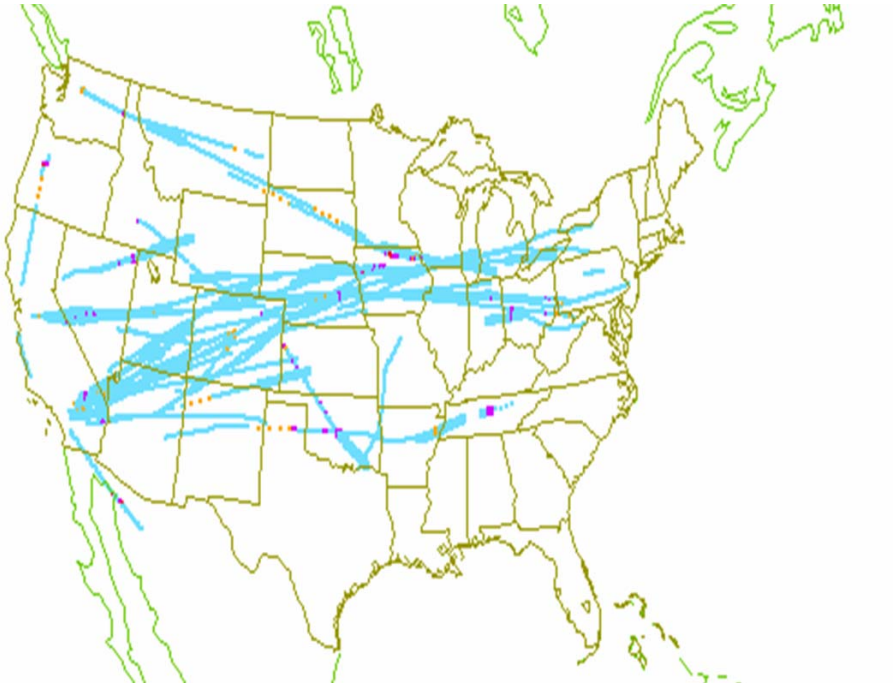

Figure 10. Typical EDR observation map from NOAA/ESRL/GSD website (http://acweb.fsl.noaa.gov/). Illustrates the lack of flights by EDR equipped aircraft over certain regions like the South and Southeast CONUS. Also illustrates the great number of null turbulence reports (in light blue).

Most of the current EDR observations are constrained to the middle of CONUS and the Northeast US. Colorado and the Southwest US are fairly well represented which is helpful for observing mountain wave turbulence over the Rockies. The Pacific Northwest, the northern Midwest, and the South and Southeast US are poorly covered by EDR equipped aircraft. In these areas, and outside the CONUS, PIREPs are still the only observing platform in use for turbulence.

One commonly noted pitfall of PIREPs is the fact that commercial pilots are always trying to avoid turbulence for the sake of the safety of the passengers, the crew, and the aircraft which results in less reports of turbulence. This pitfall is not solved by the use of EDR observations. The objective of any pilot will be to avoid turbulence when possible and so many turbulence events may occur unobserved by either of the two observing methods currently employed. Furthermore, even if more aircraft did have EDR observation capability, the fact remains that aircraft flying standard routes are sampling a very small volume of the air with respect to the Earth's atmosphere. The solution to

these problems will be to develop an observing system which does not require humans to risk their lives or their expensive equipment and which can observe a much broader and larger volume of the Earth's atmosphere.

To summarize this analysis of turbulence observation systems, turbulence is a microscale phenomenon in an atmosphere where existing observations are made at the mesoscale at best. The two methods of observing the turbulence have plenty of insufficiencies, but each offers their own advantages. For the time being, PIREPs are still to be relied upon for operational purposes especially within the USAF where no EDR network exists. It seems clear through recent studies (Brown et al. 2000, Frehlich and Sharman 2004, Takacs et al. 2006, etc.) and the author's own data that the EDR observation method provides the most accurate and realistic representation of the true atmosphere. As more aircraft are equipped with EDR observation capability in the near future, further studies will be needed, but more emphasis should be placed on using EDR observations for forecasts and verification and less on PIREPs. The addition of EDR observations to USAF aircraft would be very beneficial to USAF weather personnel. Not only would it give more spatial coverage for turbulence observations over the CONUS, but it would allow for much better spatial coverage around the globe, and most importantly, it would give far superior turbulence observations to the most current area of operations allowing the forecaster a much better understanding of the mission current atmosphere which can only result in a better forecast.

B. OWS FITL PRODUCTS (BASED ON AFWA TN 98-002)

The Air Force Weather Agency (AFWA) uses several methods to generate and disseminate turbulence forecasts. The AFWA employs a forecast-funnel approach using three levels: the strategic level, the operational level, and the tactical level. Strategic-level forecasts are created at the AFWA located at Offutt Air Force Base, Nebraska (Air Force Instruction 15-128, 2005). Strategic level forecasts will be discussed in more detail in Section D of this chapter. Operational-level forecasts are created at all of the seven OWSs located throughout the world (Cunningham 2006). Tactical-level forecasts are issued at the base level by combat weather teams (CWTs). Each level issues their own forecasts based on their area of concern and their operational level. OWSs issue forecasts for their specific region in the form of a forecaster drawn graphical chart. These charts

are produced by the current forecaster in the rotation and are termed forecaster-in-the-loop (FITL) charts. The charts are then used by CWTs who issue a forecast directly to the pilot in the form of a written one page text forecast describing where they will experience turbulence on their mission (Cunningham 2006). CWTs also give various briefings tailored to specific customers and often include the OWS FITL product in their briefings.

Operational-level forecasts of turbulence are generally traditional human forecasts in regional chart form (Cunningham 2006). The forecasters at the OWS are trained to use the strategic level turbulence forecast as guidance, as well as the guidance provided in AFWA TN 98-002 (2005), to produce their forecast charts.

A hand drawn, two-dimensional, representation of a sparse, three-dimensional microscale event like turbulence represents a great challenge to the forecaster. This is evident by the very poor verification statistics of the FITL product versus both EDR observations and PIREPs. Figure 11 below shows an OWS FITL product next to the EDR observations for 1800 GMT, 12 March 2006. The tiny pink dots on the EDR observation chart are moderate turbulence reports.

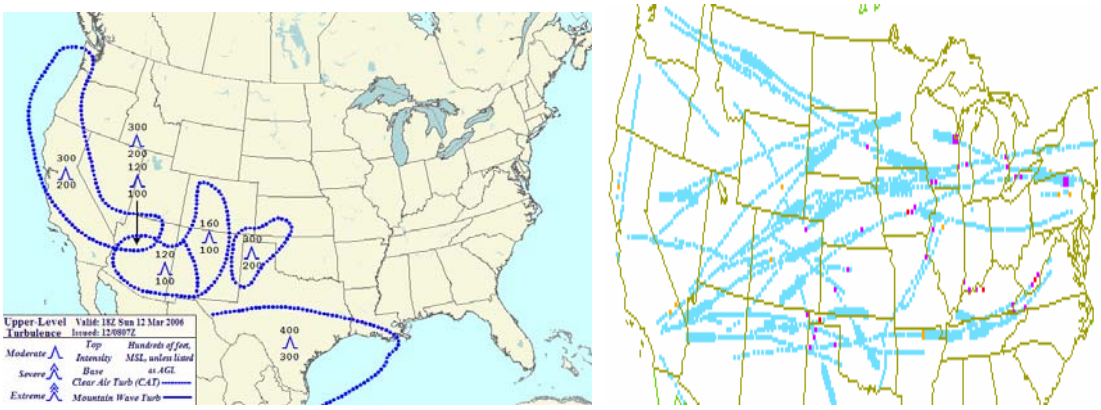

Figure 11. On the left is an OWS FITL product from the 15th OWS for 1800 GMT, 12 March 2006. On the right is the EDR observations for 17-19 GMT, 12 March 2006, with the orange representing no report available, blue representing null observations, and the pink representing moderate turbulence. Note that nearly all EDR observations in the OWS forecasted areas are null observations indicating a false alarm.

In this case, the FITL product verifies extremely poorly against the EDR observations. Forecasted turbulent areas contain mostly nonturbulent observations and

forecasted non-turbulent areas contain turbulent observations (e.g., over Iowa, Nebraska, Wisconsin, etc.). But the EDR observation chart in Figure 11 also clearly demonstrates the challenge of forming a hand drawn turbulence forecast. Imagine an OWS forecaster trying to draw a chart that looked like the above EDR observation chart. The forecaster would have to draw extremely small circles around all the pink dots, small enough to not include too many blue dots. Obviously such a task seems nearly impossible; the forecaster would be left to guessing. So the forecaster is left to draw larger areas such as those drawn in Figure 11 to encompass the range of possibilities for turbulent events and the forecaster must relate to the user that there is a certain degree of uncertainty in the forecasts. Operational decisions then should be left to the user to determine if the degree of uncertainty is worth the risk. This suggests that perhaps turbulence should be forecast from a probabilistic approach as opposed to a deterministic approach. Dutton (1980) finds that forecasts of CAT must be stated in terms of probability if they are to convey the maximum possible information to the user. This argument is made and supported by Cunningham (2006), who concludes ensemble-based probabilistic turbulence forecasts hold a distinct advantage over deterministic turbulence forecasts.

The very nature of the OWS FITL chart makes it difficult to properly relay a turbulence forecast to the user. An automated chart which can provide more detail may be of more benefit than a hand drawn chart. The forecaster is needed still to interpret the automated chart, and to relay the forecast to the user. Ideally, this would be done in a probabilistic format, to give the user some idea of the uncertainty in the forecast and to allow decision makers to be more properly informed. But even so, the OWS FITL charts do suffer from the outdated guidance in AFWA TN 98-002 as noted by Schrumpf (2006) and discussed in Chapter I of this thesis. This can be seen in Figure 11. This thesis will aim to update and improve that guidance, and one result of that will hopefully be improved and more accurate OWS FITL charts.

C. DIAGNOSTICS

Over the past 40 years there have been a large number of aviation turbulence diagnostics (or indices) developed to help diagnose and forecast the occurrence of turbulence, especially CAT. These forecast techniques are usually based on parameters derived from upper air numerical weather prediction (NWP) data such as vertical wind

shear, scalar wind speed, horizontal wind shear, deformation, and the non-dimensional Richardson number. The diagnostics have been developed based on the well understood dynamics and forcing which cause turbulence and the well observed synoptic conditions which favor turbulent conditions. The objective of these diagnostics is to take the conditions which have been known to cause turbulence, such as strong wind shear, and use models to forecast specifically these conditions. Usually, a model like AFWA's MM5 is run and then through post-processing, a diagnostic is computed using the model predicted fields. This diagnostic is then mapped like any other model output and areas where the diagnostic predicts strong turbulence will occur are noted. Every diagnostic is model dependent since the diagnostic is computed after the model has run. This means that a diagnostic applied to one model output with a certain grid resolution may look totally different applied to another model with a different grid resolution. Thus, results will not only vary between the different diagnostics, but also will vary for any single diagnostic applied to different models.

Each diagnostic has different thresholds, and extensive research and testing has to be done to determine what those thresholds are and how they might change for different synoptic conditions. However, none of these diagnostics have been shown to capture all of the turbulence forecasting problems. The NWP diagnostics were designed to attempt to capture grid scale processes that produce the mesoscale (10-100 km) meteorological conditions conducive to sub-grid scale turbulence. Thus, they cannot explicitly forecast turbulence on the scales sensed by aircraft (10-100 m) (Knox 1997). No single diagnostic should be used as a sole source for forecasting turbulence. Forecast skills of these diagnostics depend on the forecaster and how the forecaster interprets and uses the information the diagnostic provides. No diagnostic to date has been able to meet the TJSIT recommendations, either alone or combined with other diagnostics. The diagnostics' skills reflect researchers' imperfect understanding of the atmospheric processes involved (Abernathy and Sharman 2006).

Tebaldi et al. (2002) reviewed many of the turbulence diagnostics developed over the years, and performed a comprehensive statistical evaluation of the diagnostics. Diagnostics were tested individually and combined through the application of different multivariate techniques. A complete list of the diagnostics used in their study, with

complete descriptions and equations, can be found in Tebaldi et al. (2002). Three diagnostics are analyzed below and illustrate how the diagnostics help to predict turbulence. The choice of diagnostics has no significance as Tebaldi et al. (2002) show that no one diagnostic is superior to another. Notice that the three diagnostics are not entirely unique to one another (i.e., each of the three diagnostics below use vertical wind shear).

1. Ri (Kronebach 1964)

Turbulence can occur in statically stable air if the wind shear is strong enough. The air is considered to be dynamically unstable when this happens. The Richardson number has been commonly used as a measure for possible turbulent conditions since it relates shear and stability. The Richardson number (Ri) is a ratio that compares the relative strength of the static stability versus the wind shear and was discussed in Section F of Chapter II of this thesis. Recall Ri was defined as:

$$\text{Ri} = \frac{g\left(\frac{\Delta\theta}{\Delta z}\right)}{\left(\frac{\Delta v}{\Delta z}\right)^2}$$

where g is the acceleration due to gravity and Δ V/ΔZ is the vector wind shear occurring over the vertical distance ΔZ (Kronebach 1964).

Also recall that theory and experiment have shown that dynamic turbulence can only occur when Ri is less than or equal to 0.25. The Ri diagnostic then simply automates the calculation of Ri. Post-processed model fields are used to calculate the Ri as defined above, and every grid point in the model atmosphere will have a forecasted Ri value. The forecaster will then be alerted to areas in the atmosphere where the model predicts the Ri to be less than 0.25. If the forecaster were to simply forecast turbulence for every area that the Ri is less than 0.25, an extreme amount of over-forecasting would result. Recall that the Ri does not explicitly forecast turbulence; the mere fact Ri is less than 0.25 does not necessitate turbulence will exist, only that conditions are very favorable for turbulence. Furthermore, there is currently an inability to accurately measure vertical wind shear at the resolution necessary to detect areas prime for

turbulence. For these reasons, the Ri diagnostic cannot be relied upon as a sole source for turbulence forecasts, but rather should be used only as guidance to the forecaster.

2. Ellrod (Ellrod and Knapp 1992)

One diagnostic frequently used by AWC forecasters is the Ellrod index (Ellrod and Knapp 1992). The Ellrod index is defined as the vertical wind shear (VWS) times the sum of the horizontal deformation (DEF) and convergence (CVG). All three of the above components of the Ellrod index are known to increase frontogenesis, which increases the likelihood of CAT occurrence (Ellrod and Knapp 1992). The first two components, VWS and DEF, are easily calculated by using u and v wind-component forecasts. Ellrod and Knapp (1992) define VWS as:

$$VWS = \frac{(\Delta u^2 + \Delta v^2)^{1/2}}{\Delta z}$$

The vertical layer thickness is given by Δz. Ellrod and Knapp (1992) define deformation as:

$$DEF = (DST^2 + DSH^2)^{1/2}$$

where DST is the stretching deformation and DSH is the shearing deformation and are defined as:

$$DST = \frac{\partial u}{\partial x} - \frac{\partial v}{\partial y}$$

$$\text{DSH} = \frac{\partial v}{\partial x} - \frac{\partial u}{\partial y}$$

The final component, CVG, is defined as:

$$CVG = -\left(\frac{\partial u}{\partial x} - \frac{\partial v}{\partial y}\right)$$

AFWA uses the Ellrod TI2 index to produce their strategic level turbulence forecast. The Ellrod TI2 index is defined as:

$$TI2 = VWS \times [DEF + CVG]$$

Ellrod index guidance displays are generated for all NCEP models and are utilized by both military and civilian forecasters. The Ellrod index over the US from the NCEP's

North American Model (NAM) is available at http://aviationweather.gov/exp/ellrod/eta. The Ellrod index has been found to be quite skillful in determining the existence of turbulent conditions. However, both the original paper and case studies have shown the index to be limited in skill in determining the intensity of the turbulence, so the Ellrod index is frequently used in conjunction with other indices. Like the other diagnostics, the Ellrod index does not directly calculate the phenomenon that is turbulence, but only attempts to calculate its cause.

3. Dutton (Dutton 1980)

Dutton (1980) performed a study on different indices on data collected during the 1976 Turbulence Survey. Data from over 4,500 flights over the North Atlantic and north-west Europe were collected. The goal of the study was to assess the potential, as predictors of CAT, from various synoptic-scale meteorological indices computed by an automated NWP model. Dutton (1980) found that an index combining the predictive abilities of vertical and horizontal wind shear significantly out-performed concurrent conventional CAT forecasts.

The empirical index Dutton (1980) claimed as the best predictor of CAT is:

$$\text{Dutton} = 1.5 \times \text{HWS} + 0.25 \times \text{VWS} + 10.5$$

where HWS represents horizontal wind shear and VWS represents vertical wind shear. It is not surprising that vertical and horizontal wind shear were the best indicators of CAT in Dutton's study, since it is known that these two physical processes create CAT. So formulating an automated index which is calculated based upon the HWS and VWS would logically be a good indicator of areas favorable for turbulence. Previously, the forecaster was tasked to look at synoptic charts and find areas where strong HWS and VWS were likely to occur and then (after considering other synoptic factors as well) draw on their forecast charts these areas as favorable for turbulence. With diagnostics like Dutton's (1980), which automate this process by directly calculating specific areas of HWS and VWS, the forecast can be made more detailed and more precisely. Furthermore, when diagnostics like Dutton's and Ellrod's are combined with other diagnostics a more complete representation of the synoptic conditions which generate

turbulence are automated and can result in a better forecast as shown by Tebaldi et al. (2002) and Sharman et al. (2006).

D. AFWA MM5

At the strategic level, AFWA produces automated upper-level turbulence forecast guidance based on post-processed MM5 output using the second version of Ellrod's objective CAT turbulence index, as defined in Ellrod and Knapp (1992) and described briefly above in section C. Figure 12 shows an example AFWA strategic level turbulence forecast.

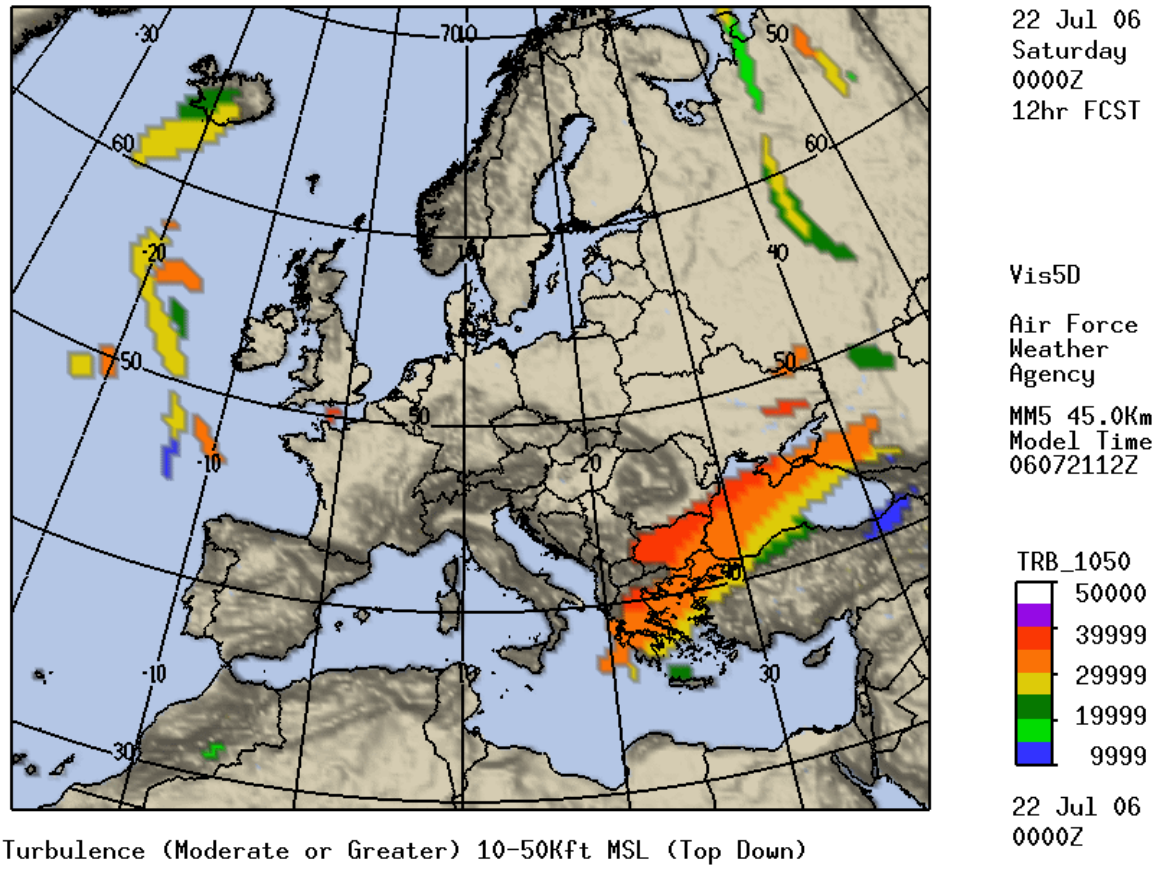

Figure 12. An upper-level (10-50 thousand feet) turbulence forecast produced by AFWA for Europe, valid 0000 GMT, 22 July 06. Forecast was derived from the Ellrod TI2 index computed from the 1200 GMT, 21 July 2006 AFWA MM5 45 km Europe model run. Altitude of predicted turbulence is denoted by color as shown.

These forecasts are easily accessible to military forecasters through the Joint Air Force and Army Weather Information Network (JAAWIN). Access to JAAWIN is restricted to .mil domain users, however, access can be granted to civilian personnel through a simple

application process. The site is located at https://weather.afwa.af.mil/. AFWA also produces low-level turbulence forecast guidance based on post-processed MM5 output using an AFWA modified version of the Panofsky (Colson and Panofsky 1965) index (Cunningham 2006). The forecaster should not singularly rely upon AFWA MM5 turbulence forecasts as they are derived from single diagnostics and cannot explicitly forecast turbulence. The forecaster should understand that the AFWA MM5 uses the Ellrod TI2 index, and should have an idea of how the Ellrod TI2 predicts turbulence as described above in Section C. With this understanding the forecaster can extract the full value of the AFWA MM5 product as it can provide good guidance on where favorable areas of CAT may occur.

E. GRAPHICAL TURBULENCE GUIDANCE

To best utilize the various turbulence indices, the NCAR has developed the Integrated Turbulence Forecast Algorithm (ITFA). The ITFA has recently become an operational NWS product generated at the AWC and has been renamed the Graphical Turbulence Guidance (GTG). The GTG generates up to 31 different turbulence diagnostics from the Rapid Update Cycle (RUC) numerical model data, normalizes the various diagnostics into a turbulence potential, scores their current skill as compared to current pilot reports, and then weights the various diagnostics into a combined index. The diagnostics used include those mentioned in Section C above and those found in Appendix A. This dynamic weighting of turbulence indices is repeated hourly for the analysis of turbulence and every 3 hours for the forecast so as to capture the best possible guidance for turbulence over the CONUS. The GTG is only generated from RUC data so it is only available over the CONUS for up to a 12-hour forecast. The GTG also is limited to flight levels above 10,000 ft.

1. GTG Procedure

The GTG process starts by automatically ingesting gridded NWP, which should accurately represent the large-scale features of the atmosphere that may be related to aircraft-scale turbulence. In principle, any high resolution NWP model could be used, but the National Centers for Environmental Prediction's (NCEP's) RUC model was chosen because of the higher effective vertical resolution provided by the isentropic vertical coordinate system at upper levels in the model (Benjamin et al. 2004). The main

task of the GTG forecasting method is to integrate a combination of several separate turbulence diagnostics, and to weight each diagnostic so as to get the best agreement with available observations (i.e., PIREPs). Using a weighted combination of diagnostics for turbulence forecasts is not a new concept, and has been tried in previous studies (i.e., Dutton 1980, Clark et al. 1975, etc.). However, in these previous studies the weights were always static. They were determined on the basis of some set of observations, and once set, the weights never changed. The GTG procedure also obtains weights for a set of diagnostics based on the best fit to observations, but when a sufficient number of PIREPs are available in real time the weights are determined dynamically and updated with every RUC model update. When there is an insufficient number of PIREPs available (i.e., at night when commercial flights are significantly reduced), a set of climatologically derived static weights are used (Sharman et al. 2006). The GTG process involves a six-step procedure as explained in Sharman et al. (2006):

1. A set of ten turbulence diagnostics D_n (e.g., Ellrod index) is computed for upper (>20,000 ft) levels and a separate set of nine diagnostics is computed for middle levels (10,000-20,000 ft). See Appendix A for a list of these diagnostics and their references.

2. D_n is interpolated to common flight levels in increments of 1000 ft and mapped to a common turbulence intensity scale which ranges from 0 (no turbulence) to 1 (extreme turbulence). The scale is designed to match with PIREPs intensities for easy calibration.

3. When using the dynamic weighting strategy, each diagnostic is compared with the available observations (PIREPs) within a time window (currently ±90 min) around the current NWP model time. For each altitude band of interest, a "score" is determined that measures the relative error between the turbulence intensity as predicted by each diagnostic and the available turbulence PIREPs.

4. A set of weights W_n is formed for each diagnostic based on the scoring function from the previous step. Note because the number of PIREPs available at any given time is still a small number, it is not possible to form weights regionally or vertically, so the weights assigned are constant throughout the domain of interest.

5. The weighted diagnostics are combined to form the GTG combination. At this point all the diagnostics have been computed and remapped to the 0–1 scale at the initialization time at each grid point. The GTG diagnostic is then computed for the initialization time as the weighted sum of the diagnostics, or:

$$\mathrm{GTG}(i, j, k) = \sum_n W_n D_n^*(i, j, k)$$

6. The GTG forecasts are formed. Currently forecasts are made out to 12 hours, the maximum forecast duration for the RUC-2. Using a different model, one could extend the forecast time.

Currently, the entire cycle repeats with every major NWP update; for RUC-2 this is every 3 hours. A flow chart showing the GTG processes along with its inputs and outputs is shown in Figure 13. The process is performed separately for middle and upper levels, and the results are merged at the flight level 20,000 foot boundary. When using weights based on climatology, steps 3 and 4 are bypassed and a constant set of weights are used for the analysis time and all forecast times. The procedure for deriving these climatology-based or default weights, along with their current values is given in Sharman et al. (2006). An example of the GTG product is shown in Figure 14 and the GTG product is available at:

(a) http://adds.aviationweather.gov/turbulence/ or,

(b) http://aviationweather.gov/exp/gtg/mdt.shtml.

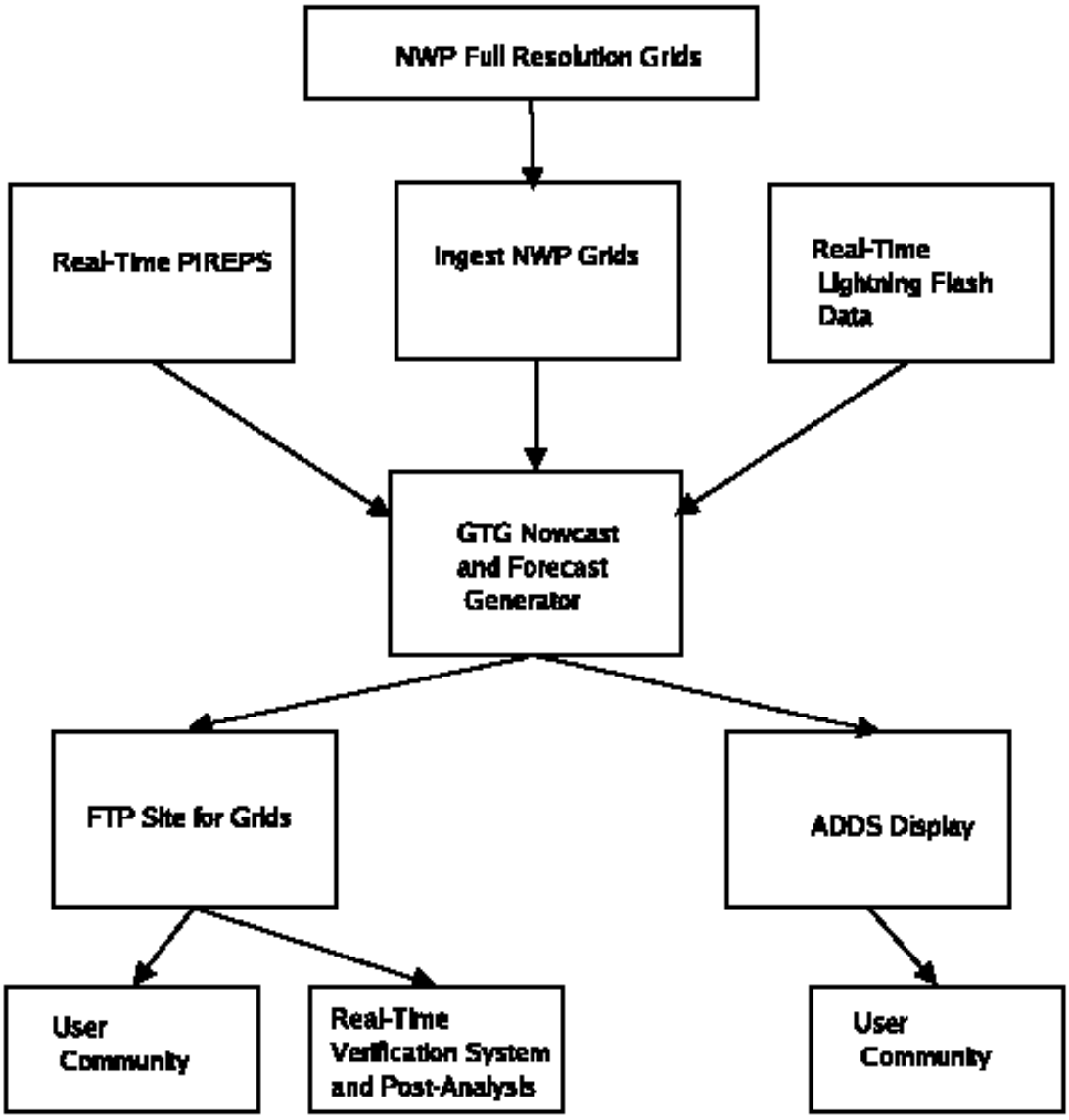

Figure 13. The GTG forecasting system and its inputs and outputs from Sharman et al. (2006).

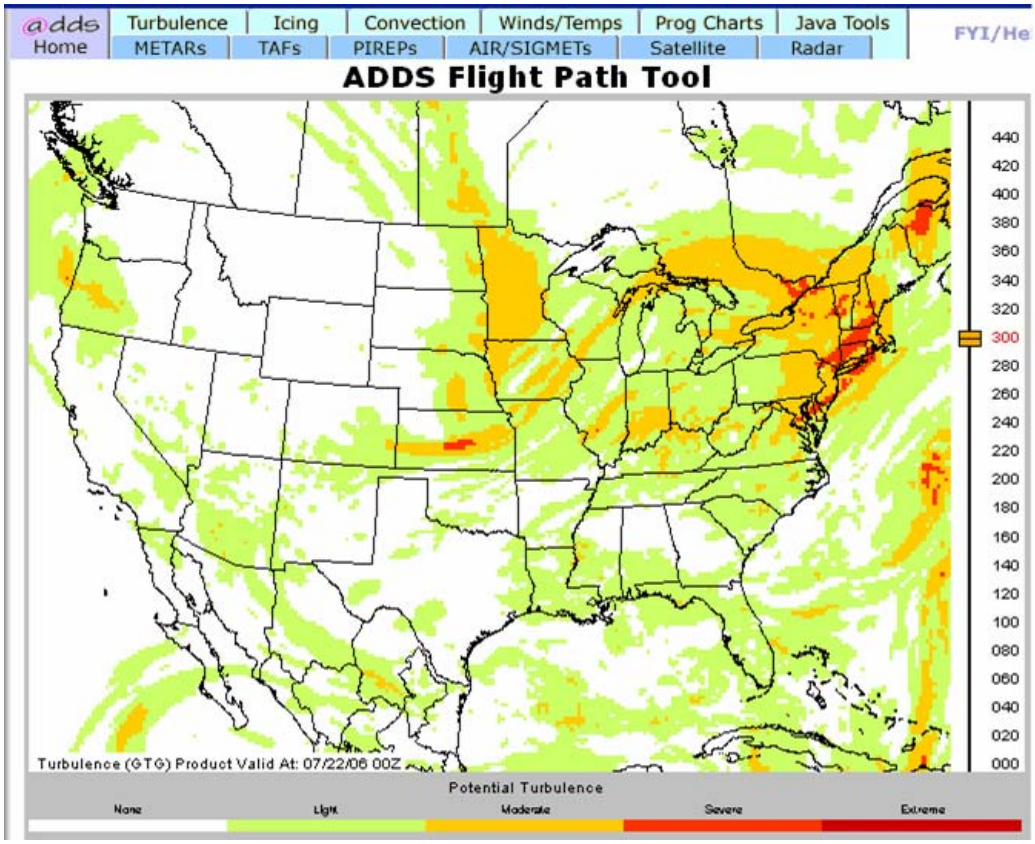

Figure 14. Example of the GTG product from the AWC for FL 3000 ft valid 0000 GMT, 22 July 2006 and produced at 1800 GMT, 21 July 2006.

A vast assortment of testing and verification of the GTG has been in progress since its development. Several objective and subjective tests have been done on the procedure and it has been found to be quite skillful. Sharman et al. (2006) describes some of the rigorous testing and verification done on the GTG recently and found the overall performance of the GTG "to be skillful enough to provide useful information to meteorologists and dispatchers for strategic planning for turbulence avoidance." Sharman et al. (2006) also concludes the GTG combination provides superior guidance than any single turbulence diagnostic in detecting CAT.

2. GTG Shortcomings

Even though the GTG does appear to be the superior method for automated turbulence forecasting, the ability to provide still more accurate aircraft-scale turbulence nowcasts and forecasts is hampered by several fundamental difficulties, which are detailed below.

a. Resolution

The resolution of current NWP models (several 10s of km) is still about two orders of magnitude too coarse to resolve aircraft-scale turbulence (roughly 100s of m). Therefore, aircraft-scale turbulence diagnoses and predictions must be based on resolvable- (by the NWP) scale features.

b. Cascading Energy Assumptions

The performance of turbulence diagnostics is hampered by our current lack of understanding of the linkage between NWP observable-scale features and aircraft-scale turbulence. An implicit assumption underlying the use of all these diagnostics is turbulence-generating mechanisms have their origin at resolvable scales and that energy cascades down to aircraft scales, but it is unclear what the exact cascade mechanism is. Recent high-resolution simulations by Lane et al. (2004, 2005) indicate the linkage is related at least in some cases to gravity wave production by features such as upper-level fronts and convection, and subsequent breakdown of the waves into turbulence (Sharman et al 2006).

c. PIREP Errors

The GTG system uses PIREPs for weighting, tuning and verification. But as discussed previously, an individual PIREP is subject to spatial, temporal, and intensity misrepresentations.

The quantitative automated in-situ turbulence reporting system should eliminate most of the uncertainty associated with PIREPs but will still not alleviate the night-time underreporting bias. The amount of data will be vastly increased, since the turbulence is reported every minute in flight. This will provide a much more complete mapping of the turbulent state of the atmosphere (at least at upper levels), and will allow GTG to fit that state much more precisely than has been possible using the current set of scattered PIREPs. Just as the accuracy of upper-level winds in NWP models has increased with the use of Aircraft Communications Addressing and Reporting System wind data (e.g., Schwartz et al. 2000), the GTG upper-level forecasts should become more accurate with the ingest of in-situ data (Sharman et al 2006).

3. GTG Evaluation

During the winter seasons of 2000 thru 2003 operational forecasters at the AWC performed a subjective evaluation of the forecasting capability of the GTG (Mahoney et al. 2002). The evaluation was funded by the FAA Aviation Weather Research Program (AWRP) Turbulence Product Development Team (PDT) (Mahoney et al. 2002). These subjective evaluations were designed to supplement the objective verification being done by Brown et al. (2002) and to identify strengths and weaknesses of the GTG from the operational forecaster's perspective. The versions of the GTG evaluated focused on CAT above 20,000 feet and consequently, the evaluations were limited to the atmosphere above 20,000 feet.

A detailed description of the evaluation process can be found in Mahoney et al. (2000, 2001, 2002). To summarize, the forecasters compared displays from the GTG to their assessment of the location of CAT, its strength, and its source (e.g., jet stream, mountain waves, etc.) every day. Forecasters were allowed to use all available sources of data and observations [e.g., PIREPs, satellite data, model forecasts] to evaluate these CAT features. Additionally, the forecasters formulated a brief discussion of: the weather situation of the day, the character of the turbulence, and an assessment of the GTG performance.

For the 2002 evaluation, seven AWC forecasters completed 165 evaluation forms from 9 February thru 9 April 2002. According to the forecasters' evaluation, more than half of turbulence events were caused by the jet stream and about a third were from unidentified causes. Figure 15 shows the forecaster identified cause of turbulence for all turbulence events identified for the 2000 thru 2002 winters over CONUS while Figure 16 shows the individual yearly results.

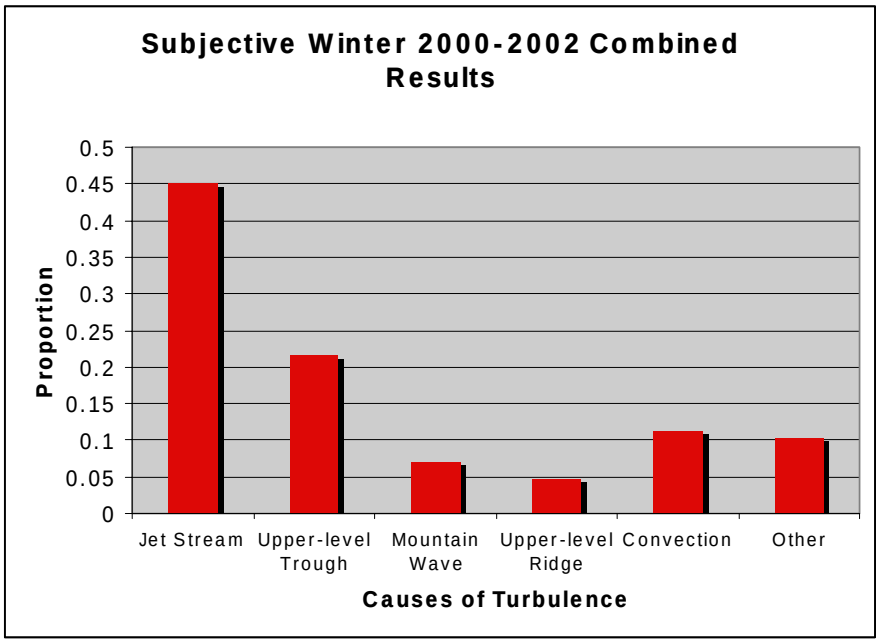

Figure 15. Forecaster identified cause of turbulence for winters of 2000 thru 2002, as reported in Mahoney et. al. (2000-2002).

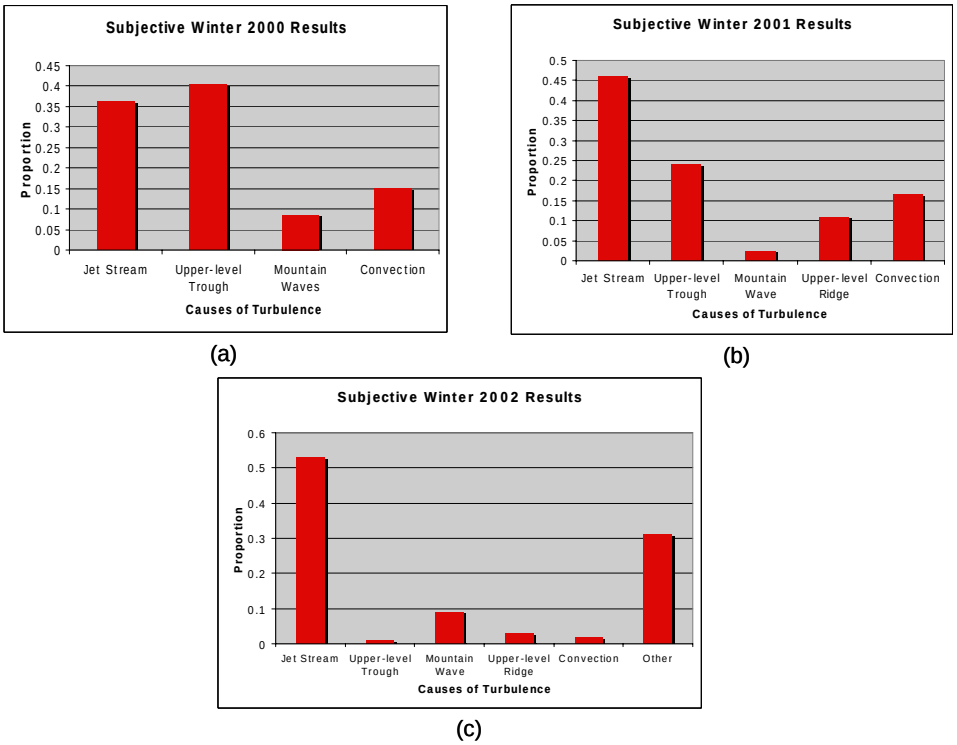

Figure 16. Same as Figure 15 except yearly results shown for: (a) 2000, (b) 2001, and (c) 2002.

In 2003 the AWC forecasters were asked to evaluate the GTG based on the predicted turbulence intensity, area of coverage, and altitude. They were also asked to assess the overall performance of the GTG, including all of the above factors, as excellent, good, fair, or poor with results shown in Figure 17. In the fair and poor cases there was a tendency for the turbulence prediction to be too broad in both, area of coverage and the altitude. According to the AWC forecasters, the GTG generally rated better for regions east of the Rockies.

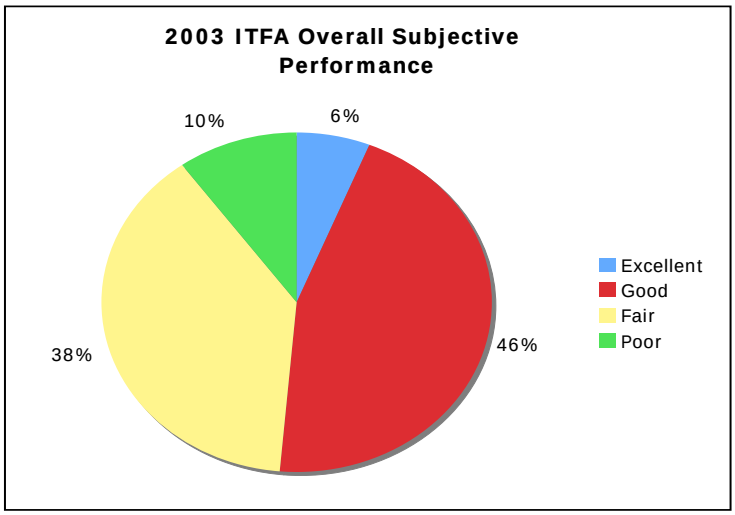

Figure 17. AWC forecasters' assessment of GTG overall performance considering the area, altitude, and intensity for 23 January thru 1 April 2003 (from Mahoney et al. 2003).

As mentioned previously, there is also a significant effort in progress to evaluate the GTG objectively. An important part of the winter 2003 GTG evaluation was to compare the results of the forecasters' subjective evaluation with the objective verification scores. There was a positive correlation between the objective verification numbers and the forecasters' assessment for days where there turbulence is very active. That is, if the forecasters said the GTG performed well, the objective verification numbers supported this. However when all times and all regions were considered the correlation between objective and subjective assessments was weaker (Mahoney et al. 2003). Low activity days sometimes had objective numbers that suggested very different GTG performance than the forecasters indicated (Mahoney et al. 2003). Conclusions on this subject were hard to make due to very nature of turbulence verification techniques used in the objective evaluations. Furthermore, the objective scores are numerical and

the subjective overall performance rating is a qualitative assessment, and therefore, the subjective assessments were converted to a numerical scale where additional error could have been injected into the results.

The GTG algorithm is designed primarily for CAT and mountain wave-induced turbulence. It is not exclusively designed to denote regions of severe turbulence but a broad cross section of turbulence intensities including light, moderate, and severe (Kaplan et al. 2004). This can be a problem because most severe aviation turbulence encounters that result in aircraft damage or human injuries are closely associated with severe outbreaks of turbulence caused by deep, moist convection.

4. GTG and OWS FITL Comparison

The GTG gives a much more detailed forecast than the AF OWS hand drawn FITL product can give as shown in Figure 18. OWS FITL forecasts tend to over-forecast turbulence as noted previously. Some over-forecasting of turbulence is unavoidable by the nature of the phenomena itself and by the requirement of hand drawing such a complex three-dimensional event on a chart. But this does not account for the persistent over forecasting of turbulence categories by OWS FITL products as noted by Schrumpf (2006): "15th OWS FITL products are overly pessimistic by at least one-half an intensity category across the board, as evidenced by observations of nearly 50,000 flight missions per year at Tanker Airlift Control Center Weather Operations." The GTG forecasts do address this problem and forecast light turbulence in broader areas, with moderate and the occasional severe turbulence forecast made in much more confined areas than the OWS FITL forecasts. OWS FITL forecasters don't forecast a light turbulence category; forecasts are only drawn for moderate or greater. The moderate turbulence forecasts are often too broad in the horizontal and the vertical as shown in Figure 18.

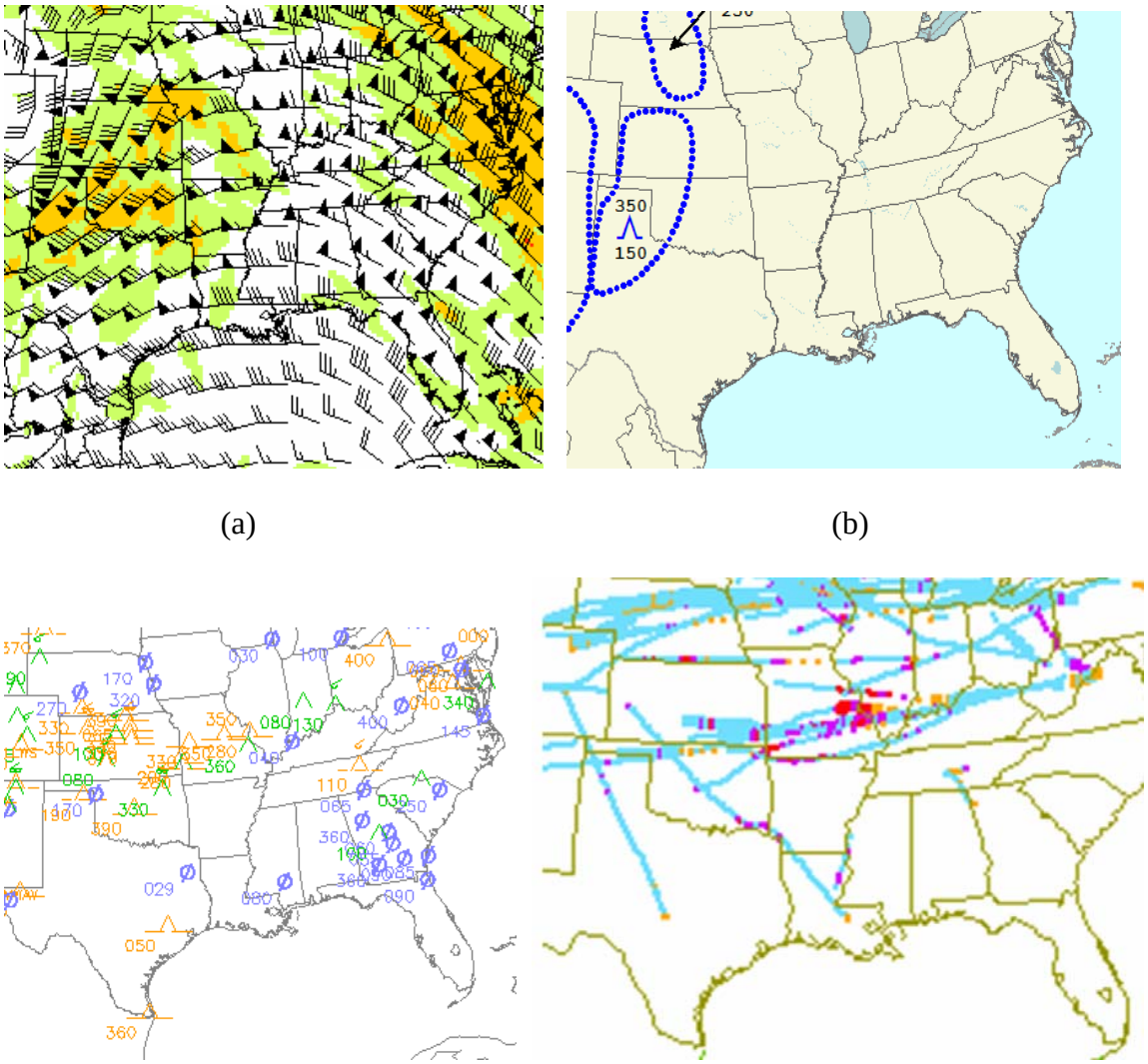

(a) (b)

(c) (d)

Figure 18. (a) and (b) are turbulence forecasts for 1800 GMT, 6 April 2006 while (c) and (d) are turbulence observations for 1700-1900 GMT, 6 April 2006. (a) is the GTG product with green indicating probable light turbulence, and orange probable moderate turbulence with the 30k ft forecasted winds overlaying the turbulence forecasts. (b) is the AF OWS turbulence forecast product with areas inside of the blue indicating predicted moderate turbulence areas. In (c) are the PIREPs observations from the AWC with green representing light turbulence, and orange open triangles representing moderate turbulence. In (d) are the EDR observations from the ESRL/GSD with light blue indicating null report, purple-light turbulence, and red-moderate turbulence.

Notice in Figure 18 the very large regions of moderate forecasted turbulence in the OWS FITL product versus the very specific and localized areas of moderate

forecasted turbulence in the GTG product. Also note the "patchiness" the GTG is able to capture with the automated grid forecasts which more closely represents the "patchiness" of the observed turbulence. Over Kansas and Oklahoma both the GTG and the OWS forecasters verify well, but the OWS forecasters miss the turbulence over Missouri all together, while the GTG does a good job in this region and the same is true over Virginia. In Figure 18 there is no elevation given by the GTG forecast. The GTG makes a different forecast for all elevations above 10,000 ft. That is, the GTG has no product like the OWS FITL product which shows a complete horizontal and vertical forecast for turbulence. This is both an advantage and a disadvantage of the GTG. The disadvantage is that the user must view a single elevation at a time. The advantage is the forecasts are much easier to read then the OWS FITL forecasts since they only show one elevation and the fact that the GTG breaks it down by elevation allows the forecaster to make again, more detailed, and localized forecasts. Figure 19 shows an example of how an OWS FITL forecast can become cluttered and confusing on an active turbulence day.

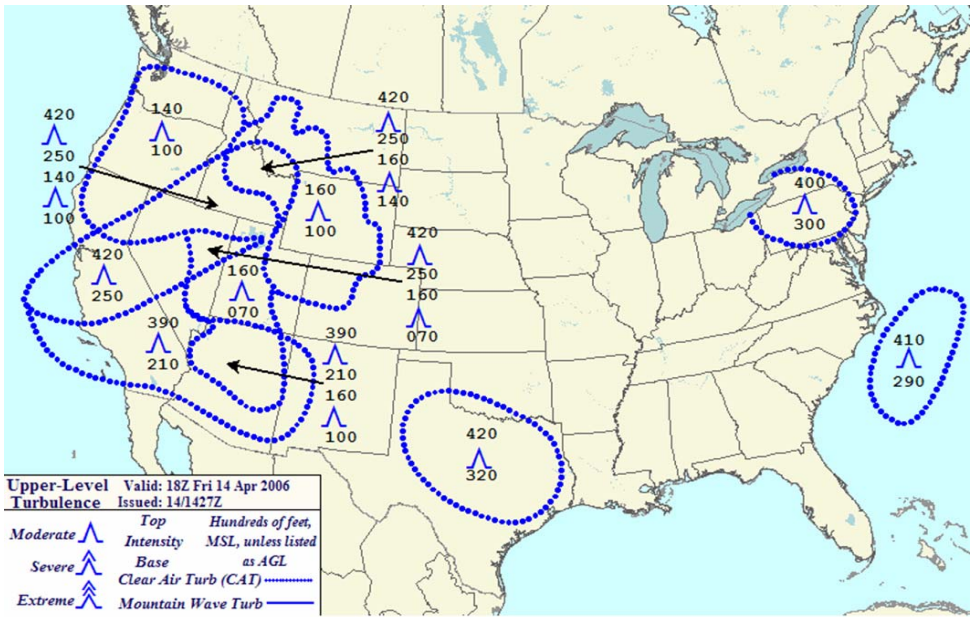

Figure 19. OWS FITL forecast product for an active turbulence day, 1800 GMT, 14 April 2006. On very active turbulence days OWS FITL forecasts can be very confusing and become cluttered as forecasters try to capture the various vertical variations in the turbulence.

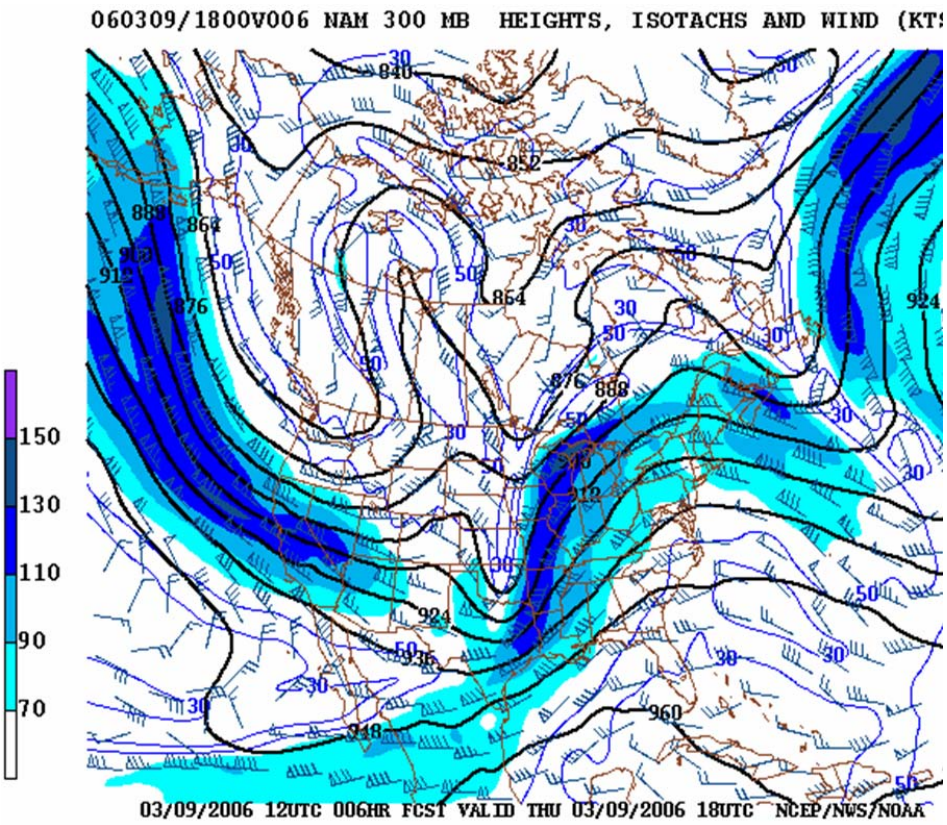

Figure 20. NWS produced 1800 GMT 300mb wind (kts) forecast for 1800 GMT, 9 March 2006. Note the strong north-south jet axis over the middle of the US.

Figure 20 shows the NWS 6 hour forecast for 300mb winds (kts) for 1800 GMT, 9 March 2006. The area of interest is the strong north-south jet axis over the middle of the CONUS spanning from eastern Texas to the Great Lakes. Figure 21 shows a typical GTG forecast for the same time period as Figure 20, where the forecaster would want to consider at least three different vertical levels, 25k ft, 30k ft, and 35k ft. As shown in Figure 21 there is a significant difference in the area and intensity of the forecasted turbulence at each different vertical level.

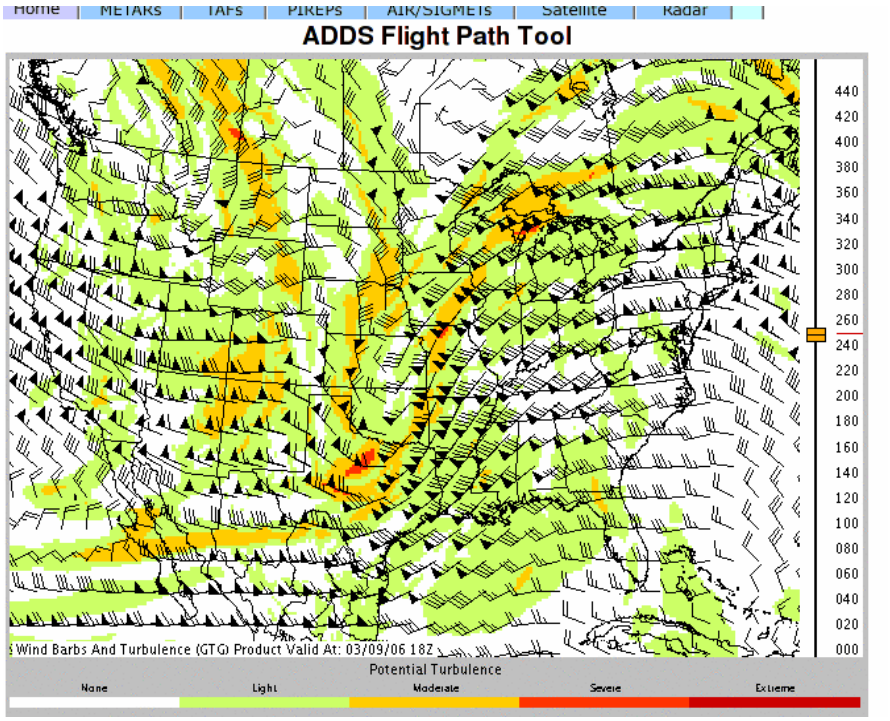
Home
METARs
TAFs
PIREPs
AIR/SIGMETs
Satellite
Radar
ADDS Flight Path Tool
440
420
400
380
360
340
320
300
280
260
240
220
200
180
160
140
120
100
080
060
040
020
000
Wind Barbs And Turbulence (GTG) Product Valid At: 03/09/06 18Z
Potential Turbulence
None
Light
Moderate
Severe
Extreme

(a)

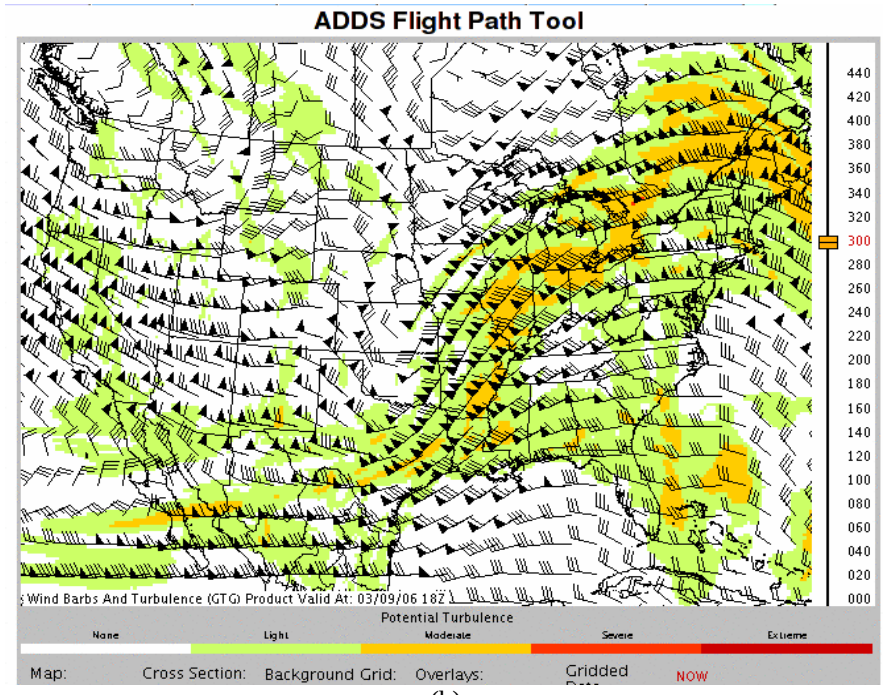
ADDS Flight Path Tool
440
420
400
380
360
340
320
300
280
260
240
220
200
180
160
140
120
100
080
060
040
020
000
Wind Barbs And Turbulence (GTG) Product Valid At: 03/09/06 18Z
Potential Turbulence
None
Light
Moderate
Severe
Extreme
Map:
Cross Section:
Background Grid:
Overlays:
Gridded
NOW

(b)

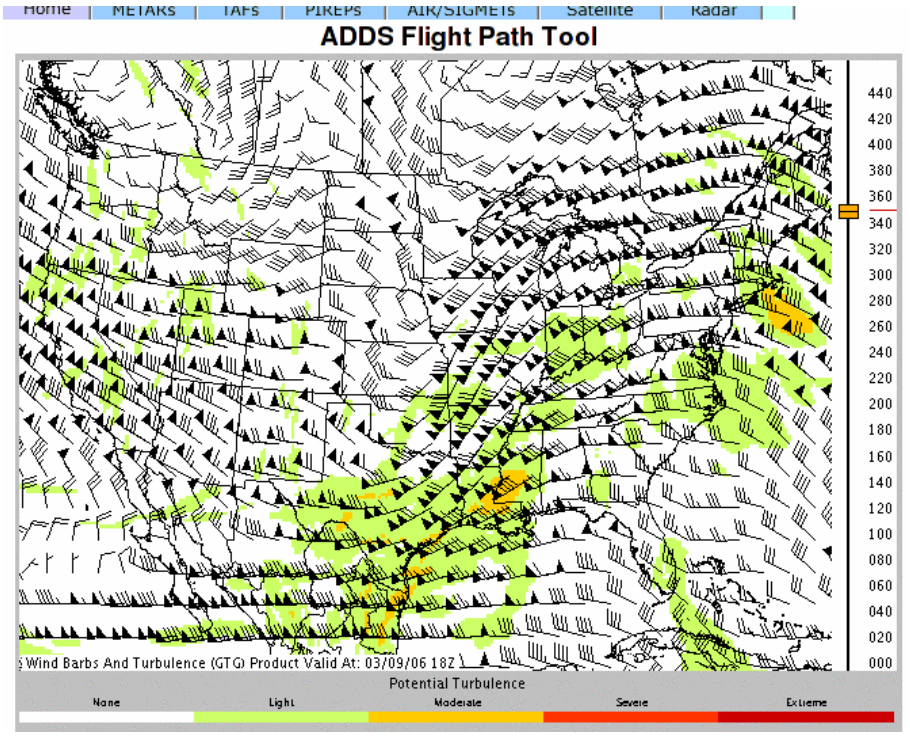

(c)

Figure 21. GTG forecasts for 1800 GMT, 9 March 2006 by vertical level, (a) 25k ft, (b) 30k ft, and (c) 35k ft. Note the significant variation in forecasted turbulence intensity between the levels.

Figure 22 shows the OWS FITL product for the same time period. The OWS forecast agrees well with the horizontal coverage of turbulence near the area of interest, however, the vertical forecast by the OWS forecasters is much broader and more general. From Missouri to the Great Lakes, the forecast is for moderate turbulence from 24,000 to 36,000 feet, a span of 12,000 feet. That span entirely covers the 3 different vertical levels shown above for the GTG forecast and then some. From Texas to Missouri the vertical span of moderate turbulence forecasted is 20,000 feet. Outside the area of interest the horizontal span of moderate turbulence forecasted covers nearly all of the Ohio Valley and the Southeast with a vertical span of 10,000 feet.

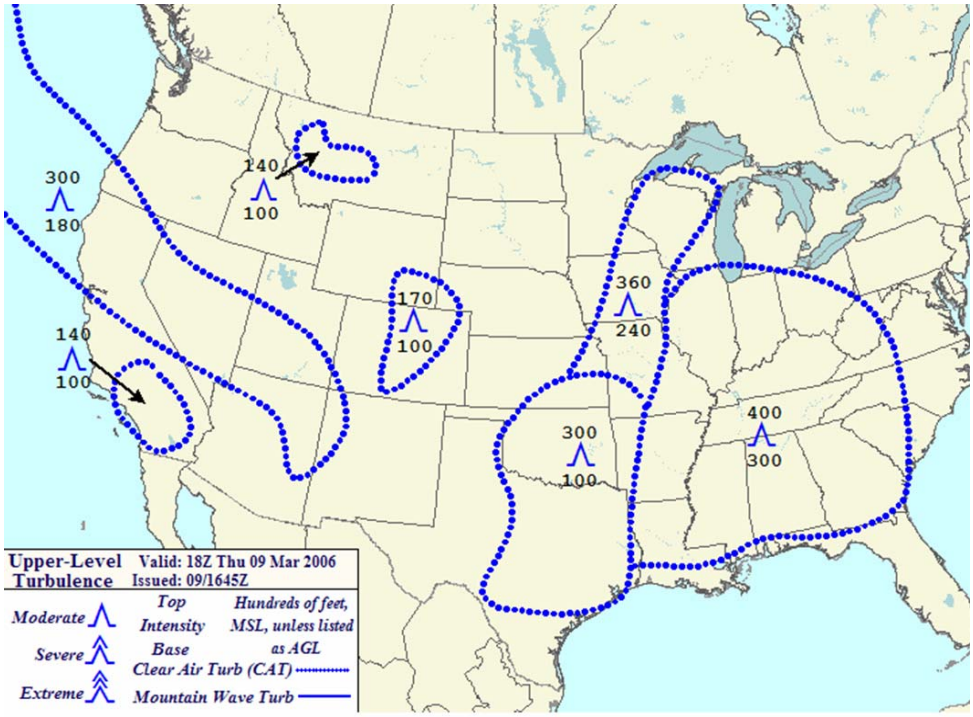

Figure 22. The OWS FITL product for 1800 GMT, 9 March 2006. Notice that the forecast for the north-south jet region is for moderate turbulence spanning 12,000 feet in the vertical and covers all 3 levels of the GTG forecast shown in Figure 21. South of the jet the vertical forecast for moderate turbulence spans 20,000 feet.

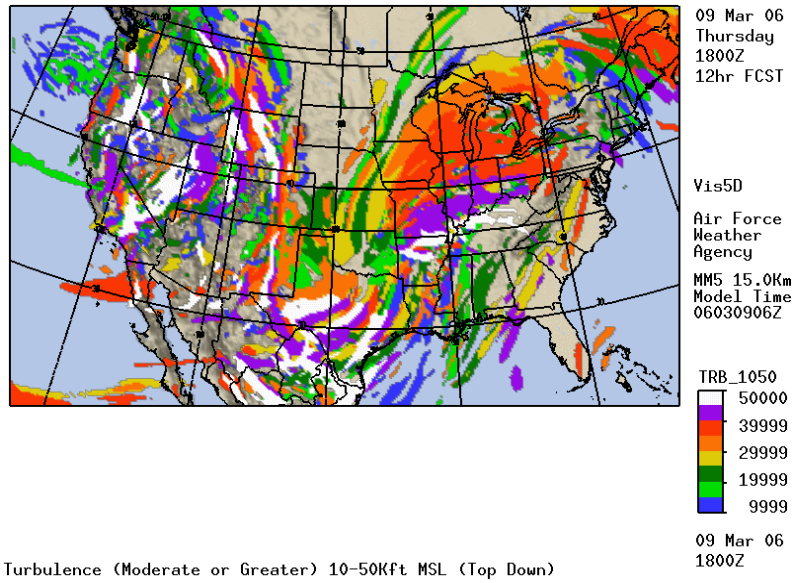

Figure 23. The AFWA MM5 upper-level turbulence forecast for 1800 GMT, 9 March 2006 gives some indication of why the OWS forecast is so broad. Only moderate or greater turbulence is forecasted above. On this day, it is predicted that nearly all of CONUS will have moderate or greater turbulence at some level.

Figure 23 shows the AFWA strategic-level turbulence forecast. Vertical variations are shown by the different colors as indicated. The fact that the OWS forecasters use this strategic-level forecast when making their OWS FITL product may explain why the forecast was so broad and general. Figure 24 shows the EDR observations for this time period to give the reader some indication of how these forecasts verified. The vertical level is not displayed in the figure but is easily accessible from the online java-based display. For this case all EDR observations of moderate turbulence were between 32,000 and 39,000 feet. The reader can see that moderate turbulence in the area of interest does exist but in very specific areas, and that from a broader perspective, most of the area of interest is actually covered by null or light turbulence reports. From these observations it seems that the GTG forecast conveys to the forecaster much more valuable information than the OWS FITL forecast or the AFWA MM5 forecast does. The OWS FITL product does convey good information; the turbulence observed is in the turbulence forecasted areas of the OWS FITL forecast. However, mission planners may take a look at the OWS FITL forecast and avoid all regions forecasted which, as the EDR observations show, is not necessary and represents the most challenging problem OWS turbulence forecasters have; effectively minimizing the false alarm ratio for turbulence forecasts while not risking the safety of AF personnel and equipment by under-forecasting turbulence.

Figure 24. The EDR observations for 1700-1900 GMT, 9 March 2006 from the ESRL/GSD (2006). The vertical level of the observation can be viewed on the website by clicking on the observation but are not shown here. Light blue indicates null turbulence, purple-light turbulence, red-moderate turbulence, and orange-no data.

The previous figures highlight some of the advantages that an automated forecast like the GTG has over the traditional OWS FITL forecasts and it has been shown that the GTG is currently the most effective automated turbulence forecast available. The GTG contains all the best developed automated turbulence diagnostics in the past 40 years. These diagnostics effectively automate the process of identifying the synoptic conditions favorable for turbulence development as described in Section C of this chapter. Furthermore, the GTG calibrates itself every three hours with PIREPs observations to make sure it's using the best diagnostics for the current weather environment. With the inclusion of the EDR observations into the GTG system in the near future and for all of the above reasons, it is clear that the GTG should be utilized by OWS forecasters and all aviation weather forecasters for forecasting upper-level turbulence.

THIS PAGE INTENTIONALLY LEFT BLANK

IV. TURBULENCE FORECAST APPROACH

This chapter outlines a suggested forecast approach for AFWA OWS turbulence forecasters or any newly trained turbulence forecaster. As is the case with all forecasting, a good forecast starts with a good analysis. The forecaster must first understand the current and past conditions of the atmosphere before being able to predict the future state of the atmosphere. A complete synoptic analysis which includes recognizing distinct synoptic patterns and features which favor turbulent conditions is presented in Section A for each of the types of turbulence. Observations, discussed in Section B, should be used to verify patterns and favorable areas identified in the forecaster's analysis, and to alert the forecaster of all reported turbulent areas. Section C discusses the turbulence diagnostics and how they should be used in the turbulence forecast process. The use of models and the GTG will be discussed in Section D. Finally, Section E will summarize the overall suggested turbulence forecast approach.

A. SYNOPTIC ANALYSIS

In Chapter II three types of turbulence were defined; thermal turbulence, CAT, and mountain wave turbulence. Recall that atmospheric turbulence was classified into the above categories because each type of turbulence is caused by different physical processes which were discussed in Chapter II. It is important that, when beginning the turbulence forecast process, the forecaster separate the different types of turbulence and analyze/forecast each type individually. Once this is done, the forecaster can then combine the three types together on one chart for the finished forecast product. Bearing this in mind, the following subsections are broken down by the type of turbulence, similar to the approach the forecaster should take. That is, the forecaster should start with an analysis of thermal turbulence, then CAT, and finally mountain wave turbulence. For the different types of turbulence, the forecaster should take different approaches, looking at different analyses and data and these will be described below.

1. Thermal Turbulence

Recall from Chapter II that surface heating can generate turbulent conditions. As solar radiation heats the surface, the air above it is warmed by contact. Warmer air is less dense, and "bubbles" of warm air rise upward as updrafts. Uneven surface heating, and

the cooling of rising air, allows for areas of downdrafts as well. Characteristics of boundary layer turbulence include:

- The maximum occurrence is between late morning and late afternoon.
- The impact on flight operations is greatest during terminal approach and departure and during low-level flights.
- Moderate turbulence may occur in hot, arid regions, as the result of irregular convective currents from intense surface heating (AFWA TN 98-002, 2005).

When vertical motions break through the boundary layer they can generate cumulus clouds that can grow to great heights as thunderstorms (AFWA TN 98-002, 2005). Within these thunderstorms, intense updrafts can exist alongside intense downdrafts. This is another prime area for turbulence, appropriately referred to as convective turbulence. Convective turbulence is often found in and around thunderstorms, especially strong and severe storms where deep convection is persistent. The stronger the convection becomes, the stronger the turbulence will be. While moderate or severe turbulence can be found anywhere within the storm, including the clear air along its outer edges, the highest probability of turbulence is found in the storm core (AFWA TN 98-002, 2005).

The early morning sounding from Davenport, Iowa for 1200 GMT, 10 August 2006 shown in Figure 25 exemplifies a convective regime sounding which should alert the forecaster to possible convective turbulence. The high value of the Convective Available Potential Energy (CAPE) as well as the low value of the Lifted Index indicates the weak atmospheric stability in which strong updrafts and downdrafts can occur and cause turbulence. A stronger CAPE will result in more energy being available to support stronger updrafts and potentially violent convection and thunderstorms. The sounding reveals an important low-level inversion which will temporarily inhibit convection. But as the day progresses and the surface is heated by solar energy the inversion will dissipate in which case all of the built up CAPE can be realized and intense convection can develop. Therefore, a strong low-level inversion can allow the CAPE to build up creating a greater potential for strong convection, but at the same time if the inversion becomes too strong, the boundary layer may never warm enough throughout the day to “break” the

inversion and realize the CAPE. EDR observations over Iowa for this day in August confirm that turbulence was present over the Davenport region and surrounding areas. Radar data also showed convective activity in this region.

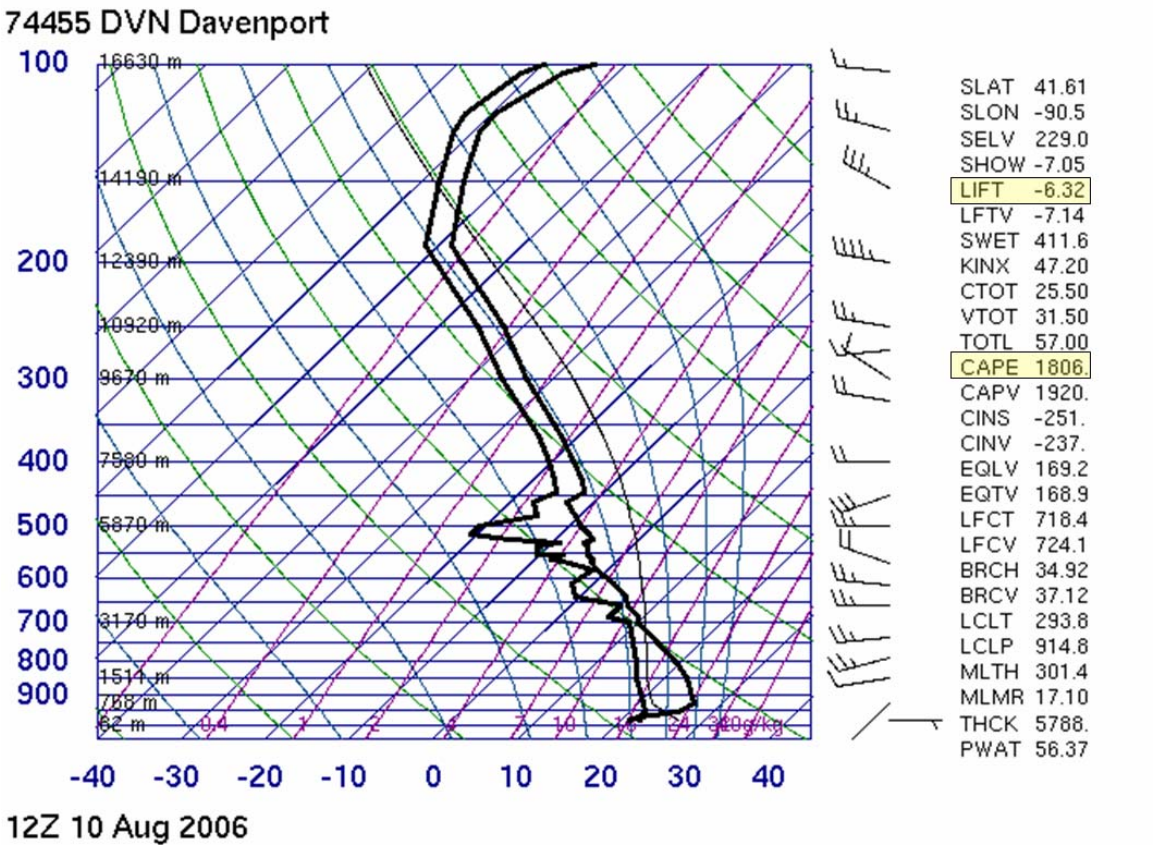

Figure 25. Atmospheric sounding for Davenport, Iowa on at 1200 GMT, 10 August 2006. The sounding has a CAPE of 1806 J/kg and a Lifted Index of -6, indicating conditions are favorable for significant convection to develop.

Significant downdrafts can exist beneath the convective cloud base, usually associated with areas of heavy rain and generally the areas of highest water concentration are the areas of heaviest turbulence (AWS TR/105-39, 1949). Thus, the forecaster should expect significant turbulence where the most intense rain columns are seen on the radar (AWS TR/105-39, 1949). Potentially hazardous turbulence is present in all thunderstorms, and a severe thunderstorm can severely damage an aircraft (AWS FM/83-002, 1983). Turbulence has been encountered several thousand feet above and 20 miles laterally from a severe storm (AWS FM/83-002, 1983). A low-level turbulent area is often associated with the shear zone in the gust front of a strong thunderstorm. A roll

cloud on the leading edge of a storm marks the top of the eddies in this shear and it signifies an extremely turbulent zone as shown in Figure 26. Gust fronts extend 10 to 20 miles away from the thunderstorm with extreme turbulence-causing wind shears existing behind and across the gust front (AWS FM/83-002, 1983).

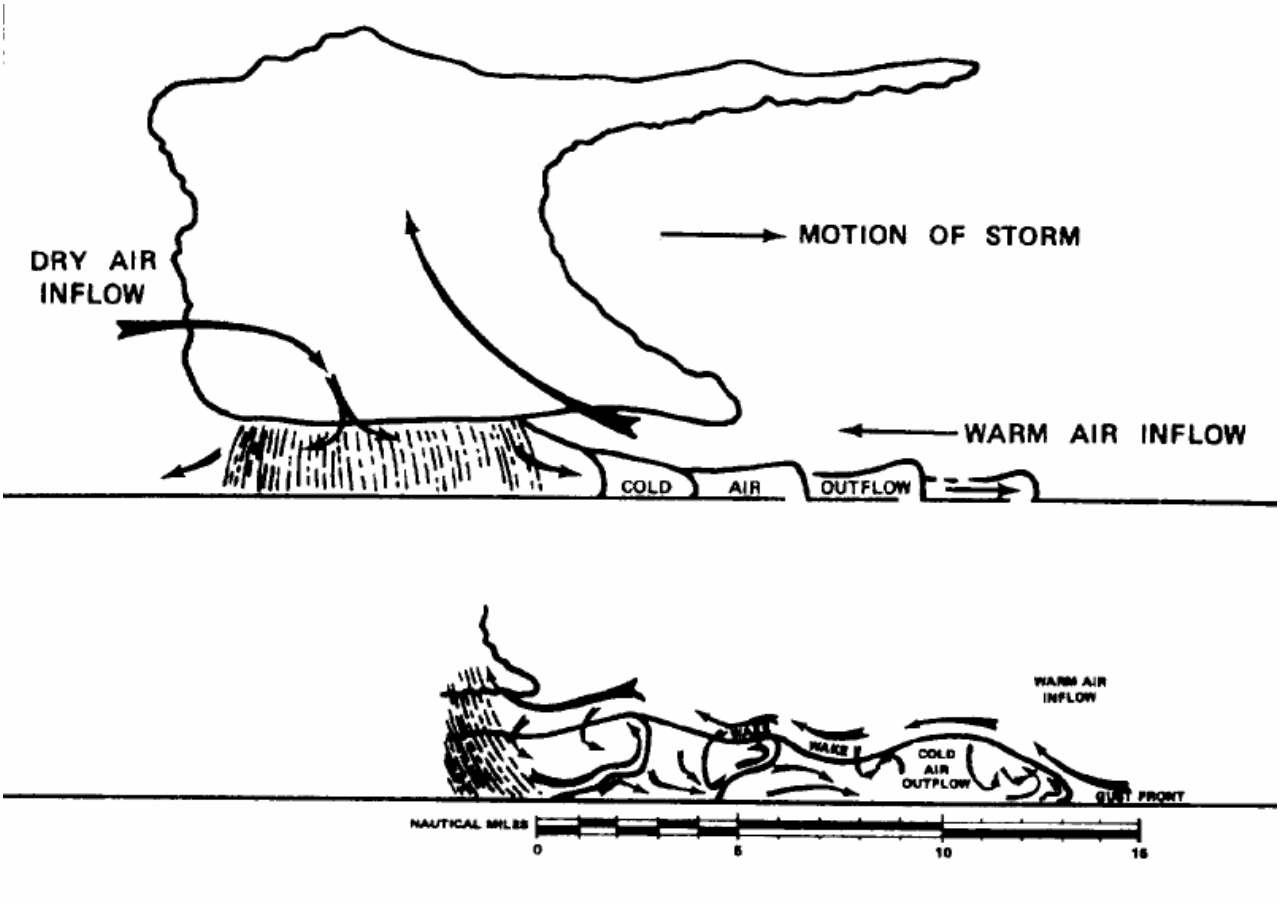

Figure 26. Typical thunderstorm with up/downdrafts and outflow shown (from AWS FM/83-002 1983). The eddies shown in the outflow region signify an extremely turbulent zone.

A common feature of a capped boundary layer where a strong inversion exists aloft is significant low-level wind shear (LLWS). In a capped boundary layer turbulence may not exist at the surface and boundary layer where the atmosphere is stable, but as aviators cross the interface from the boundary layer to the free atmosphere through the inversion, they will likely experience LLWS which is very similar to turbulence and can have the same damaging effects.

Turbulence forecasters should expect turbulence to exist in and surrounding any significant convective regions and should utilize tools like the radar, visible and IR satellite imagery, and atmospheric soundings to identify areas of strong convection. For more guidance on convective weather see Chapter 3 of AFWA TN 98-002 (2005).

2. CAT

a. Jet Identification

When performing an analysis for CAT the suggested starting point is an upper-level chart such as the 200mb, 250mb, or 300mb chart. Jet streams can almost always be identified in these upper-level charts. Normally the polar jet stream is found on the 300mb chart (most prominent in the winter for midlatitude regions), while the subtropical jet can best be seen in the 200mb chart (most prominent in the summer for midlatitude regions). When forecasting for tropical regions, the 200mb chart is preferred and similarly, for polar regions the 300mb chart is preferred. Figure 27 is a typical 300mb chart for 1800 GMT, 9 March 2006 showing 300mb heights and isotachs. On this day there was a very strong jet located over the eastern Midwest region making the jet identification quite simple. Figure 28 shows the EDR turbulence observations over a period of 2 hours (1700-1900 GMT) on top of the same chart as in Figure 27.

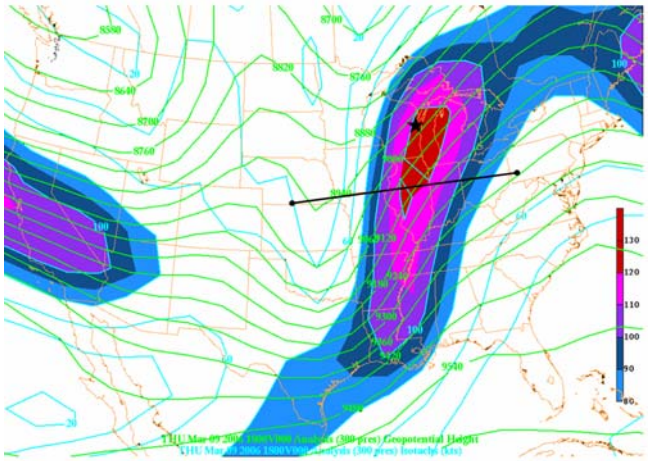

Figure 27. 300mb heights (m; green solid lines) and isotachs (kts; blue solid lines) are shown here for 1800 GMT, 9 March 2006. Isotachs greater than 80 are filled according to color scale in bottom right corner. A strong north-south oriented jet exists from the Great Lakes down to Louisiana. The black line shows the area used for the cross-section figures in this section and the black star indicates the location of the sounding shown in Figure 30.

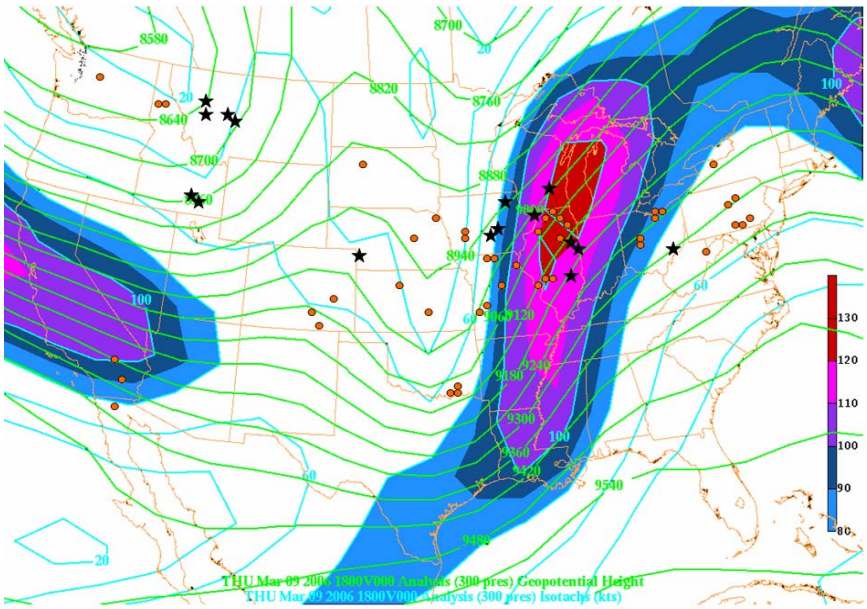

Figure 28. Same as in Figure 27 except with EDR observations shown for 1700-1900 GMT, 9 March 2006. The black stars are observations of moderate turbulence (0.25 EDR category), and the orange circles are observations of light-moderate turbulence (0.15 median/0.25 peak EDR category). The height of the moderate turbulence observations in the jet region range from 32,000 ft (275mb) to 39,000 ft (197mb) while all observations shown above are between 20,000 and 40,000 feet.

The CAT analysis begins with jet identification because the jet stream exhibits nearly all of the factors (i.e., strong thermal gradients, strong vertical wind shear, and strong horizontal wind shear) that have been associated with turbulence and that have been discussed in the previous chapters of this thesis. Additionally, the stronger the jet, the more likely turbulence will exist in its proximity. Jet entrance regions and exit regions are particularly conducive for turbulence as well as confluent jet streams. When two jet streams are within 300 nm of each other there is a high probability of CAT in the confluent zone between the jets (Lee et al. 1984). The northern jet stream is accompanied by colder temperatures and thus is usually at a lower altitude than the southern jet stream and will cut underneath the southern jet stream. This will cause an increase in static stability and strong vertical directional and speed shears in the confluent zone and a rapid backing of the wind with height between the levels of the two jets.

b. Jet Core

In Figure 27 the jet core is over Lake Michigan, Wisconsin, and Illinois and is highlighted in red with winds exceeding 130 knots. Jet cores are very favorable areas for CAT and should be investigated next. The environment accompanying the jet core includes very strong winds with weaker surrounding winds in the vertical and horizontal, and consequently is a prime location for strong vertical and horizontal wind shear. Figure 29 shows the jet core from a cross-section view of the jet in Figure 27 and comes from the global GFS model analysis with one-degree resolution. Cross sections from mesoscale models with enhanced horizontal and vertical resolution can also depict the intense shears associated with the CAT environment. It is suggested that the forecaster identify jet cores after identifying the upper-level flow and jet streams. The position of the jet core is also very important, especially with respect to curvature which will be discussed later (Section d.).

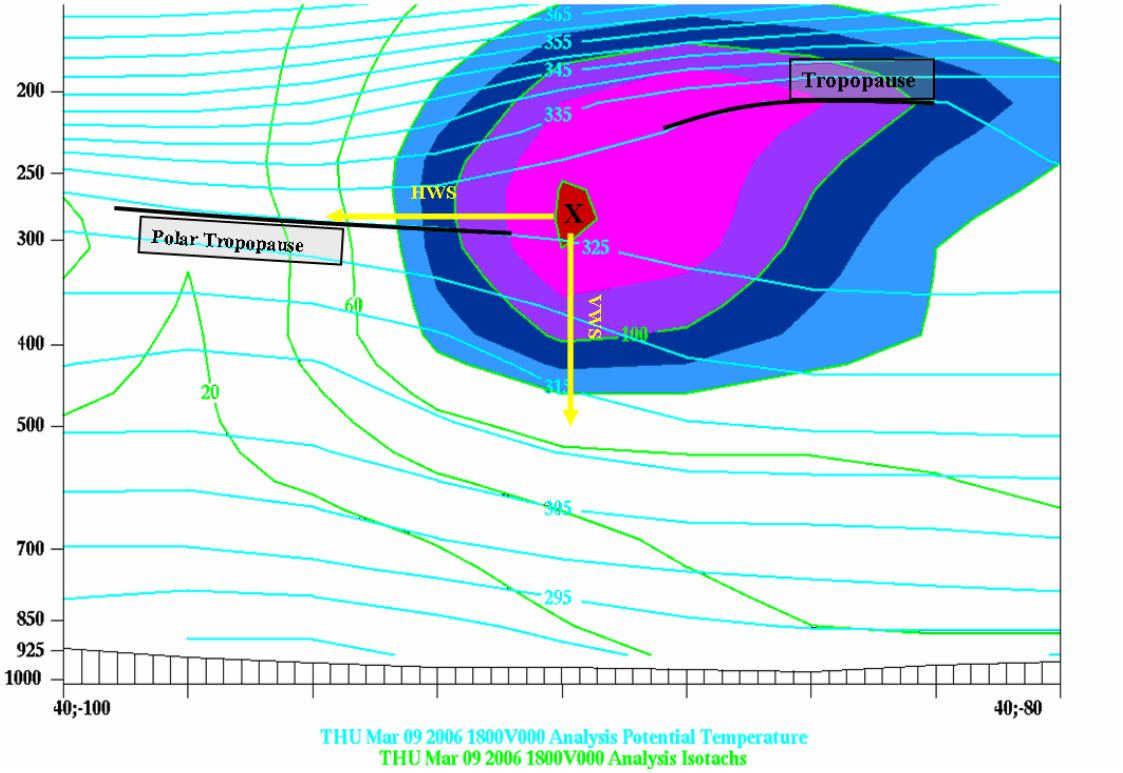

Figure 29. Cross-section from Iowa to Ohio across the jet showing isotachs (kts; solid green lines) and potential temperature (˚K; solid light blue lines) for 1800 GMT, 9 March 2006. The jet is shown with the filled-in isotachs and the jet core is indicated by the "X". Note the strong horizontal and vertical wind shear through the jet region as shown by the yellow arrows.

c. VWS & HWS

The cross-section in Figure 29 is a good example of how vertical wind shear (VWS) can be identified as well as horizontal wind shear (HWS). Cross-sections are an extremely valuable tool for forecasting turbulence and for aviation forecasting in general, especially when using high resolution mesoscale models. Drawing a horizontal line out from the jet core to the west (left) as shown by the HWS yellow arrow in Figure 29, the forecaster can see that there is significant horizontal speed shear in the upper troposphere in this region as winds decrease from 120 knots in the core to 80 knots about 200km to the west. Drawing a vertical line straight down form the jet core as shown by the VWS yellow arrow in Figure 29, the forecaster can quickly see that for that location, approximately 40˚N; 89.8˚W, there is significant vertical speed shear also. At 250mb the wind is approximately 120 knots, but decreases to 60 knots at 500mb. At the surface, the winds are under 20 knots. Another useful tool for identifying vertical wind shear (speed and directional), as well as convective turbulence, is the atmospheric sounding. Figure 30 below is the sounding for Green Bay, WI (shown as the black star in Figure 27) and illustrates how vertical wind shear can be identified using a sounding. It is important to note the smoothing associated with automated products such as the GFS analysis shown in Figure 29. This smoothing, which occurs with all models, can tend to reduce intense shears and features associated with the CAT environment and the forecaster should be aware the actual shears, temperature gradients, and atmospheric processes may be more intense than the model can resolve. Therefore, atmospheric soundings generated from rawinsonde observations can give higher vertical resolution without model smoothing and can give a more detailed picture of the vertical CAT environment which can supplement model cross sections.

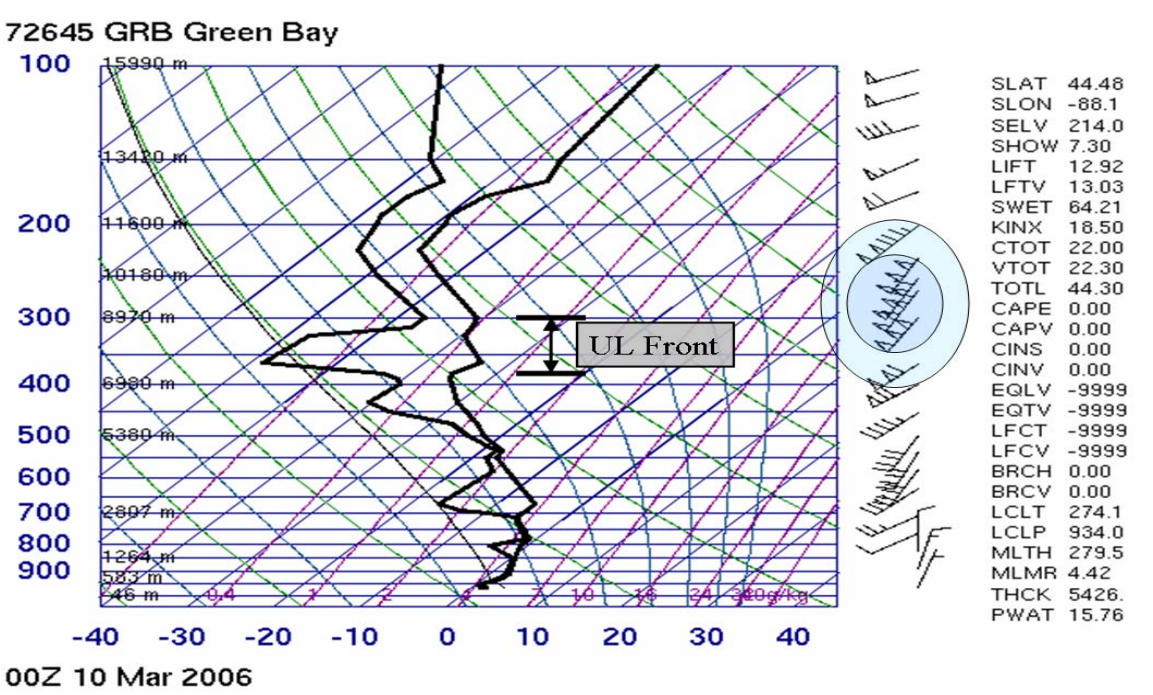

Figure 30. Sounding for Green Bay, WI for 000 GMT (6 hours after above figures), 10 March 2006. Note the vertical wind barbs to the right of the sounding, which show significant VWS near the UL front as expected, going from 70 kts at 400mb to 110 kts at 375mb and 150 kts at 300mb. Winds near the surface are 5 knots, while aloft they reach 160 knots. The blue ovals indicate the jet level, with the darker inside blue oval indicating the approximate jet core. The upper-level front is also visible in this sounding.

A difficult question for forecasters and researchers to answer is how much shear is necessary for turbulence? Because of the very nature and complexity of turbulence it is extremely difficult to define a certain amount of shear will always result in turbulence or will never result in turbulence. As has been shown, there are several other factors which can inhibit or create turbulence so a certain amount of VWS may be associated with turbulence in one region but not another. However, there have been several efforts to try to quantify the amount of shear necessary for turbulence with the understanding that the quantifications are not definitive, but rather provide general guidance to probable turbulent conditions. Table 4 below is one such attempt from AFWA TN 98-002 (2005) which the forecaster should use to understand how much shear to look for during the analysis and forecast process. Again, the forecaster must be aware of model smoothing when considering actual amounts of shear and should use either a

high resolution mesoscale model or a sounding to identify vertical shear amounts for Table 4 and similarly, a high resolution human analysis or model to identify horizontal shear.

Table 4. Wind shear critical values from Table 2-12 in AFWA TN 98-002 (2005).

	Turbulence Intensity			
	Light	**Moderate**	**Severe**	**Extreme**
Horizontal Shear		25-49 kt/90 NM	50-89 kt/90 NM	≥ 90 kt/90 NM
Vertical Shear	3-5 kt/1,000 ft	6-9 kt/1,000 ft	10-15 kt/1,000 ft	> 15 kt/1,000 ft

d. Upper-level Fronts

Upper-tropospheric fronts above and below jets are preferred regions for turbulence (Carlson 1998). Closely associated with upper-level fronts is tropopause folding. Tropopause folding constitutes an intense phase of upper-tropospheric frontal development and is closely associated with strong upper-tropospheric jet streaks. Turbulence is commonly found near the tropopause fold where the vertical and horizontal wind shear is very sharp and narrow. Furthermore, low Richardson numbers are an inherent property of upper-tropospheric fronts and their accompanying jets (Carlson 1998). Recall that low Richardson numbers mean the atmosphere is in a favorable state for turbulence to exist as the restoring effect of buoyancy is unable to overcome the VWS. Generally, a stronger jet is supported by a strong upper-level front which is characterized by vertical and horizontal wind shear and intense thermal gradients. This results in an environment prime for CAT. Figure 31 shows first a common cross sectional view of the upper-level front structure along with a tropopause fold and the resulting favorable areas of CAT and second, the same GFS analysis from Figure 29 with the upper-level front structure, tropopause folding, and favorable CAT areas all highlighted.

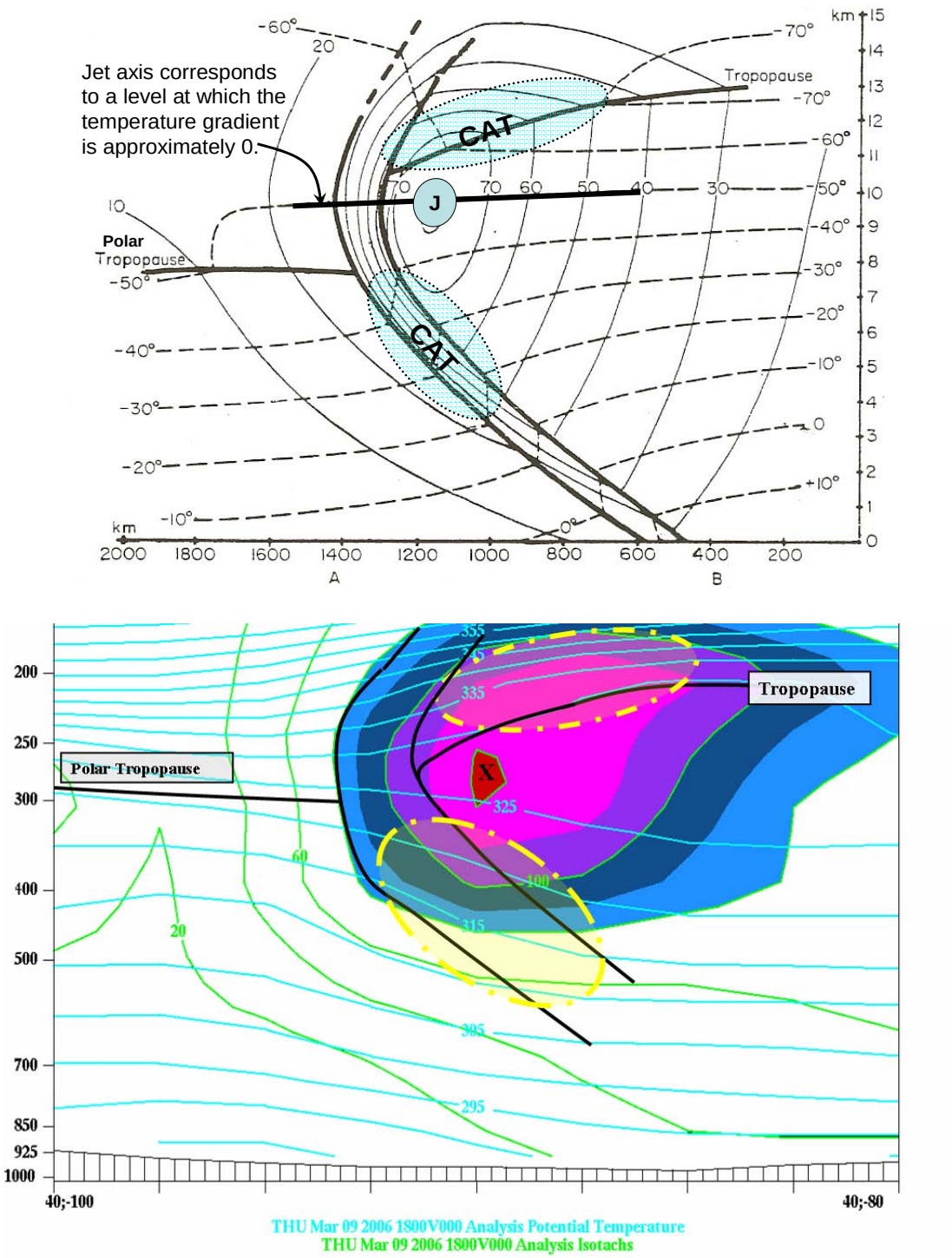

Figure 31. On top is Figure 7 from Chapter II showing the typical upper-level front structure along with a tropopause fold and favorable areas of CAT (blue ovals). The bottom chart is the analysis from 1800 GMT, 9 March 2006 (Figure 29) with the favorable CAT areas (dashed yellow ovals) and upper-level front shown.

e. Curvature

Sharp curvature in the upper-level flow indicates areas where large HWS occurs, particularly at the region of strongest curvature (such as a trough or ridge) where the direction of flow changes most rapidly. Tightly packed isotherms are usually found in these areas as well, and the vertical wind shear is, according to the thermal wind equation, proportional to the horizontal thermal gradient. These conditions are conducive to the formation of the shallow stable layers and coincident layers of wind shear associated with CAT (Lee et al. 1984). It is difficult to quantify how much curvature is needed for favorable turbulent conditions, however, there are some guidelines established by Lee et al. (1984) which are useful:

- Moderate turbulence is expected when wind speeds are between 60 and 120 knots with a wind shift greater than 120 degrees (within a 200 nm area)
- Severe turbulence is expected when winds exceed 120 knots with a wind shift of 90 degrees or greater (within a 200 nm area)

Note that with increasing wind speeds, turbulence intensity increases and less wind directional shift is necessary to sustain the turbulence. The requirement that the wind shift occur within a 200 nm area ensures that the curvature is sharp and confined.

As Kaplan et al. (2002) found, upper-level curvature is a key pattern in identifying CAT. Curvature should be identified in the upper-level charts, and should be associated with jet analysis. Areas of sharp curvature are important regions to consider for CAT potential, but more important than just the curvature is where the jet stream or core is located with respect to the curvature. As mentioned above, when strong winds exist in the curvature turbulence is likely, and the stronger winds result in an increase in turbulence intensity and probability. When there is a strong jet core in the point of maximum curvature, like shown in Figure 32, moderate or greater CAT potential is high. Figure 32 shows an anticyclonic curved ridge, but the same would apply for a sharply curved cyclonic trough as can be seen in Figure 33. Figure 34 shows the PIREPs for the example in Figure 33 which verify that turbulence does exist associated with the sharp trough and jet core.

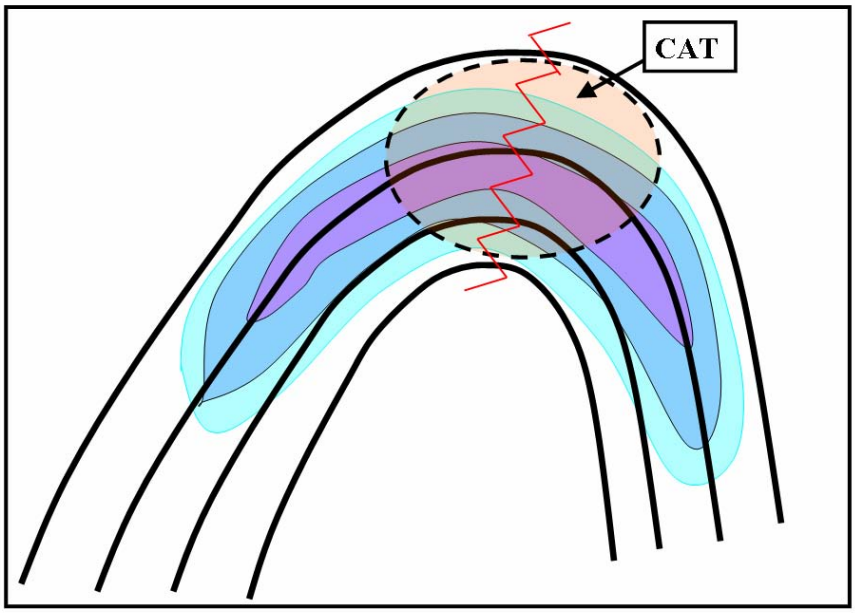

Figure 32. Example of a jet core inside peak anticyclonic curvature. 300mb heights (solid black lines), 300mb jet shown in color filled isotachs with purple indicating jet core, and potential CAT area shown in shaded orange dashed oval.

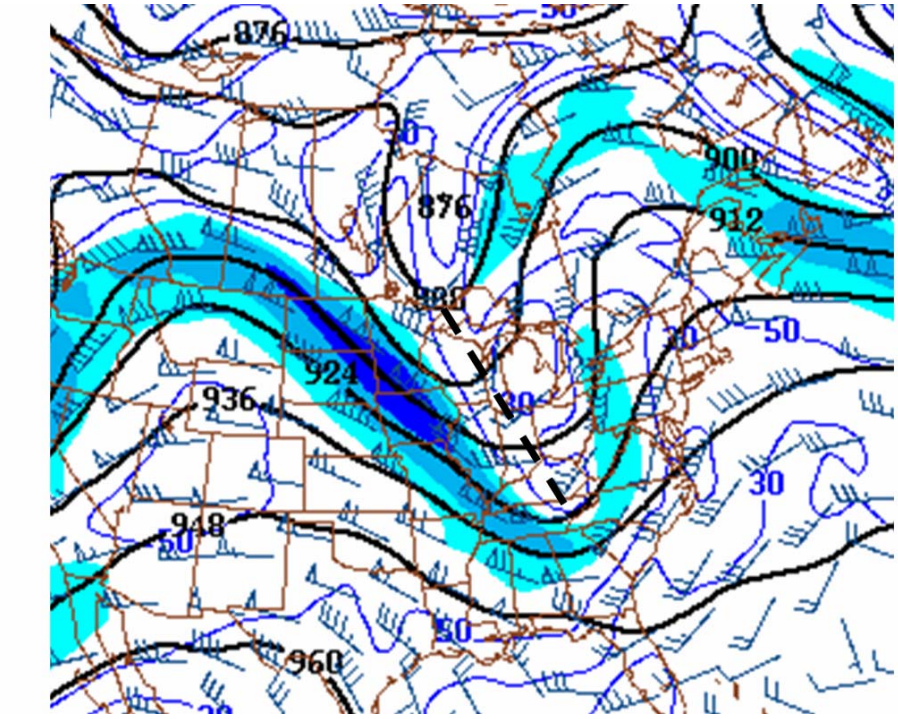

Figure 33. Sharp cyclonic curvature can be seen over the Great Lakes and the Midwest with a jet located inside the curvature although not exactly at the peak, CAT is still likely for 1800 GMT, 3 April 2006 (300mb analysis from the NWS).

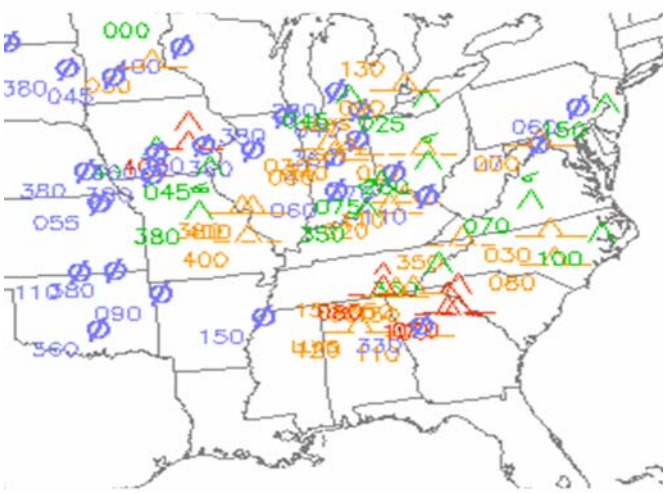

Figure 34. PIREPs for 1800 GMT, 3 April 2006. CAT reports are frequent in the area of maximum curvature from Iowa (maximum winds) to the Southwest US at the bottom of the trough (minimum winds).

f. Upward Vertical Motion

Recall from Table 3 that Kaplan et al. (2002) found that upward vertical motion was number three on their list of best predictors for CAT. When possible, vertical motion should be a part of the analysis process. The cross section is a useful way to view vertical motion as shown below in Figure 35 which goes back to the earlier example from 1800 GMT, 9 March 2006 and shows vertical motion on the cross-section plot. With the maximum upward vertical motion occurring underneath the jet core and in an area of significant vertical and horizontal wind shear, moderate or greater turbulence is very likely in this area.

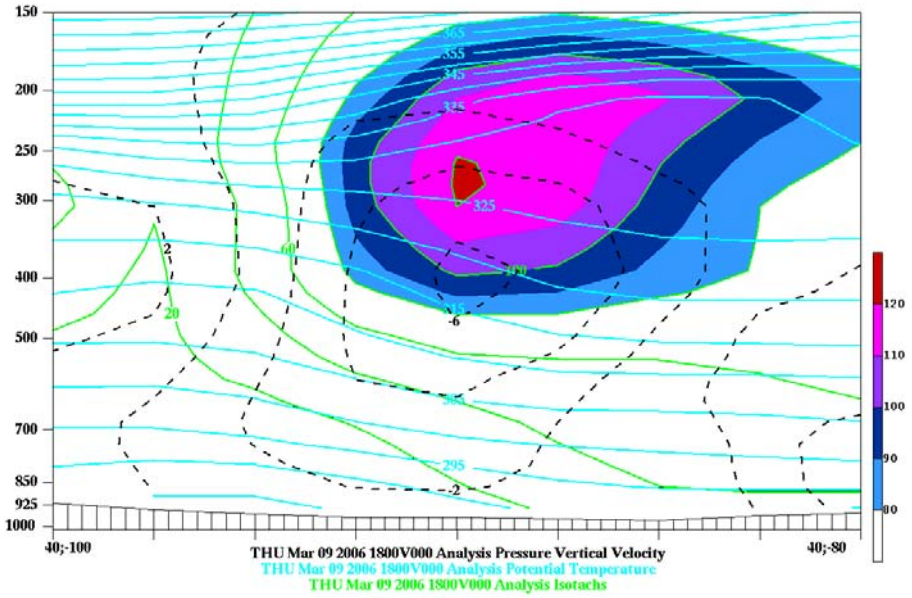

Figure 35. Pressure vertical velocity (mb/s; black dashed lines) is plotted for 1800 GMT, 9 March 2006 on this cross-section along with the isotachs (kts; green, color filled lines), and potential temperature (˚K; light blue lines). Negative values of vertical velocity indicate upward vertical motion. Maximum upward vertical motion occurs underneath the jet core around 400mb in the vicinity of the upper-level front.

g. Horizontal Deformation

Deformation zone CAT is common and found in the region where the atmosphere is undergoing contraction in one direction and elongation or stretching in the perpendicular direction, relative to the motion of the air stream (as in Figure 36) (AFWA TN 98-002). Recall Ellrod and Knapp (1992) also found horizontal deformation to be a significant factor in forming the CAT environment. A cloud border is often located near and parallel to the stretching axis. In Figure 36 a visible satellite image shows a typical deformation zone which can be favorable for the CAT environment.

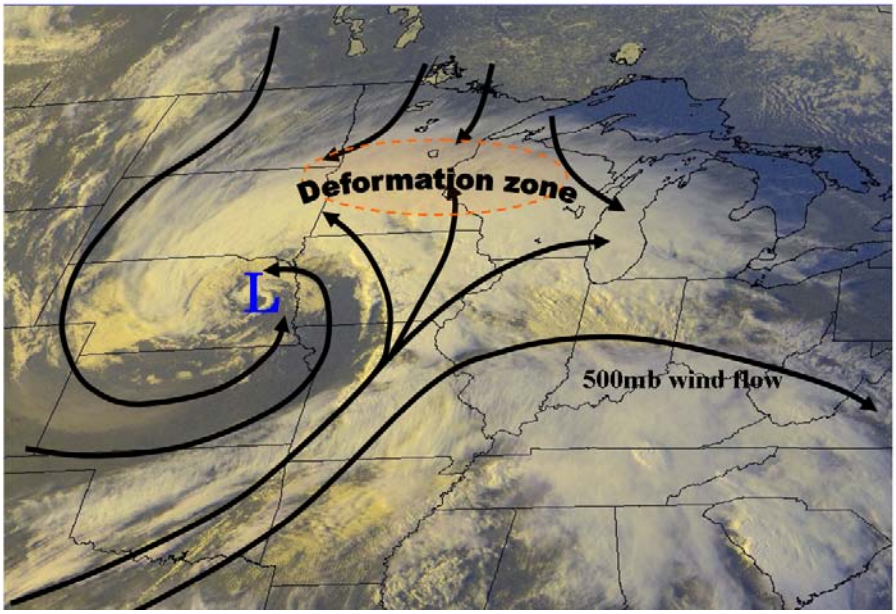

Figure 36. CAT in the deformation zone associated with the classic comma cloud pattern. Favorable CAT area shown in orange shaded region. Black stream lines represent general 500mb flow pattern. Adapted from AF 15th OWS SOP-3 (2006). Also shows how use of satellite imagery can help identify areas of CAT.

h. Horizontal Cold Air Advection

The 500 mb chart is a very common and useful weather analysis chart. Horizontal cold air advection at 500mb as well as significant positive vorticity, which is related to strong vertical motion, are often found associated with a mobile upper-level front near the jet stream. CAT frequently occurs in regions of increasing thermal gradients and increasing vertical wind shear. Consequently, using the 500mb chart to identify regions of significant cold air advection and positive vorticity can be useful in predicting favorable regions of CAT. Figure 37 below shows 500mb heights, isotherms, and absolute vorticity for 1800 GMT, 9 March 2006. Note the significant cold air advection and vorticity over northeastern Montana. In the 300mb chart this was an area of curvature, specifically it appeared to be at the bottom of a sharp, tilted 300mb trough. However, winds were not significant and no jet was shown in the area and so the forecaster might dismiss this area as not likely for turbulence. But this 500mb chart should give the forecaster some further indication that turbulence may exist in this area due to the horizontal cold air advection, vorticity, and likely significant shear that is developing over northeastern Montana. Over the Southern Plains there is significant

positive vorticity in the isotherm trough as well as some temperature advection. This area corresponds to the entrance region of the 300mb jet core that was shown in Figures 27 and 28. The observed moderate or greater CAT occurred mostly downstream of the maximum vorticity over Illinois, Wisconsin, and Iowa.

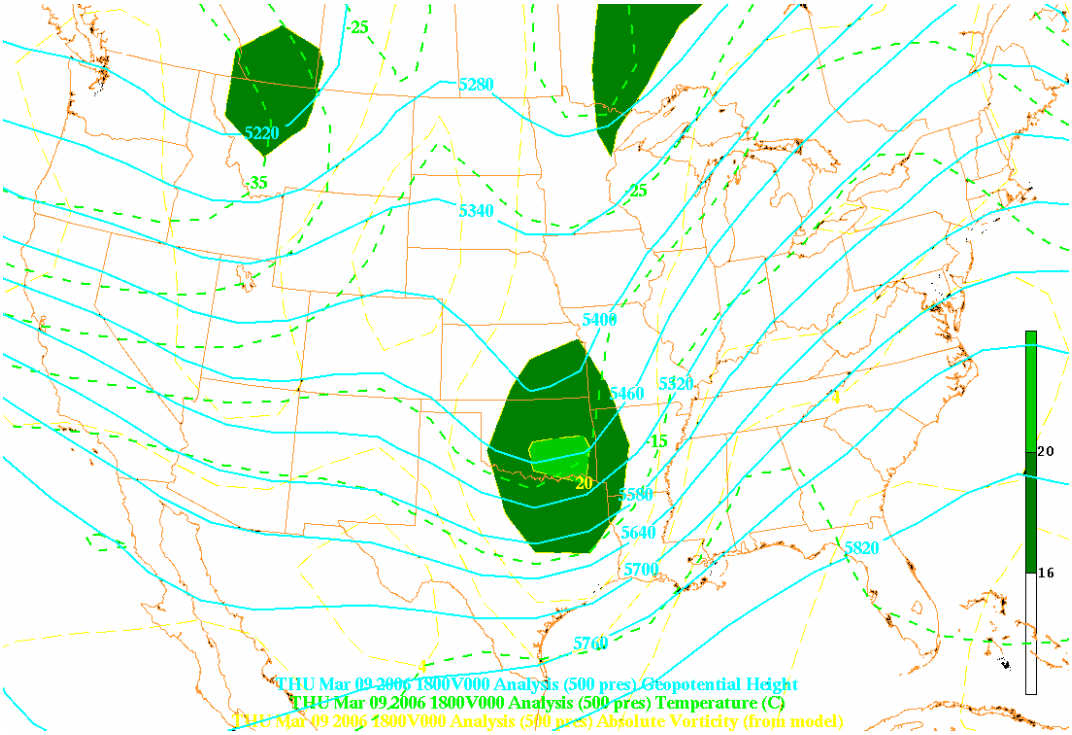

Figure 37. 500mb analysis chart for 1800 GMT, 9 March 2006 with heights (m; blue solid lines), isotherms (˚C; green dashed lines), and absolute vorticity (s^{-1}; yellow dashed and color filled) shown.

3. Mountain Wave

Mountain wave turbulence can be a significant hazard to aircraft and is most common near large, distinct mountain ranges. Mountain wave systems can occur whenever strong flow in a stable environment encounters a topographic barrier. Forecasting mountain wave turbulence has been fairly well studied, and perhaps the most useful and reliable approach is identifying where mountain waves exist by cloud identification, by eye or by satellite imagery. AFWA TN 98-002 (2005) lists the following cloud features that are indicators of mountain wave activity:

There are specific clouds associated with mountain wave turbulence. These are cap (foehn wall), roll (rotor), lenticular, and "mother-of-pearl" clouds. Figure 38 illustrates the structure of a strong mountain wave and associated cloud patterns. The lines and arrows depict windflow.

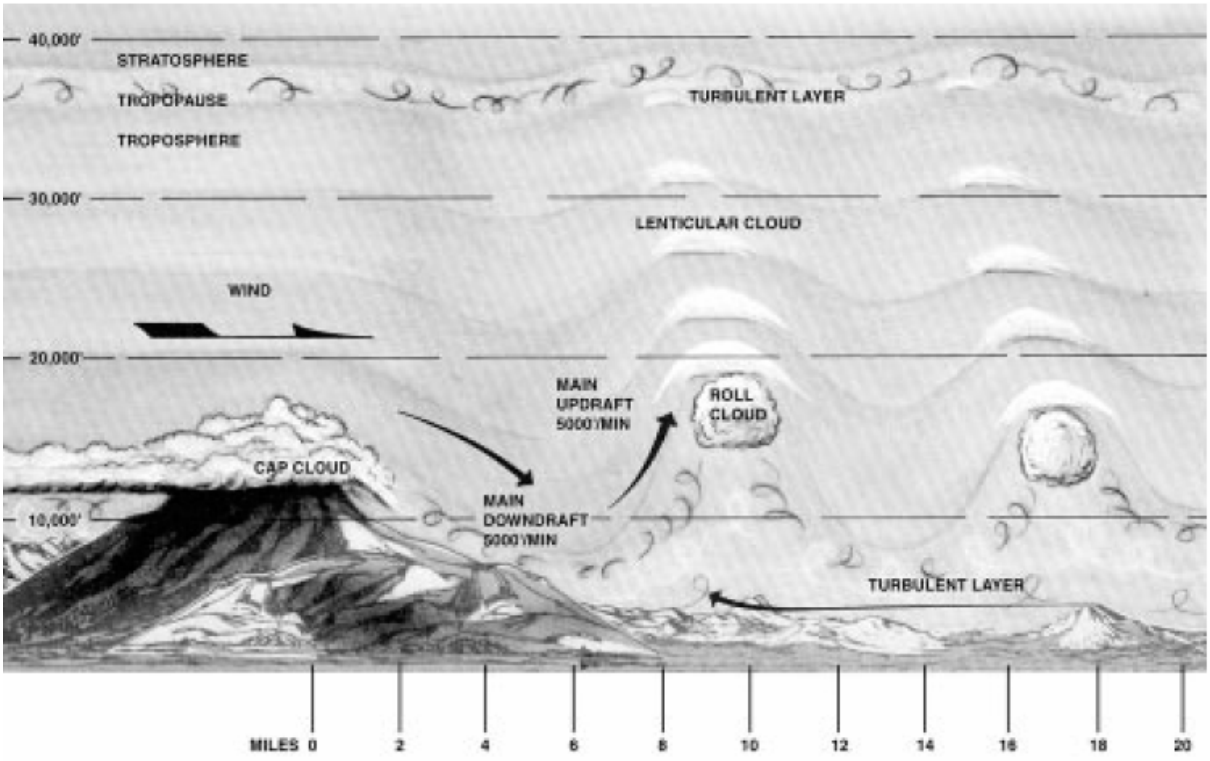

Figure 38. Mountain-wave cloud structure. The figure illustrates the structure of a strong mountain wave and associated cloud patterns. The lines and arrows depict windflow. (Figure 2-49 in AFWA TN 98-002).

a. Cap Cloud. The cap cloud hugs the tops of mountains and flows down the leeward side with the appearance of a waterfall. This cloud is dangerous because it hides the mountain and has strong downdrafts associated with it. The downdrafts can be as strong as 5,000 to 8,000 feet per minute.

b. Roll Cloud. The roll cloud, also called a rotor cloud, looks like a line of cumulus clouds parallel to the ridge line. It forms on the lee side and has its base near the height of the mountain peak and top near twice the height of the peak. The roll cloud often merges with the lenticular clouds above, forming a solid cloud mass to the tropopause. The roll cloud is dangerously turbulent with strong updrafts (5,000 feet per minute) on the windward side and dangerous downdrafts (5,000 feet per minute) on its leeward edge. This cloud may form immediately on the lee of the mountain or it may be a distance of 10 miles downwind – depending on wind speed.

c. Lenticular Clouds. Lenticular clouds are relatively thin, lens-shaped clouds with bases above the roll cloud. Their tops extend to the tropopause. These clouds have a tiered or stacked look due to atmosphere stability above the mountain ridge. All lenticular clouds are associated with turbulence. In polar regions, lenticular clouds can appear in the stratosphere as high as 80,000 feet. These clouds are called "mother-of pearl" (nacreous) clouds.

Another important feature to look for when identifying mountain wave activity is the foehn gap which indicates turbulent lee waves are present. The gap is located between the cirrus clouds and mountain range on the leeward side of the range as shown in Figure 39.

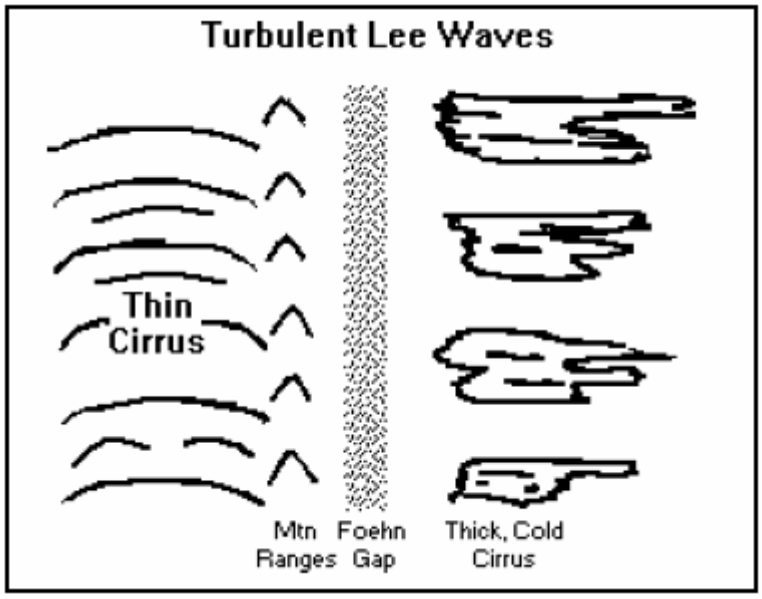

Figure 39. A foehn gap shown here with the typical mountain-wave clouds indicates turbulent waves are present (AFWA TN 98-002, 2005).

Mountain wave intensity depends on several factors, but generally is proportional to turbulence intensity. Mountain wave intensity factors include: wind speed, height and slope of the mountain (highest, steepest mountain produces most intense wave and turbulence), stability above and to the lee of the mountain (very stable air above and to the lee of the mountain produces most intense turbulence) (AFWA TN 98-002, 2005). Some necessary ingredients for significant mountain wave development are as follows:

- A minimum wind component of 25 knots perpendicular to the mountain ridge at the height of the ridge.
- Wind profile should show very little change of wind direction with height and increasing wind speeds with altitude high into the troposphere.

Table 5 and Figure 40 (used together), provide guidance in forecasting mountain wave turbulence.

Table 5. Low-level mountain wave turbulence. (Lee et al. 1984).

Low-Level Mountain-Wave Turbulence (Surface To 5,000 Ft Above Ridge Line)			
Low-Level Feature Wind Component Normal to Mountain Range at Mountain Top and > 24 kt **and**	**Turbulence Intensity**		
	Light	**Moderate**	**Severe**
dP Across Mountain at Surface is	See Figure 2-48	See Figure 2-48	See Figure 2-48
|dT| Across Mountain at 850 mb is	< 6°C	6°C - 9°C	> 9°C
|dT/dX| Along Mountain Range at 850 mb is	<4°C/60 NM	4-6°C/60 NM	>6°C/60 NM
Lee-Side Surface Gusts	< 25 kt	25 - 50 kt	> 50 kt
Winds Below 500 mb > 50 kt	Increase the Turbulence found by one degree of intensity (i.e., Moderate to Severe)		

Notes: (1) dP is the change in surface pressure across the range.
(2) |dT| is the absolute value of the 850-mb temperature difference across the range.
(3) |dT/dX| is the absolute value of the 850-mb temperature gradient along mountain range.
(4) Turbulence category forecast is the worst category obtained from each of the four parameters.

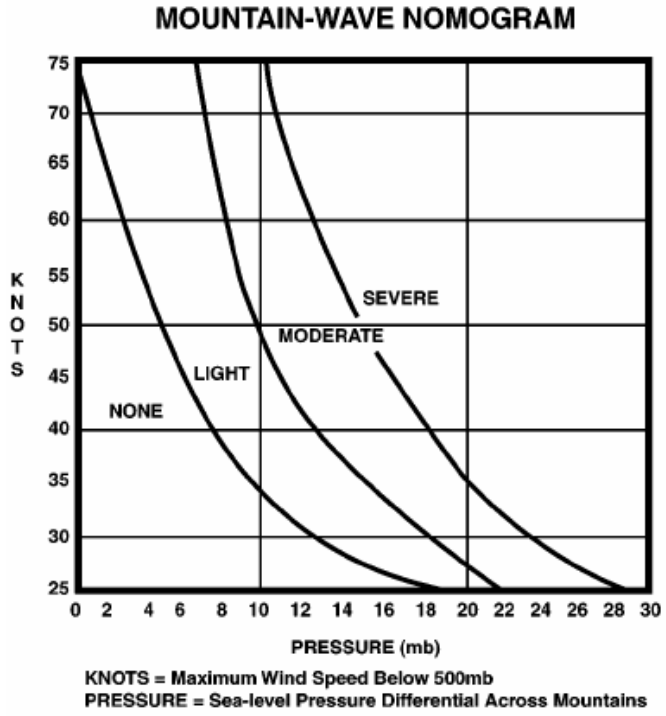

Figure 40. Mountain-wave nomogram to be used to predict mountain wave intensity (from Lee et al. 1984).

a. Trapped Lee Waves

Trapped lee waves are often found downstream of the rotor zone, although a weak rotor may exist under each lee wave. These waves are typically at an altitude within a few thousand feet of the mountain ridge crest and turbulence is generally restricted to altitudes below 25,000 feet. Strong turbulence can develop between the bases of associated lenticular clouds and the ground. Lenticular clouds form near the crests of mountain waves (UCAR 2005a). A deep, stable layer with smooth, horizontal flow that increases with height above the barrier will result in a series of shallow trapped lee waves. A general rule of thumb, called the "1.6 rule," is useful: if the wind speed at 2000 m above ridge-top level is more than 1.6 times the ridge-top wind speed, then you should expect a trapped lee wave regime (UCAR 2005a).

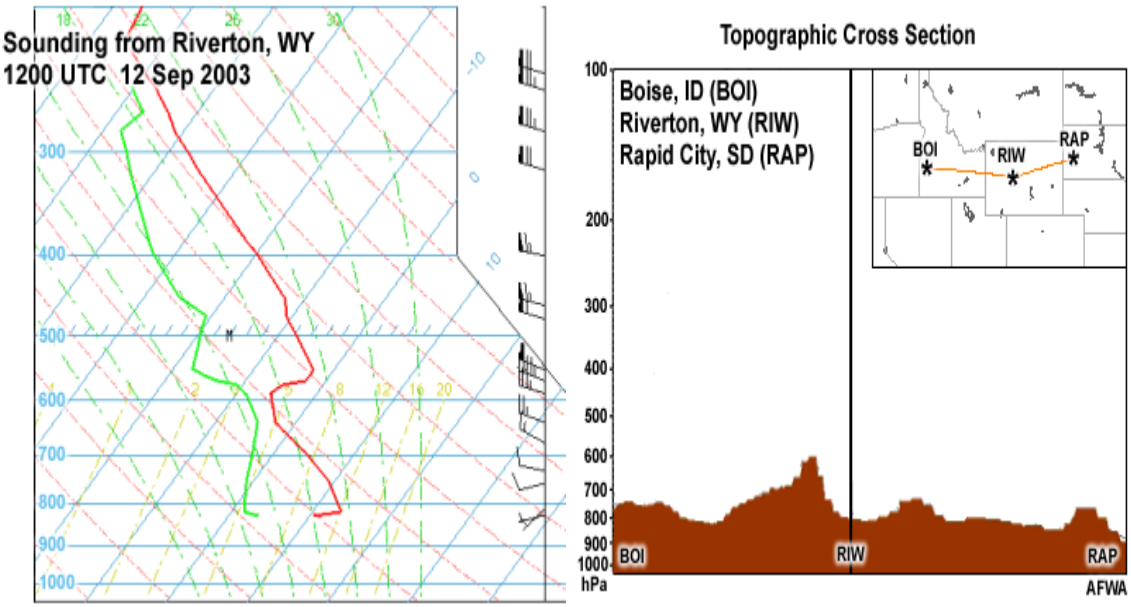

Figure 41. On the left is a sounding from Riverton, Wyoming at 1200 UTC on 12 September 2003. On the right is a vertical cross section of topography which shows that the Rocky Mountains lie immediately to the west of Riverton. The mountains are oriented north-south and ridge-top level is approximately 600 hPa (from UCAR 2005a).

The sounding in Figure 41 shows that while winds near the surface are light, winds at ridge-top level are 25-35 knots. The sounding also reveals an incredibly strong inversion immediately above ridge-top level. Under these conditions, the forecaster should expect a significant wave response. In Figure 41, wind speeds increase

from 25 knots at 650 hPa to 55 knots at 550 hPa, which clearly exceeds the 1.6 rule-of-thumb. On this day significant trapped lee waves were observed and there were several EDR reports of light and moderate turbulence near Riverton, WY ranging in elevation from 697mb to 496mb. Thus, rawinsonde observations and mesoscale analyses can be used to evaluate the vertical structure of wind and atmospheric stability. The limitation is the availability of observations at proper locations. Ideally, they should be positioned upstream of the mountain barrier where ambient atmospheric conditions can be assessed (UCAR 2005a).

b. Vertically Propagating Waves (VPWs)

VPW develop on the leeside of large-scale mountain ranges like the Rockies, and much like trapped lee waves, occur when upstream synoptic-scale flow becomes perpendicular to the mountain ridge axis. They can also develop to the lee of much smaller, isolated terrain causing additional complexity. What distinguishes a trapped lee wave response from a VPW is the atmospheric stability and shear. While increasing stability favors a trapped lee wave, it is detrimental to a VPW. Specifically, a mountain top inversion like that shown in the Figure 41 sounding will not allow a VPW to exist. However, the atmosphere must be stable in order for a mountain wave to exist, so some stability is required for a VPW. Vertical wind shear is also detrimental to a VPW while wind greatly increasing with height is favorable for a trapped wave. To excite a VPW, having a wind profile with little change in speed or direction at and above the mountain (i.e., no jet max aloft) is necessary. The 1.6 rule-of-thumb mentioned above for trapped lee waves can still be utilized for VPWs, but with VPWs the mountain top wind speed should be less than 1.6 times the wind speed 2000 m above mountain top to allow vertical propagation (Coughlin 2005). For further information on VPWs the reader/forecaster is referred to Coughlin (2005) and to UCAR (2005a) which offers a very useful online module on mountain waves.

B. TURBULENCE DATA AND REPORTS

Observations should be used to verify patterns and favorable areas identified in the forecaster's analysis, and to alert the forecaster of all reported turbulent areas. As previously discussed, there are currently two primary methods of observing turbulence in the atmosphere. PIREPs are the traditional and most widely used method, and still the

only method being used outside of CONUS, although they are highly subjective and pilot dependent. EDR observations offer a more objective approach, with potentially greater coverage capability but the majority of current aircraft are unequipped with the technology capable of reporting EDR values, resulting in limited spatial coverage to the 100 or so aircraft routes that do have EDR capability. Both types of observations offer the only insight available into the true turbulent atmosphere and should be utilized by the forecaster. Satellite imagery and radar data can and should also be used to help identify regions of turbulence and will be discussed in more detail later. Because turbulence is such a brief, microscale phenomena it can be dangerous to simply forecast persistence. That is, if a PIREP is reported in a region of interest, the forecaster should not automatically forecast turbulence for that region over the next 12 to 24 hours, or even in the region downstream of that PIREP. Rather the forecaster should attempt to understand what is causing the turbulence (i.e., strong vertical wind shear, a jet core through a sharply curved ridge, a strong upper-level front, etc.). Once the forecaster has some idea of what caused the turbulence the forecast should be made based on whether those conditions will continue to exist or not.

An effective way to use EDR and PIREPs observations is to overlay them on a 300mb (or an alternative upper-level) chart as done in Figure 42. In Figure 42 only the EDR observations are shown and the forecaster can quickly see that there is moderate turbulence being reported (via EDR observations) associated with the strong north-south jet core located over the southern Great Lakes region.

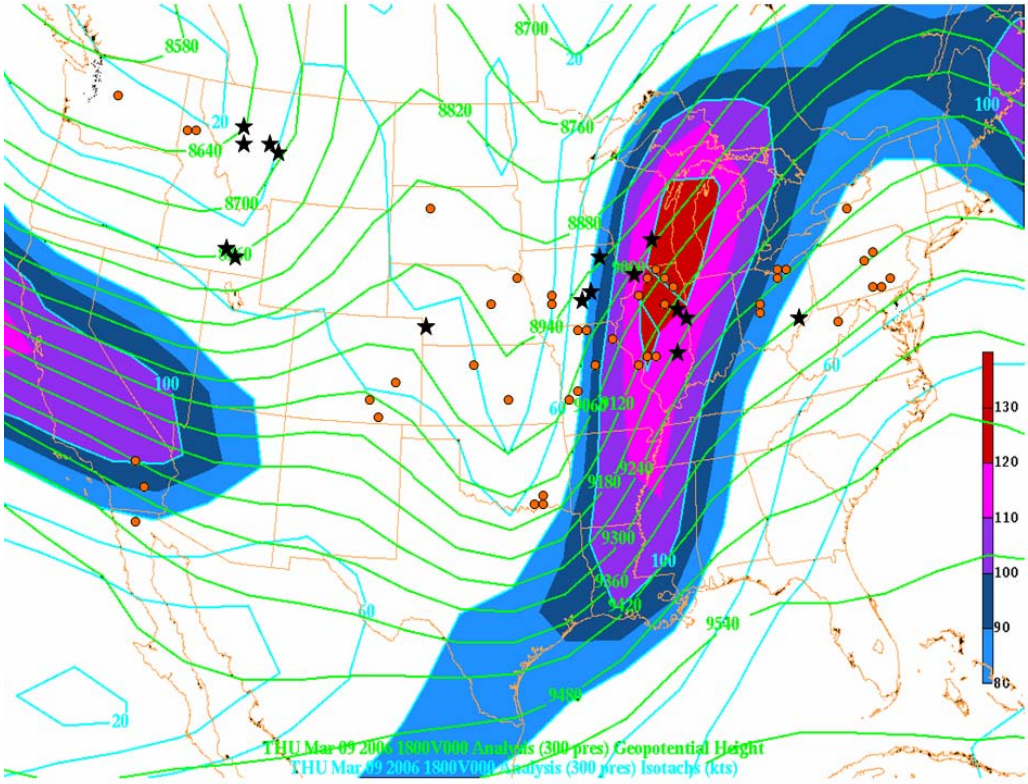

Figure 42. Same as Figure 28. The figure illustrates how EDR observations can be used to help identify and alert the forecaster as to where CAT is occurring and thereby validate forecaster's first guess at the turbulent state of the atmosphere from the synoptic analysis.

The forecaster can also quickly see that there is moderate turbulence being reported over Montana and Idaho not associated with any visible jet and as such may require further investigation by the forecaster. Upon further investigation the forecaster would find these observations are at 39,980 ft (188mb) near the tropopause. A weaker and narrow wind maximum of about 60 knots extended down through Montana and Nevada and a cross-section through Montana reveals this maximum occurs at about 250mb with sharply decreasing winds above the maximum and to the east and west which would be conducive for the CAT environment. The EDR observations over California and Nevada seem to indicate a lack of moderate-or-greater turbulence associated with the jet streak off of the Pacific Coast, however, there were three PIREPs of moderate turbulence during this time period over southwest Nevada and southeast California. Recall that the coverage of EDR observations is currently limited and thus, PIREPs can often provide very useful information where EDR observations can not as

shown in Figure 43. In Figure 43, a strong jet exists in the deep trough over the Southeastern U.S. in an area where there are no EDR observations. Fortunately, there are PIREPs available in this region which indicates that there is moderate to severe turbulence in this area.

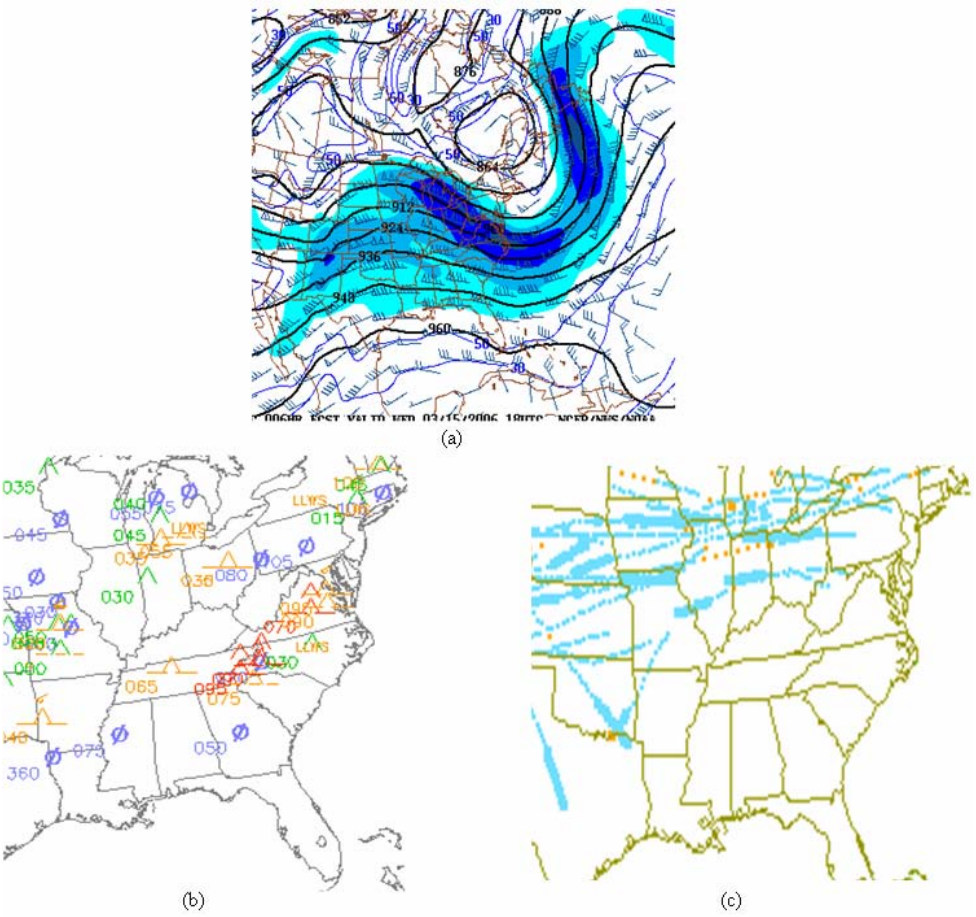

Figure 43. (a) 300mb chart from NWS showing heights and winds for 1800 GMT, 15 March 2006 (b) PIREPs over Southeastern U.S. for 1700-1900 GMT, 15 March 2006 (c) EDR observations for 1700-1900 GMT, 15 March 2006. PIREPs give vital information in an region where few EDR observations exist.

1. Accessing EDR Observations

EDR observations currently are only available via the NOAA/ESRL/GSD aircraft data web. Current EDR data is only available to NOAA sites and users with a login and password account. The term ACARS is used to designate automated weather reports from commercial aircraft and stands for Aircraft Communications Addressing and Reporting System. Because the ACARS data is proprietary to the airlines providing the

data, the following guidelines, taken from ESRL/GSD (2006), have been developed regarding access:

- Real-time ACARS data may be made available to those organizations that are performing research which is likely to benefit the airlines providing the data.
- Real-time data are available to government agencies such as NOAA in support of forecasting operations.
- Real-time data may be made available only to those airlines that provide ACARS meteorological data to the US Government at their own expense. Data may not be shared with affiliate or code-share airlines.
- Real-time data may not be made available to commercial entities that would use them to develop products or services they plan to offer for sale to the participating airlines.

ACARS data can be received in several ways: Web-based graphical displays, either java-based or not, web-based access to binary data in netCDF format, or LDM access to binary data in netCDF format. The web-based graphical display using java is very useful and shown below in Figure 44. It can be accessed at http://acweb.fsl.noaa.gov/java/. The default load page is shown in Figure 44a. For the java display the forecaster can view EDR information to include the EDR category, aircraft number, and elevation of each EDR observation. The forecaster can also right click on the observation and bring up a window like that shown in Figure 44c which shows every observation that aircraft has made on that flight route. The forecaster can slide the tabs on the ruler to right of the map in Figure 44b up and down to display observations for certain altitudes only. For example, if the forecaster wanted to focus in on CAT only, then he/she could bring the bottom tab up to 20,000 feet and EDR observations for 20,000 feet to 40,000 feet would be displayed which might rid the map of some clutter from lower altitude observations.

AMDAR Data Display from ESRL/GSD

Latest version is: 12-Dec-2005
To be sure you are using it, hold down the shift key and press 'reload' on Netscape, or restart Internet Explorer. Please notify Bill.Moninger@noaa.gov of any problems.

12-Dec-2005: new Several airports in central Africa added.
See change details (new window) for more information.

Per our agreements with participating airlines, this data may not be redstributed to third parties. (Use of images in research publications is allowed and encouraged, however.

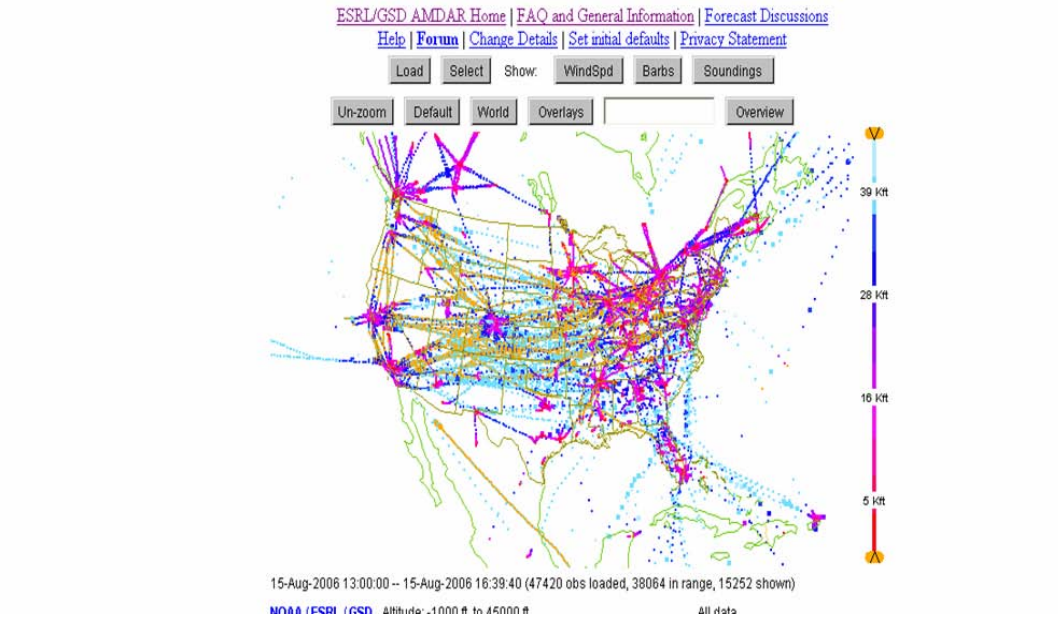

(a)

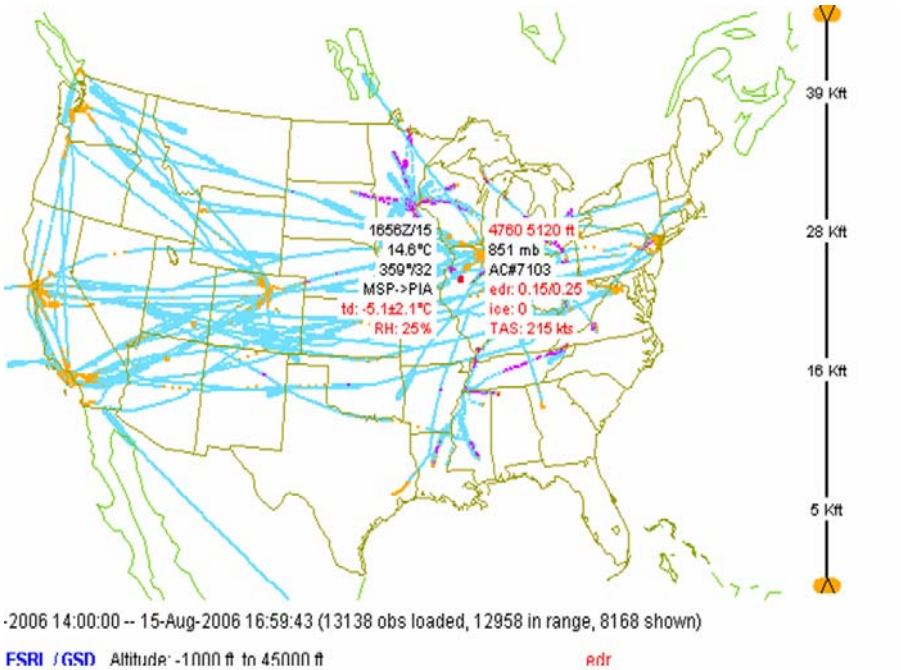

(b)

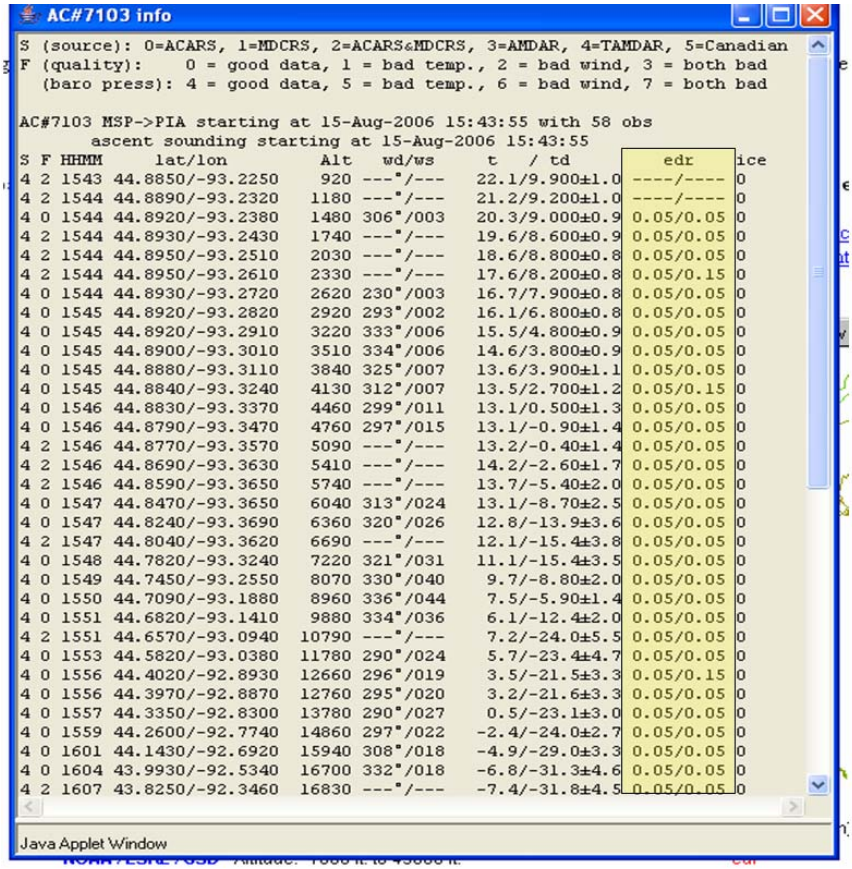

(c)

Figure 44. (a) Web-based java display default load page (http://acweb.fsl.noaa.gov/java/) (b) forecaster can move cursor over any EDR observation and that observation information will be displayed. (c) if forecaster right clicks on an EDR observation, a list of every EDR observation of that particular aircraft for that flight will be displayed along with it's elevation and lat/long position (EDR column is highlighted for clarity).

2. Accessing PIREPs

It is assumed that the forecaster already has some knowledge of using PIREPs and where to access them. PIREPs are available from a wide variety of platforms and sources, but they all share the same basic form as shown in Figure 45 taken from the NOAA/NWS AWC turbulence website; http://adds.aviationweather.gov/turbulence/.

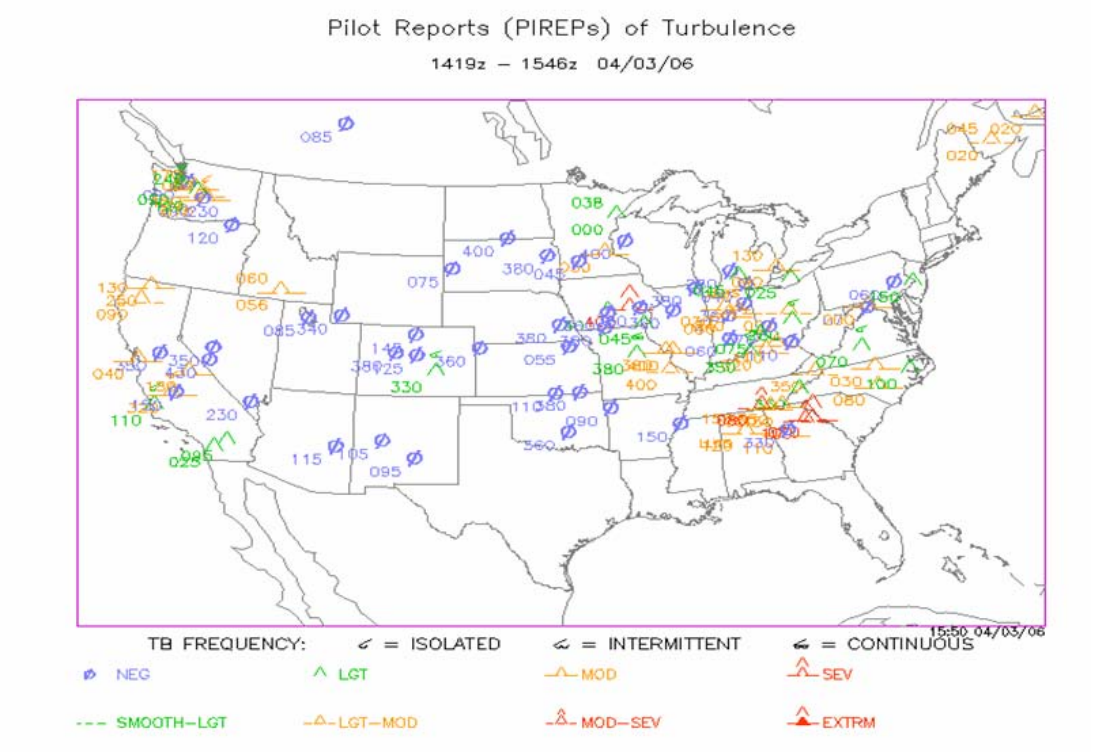

Figure 45. Typical PIREPs for 1419-1546 GMT, 3 April 2006. Intensity scale shown on bottom, elevation shown next to each PIREP.

Most PIREPs displays are shown as images and are not java-based displays like the EDR observations shown previously. This can make some PIREPs displays difficult to read, particularly the elevation of PIREPs when there are a large number of PIREPs in a small region. While not as glamorous as the EDR display shown in Figure 44, the vital information (location, elevation, and intensity of turbulence) is relayed to the forecaster.

3. Satellite Imagery

a. IR/VIS

Turbulence can sometimes be detected in infrared (IR) or visible (VIS) satellite imagery. There are two distinctive features which the forecaster should look for in IR/VIS images; transverse bands and billows. Transverse bands are defined as irregular, wavelike cirrus cloud patterns that form nearly perpendicular to the upper flow (AFWA TN 98-002, 2005) and can be seen in Figure 46 in VIS and IR images. These bands are usually associated with the low latitude subtropical jet stream and indicate large vertical and possibly horizontal wind shears. The additional presence of thermal instability commonly causes severe turbulence in the wider, thicker transverse bands and

these bands often have a carrot-shaped appearance, similar to cumulonimbus anvils. Cloud bands, in general, tend to be aligned with the cloud layer shear vector. For this reason, the presence of cirrus bands which differ in orientation from the prevailing wind direction (transverse to the flow) indicate directional shear with height (AFWA TN 98-002, 2005).

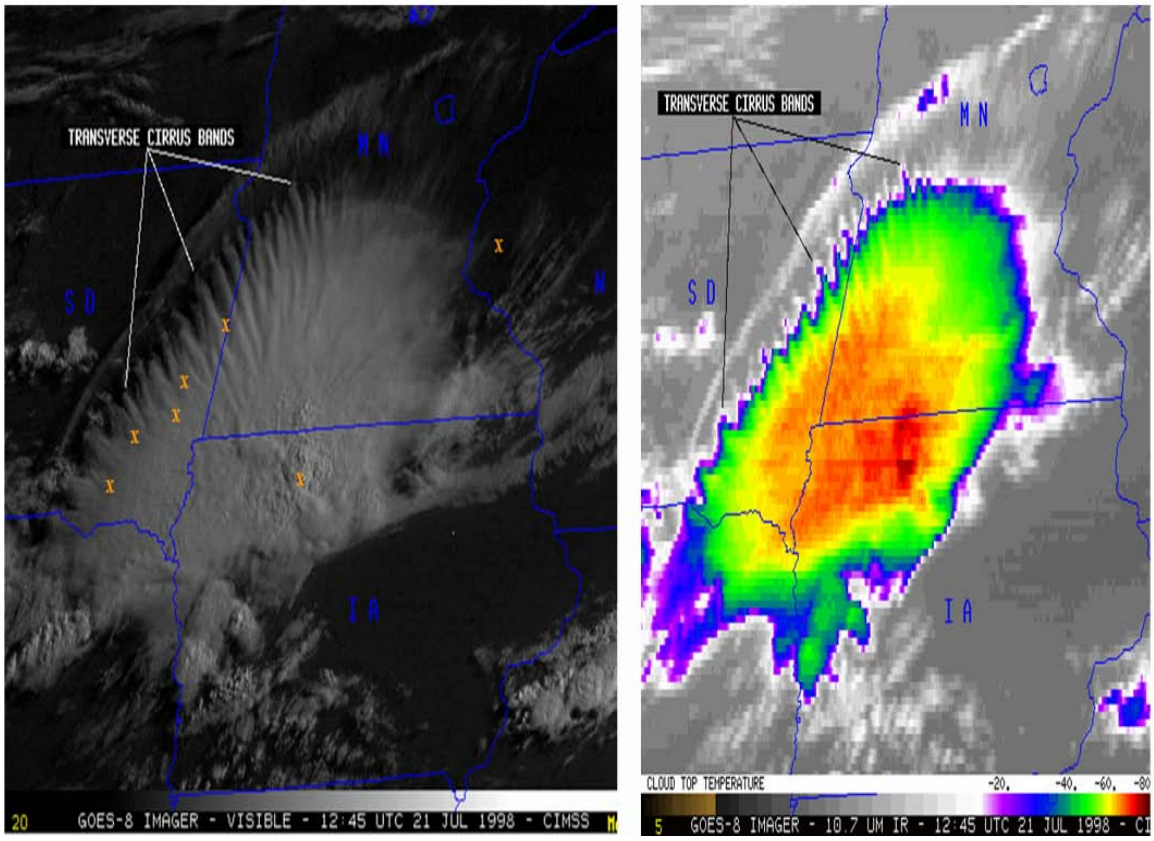

(a) (b)

Figure 46. A series of transverse cirrus bands are distinctly visible in the (a) NOAA GOES-8 VIS image and (b) NOAA GOES-8 IR image from 1245 GMT, 21 July 1998. Such transverse bands are often satellite signatures of high-altitude turbulence and can form along the northern periphery of convective storms (from CIMSS 2006). Several reports of moderate turbulence (orange 'x's in (a)) were received from aircraft flying between 33,000 and 39,000 feet across eastern South Dakota, southern Minnesota, and western Wisconsin from 1000 GMT to 1500 GMT. The moderate turbulence over northern Iowa is likely the result of convective turbulence.

Billows are wave cloud patterns in cirrus, or middle-level clouds which are regularly spaced, narrow, and oriented to the upper flow (AFWA TN 98-002, 2005). Billows are commonly visible when a strong jet intersects either a frontal cloud system or a line of cumulonimbus clouds at a large crossing angle. The anvil debris of convective clouds in these situations extends well downstream from its source. The individual wave clouds dissipate quickly (i.e., less than 30 minutes), however, new waves can reform nearby when favorable conditions exist. Turbulence intensity does seem to correlate well with the wavelength of the billows; the longer the wavelength of the billows, the better the chance for significant turbulence (AFWA TN 98-002, 2005).

b. Water Vapor

Water vapor imagery can also be very useful for identifying turbulence. The forecaster should look for water vapor darkening; elongated bands, or large oval-shaped gray regions that become darker in successive images (AFWA TN 98-002, 2005). Cold advection and convergence in the middle and upper troposphere result in compensating sinking through a deep layer. Cross sections of such features reveal sloping baroclinic zones and/or tropopause folds indicating stratospheric air may be descending into the upper troposphere and creating a very favorable environment for turbulence. Moderate or greater turbulence occurs 80 percent of the time when water vapor darkening occurs, especially if the darkening persists for at least three hours (AFWA TN 98-002, 2005) as it does in Figure 47.

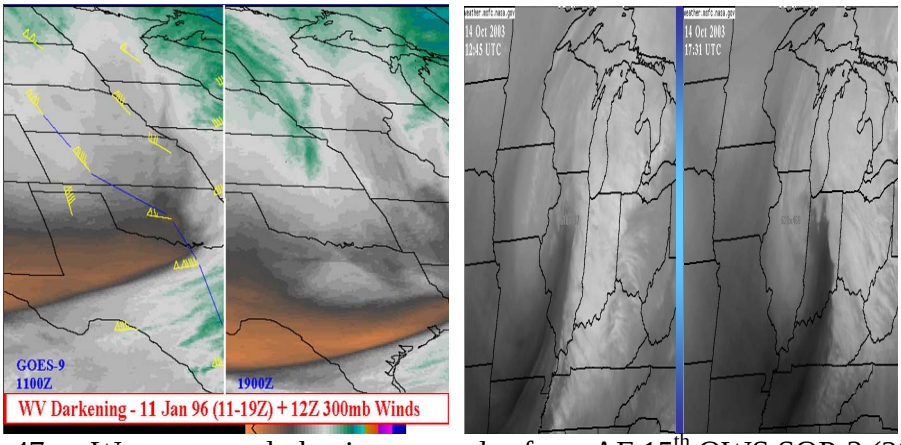

Figure 47. Water vapor darkening examples from AF 15th OWS SOP-3 (2006). Darkening exists in both of the GOES-9 water vapor images. On the left the darkening occurs over an 8 hour period, and on the right it occurs over a 5 hour period. Moderate or greater turbulence occurs 80 percent of the time in such areas of darkening (from AF 15th OWS SOP-3 2006).

Mountain waves or trapped lee waves can also often be detected in satellite imagery. Figure 9 (page 28) is a GOES-10 VIS image which clearly shows a trapped lee wave where turbulence is likely to exist. Figure 48 illustrates mountain waves in water vapor imagery.

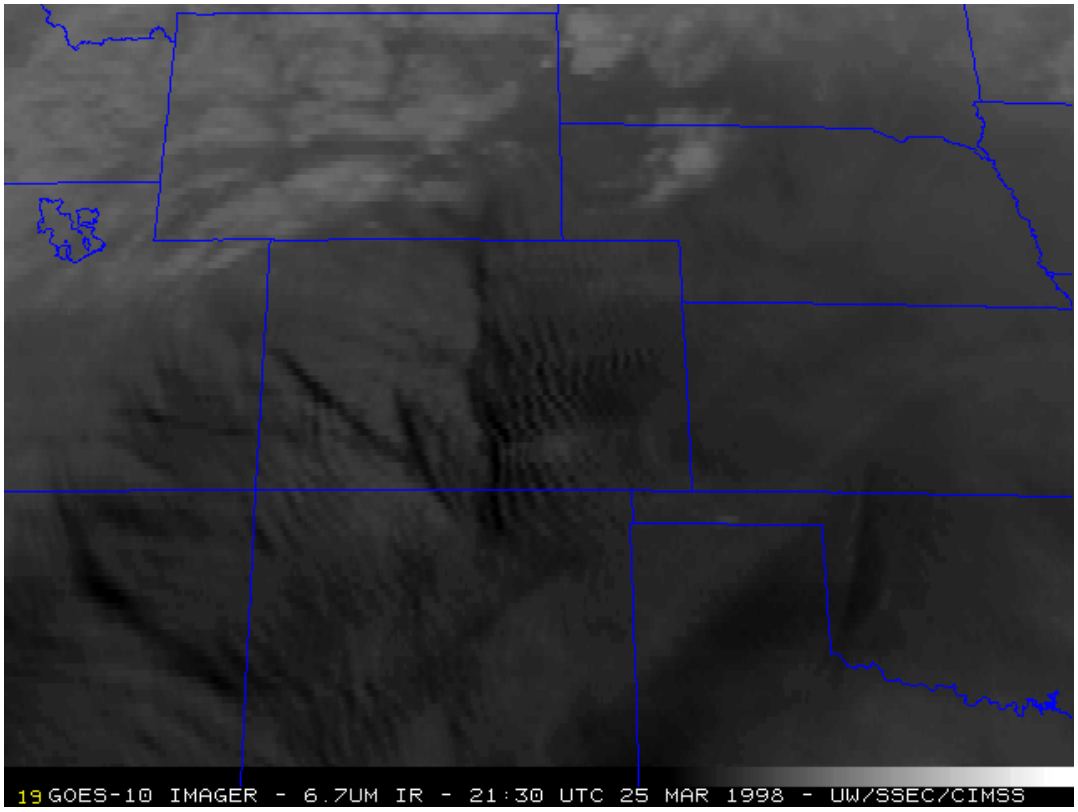

Figure 48. GOES-10 water vapor imagery shows widespread mountain waves over Colorado and New Mexico at 2130 GMT, 25 March 1998. Such a signature on water vapor imagery can often indicate turbulence (from CIMSS 2006).

4. Radar

Although the radar is not commonly associated with turbulence, it can be quite useful in identifying convective turbulent regimes. The radar's ability to display convection is of great value to the forecaster. A quick look at the current radar can highlight regions where convection is taking place, and consequently the forecaster should focus in on these areas as favorable for convective turbulence. The radar can also account for the intensity of the convection which is proportional to the intensity of convective turbulence. Figure 49 is a national composite radar image from the NWS for 1858 GMT, 10 August 2006.

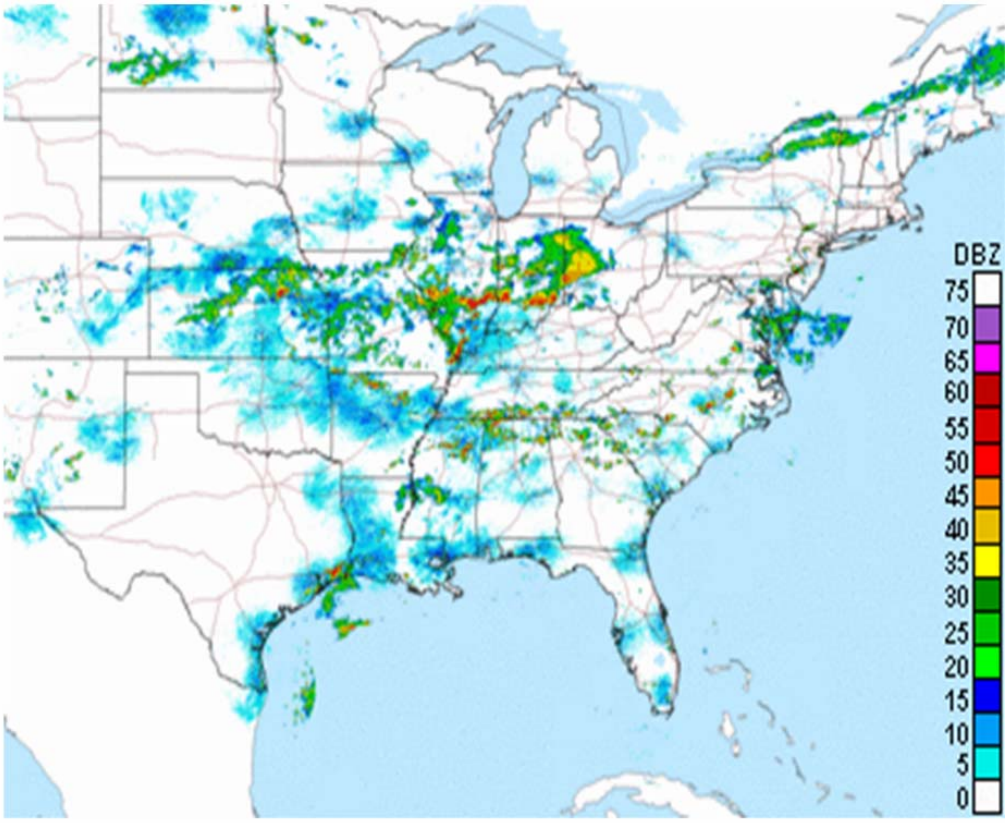

Figure 49. NWS composite radar image for 1858 GMT, 10 August 2006. Most intense convection is shown by red colors located over northeastern Kansas, southern Illinois and Indiana, and western Ohio. These are areas the forecaster should then further look for turbulence.

The intense convection over northeastern Kansas, southern Illinois and Indiana, and western Ohio should alert the forecaster that convective turbulence is likely in these areas and requires further investigation. By considering the current EDR observations, shown in Figure 50, the forecaster can see that turbulence is present in these convective areas. The forecaster can overlay the EDR or PIREPs observations onto the radar or even satellite imagery in much the same way that was done with the 300mb chart.

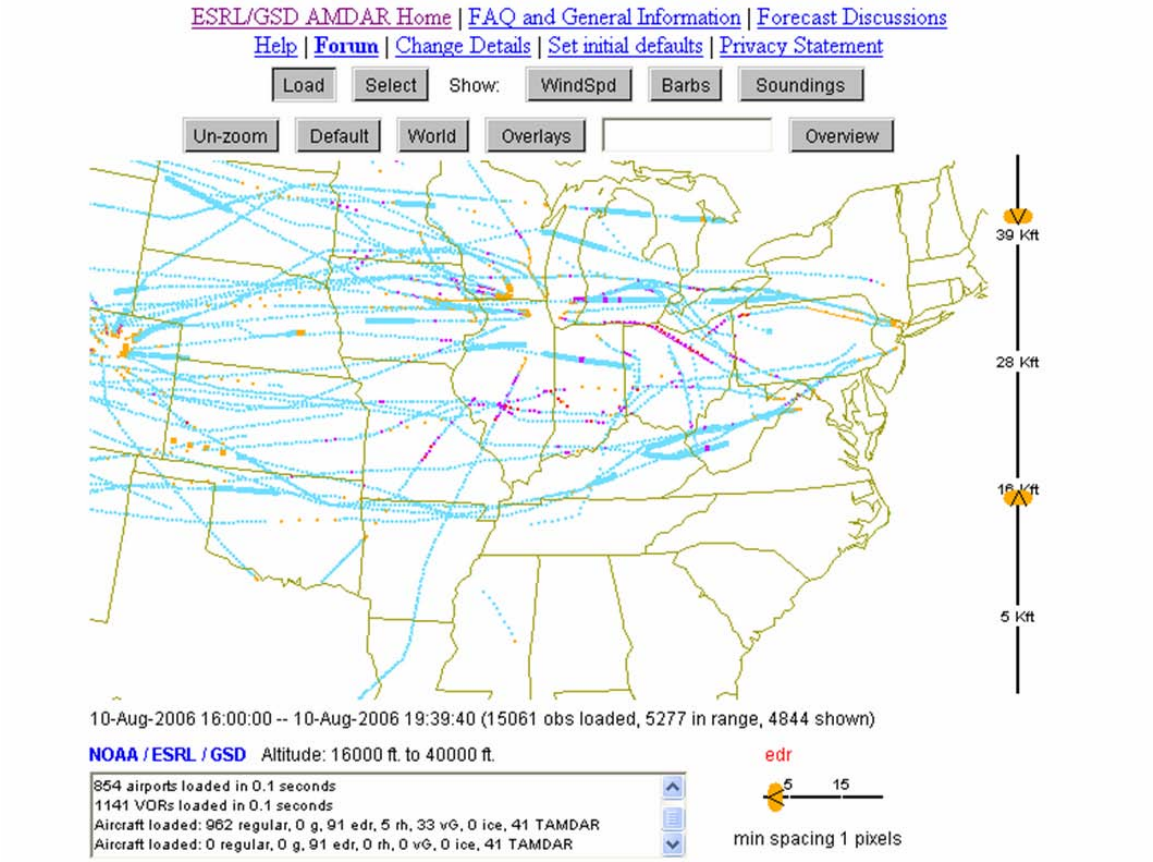

Figure 50. EDR observations from ESRL/GSD (2006) confirm the presence of turbulence in the convective areas shown in Figure 49.

The WSR-88D radar has additional functionality which can help in identifying turbulence favorable environments. This radar can provide unique, near real-time capabilities to detect and display turbulence indicators such as frontal boundaries, low-level jets, gust fronts, and upper-level wind shear (AFWA TN 98-002, 2005). Some of the WSR-88D products useful in turbulence forecasting are described here:

a. Spectrum Width

This WSR-88D radar product depicts a full 360 degree sweep of spectrum width data indicating a measure of velocity dispersion within the radar sample volume and is available for every elevation angle sampled (NWS 2006). The spectrum width provides a measure of the variability of the mean radial velocity estimates due to wind shear, turbulence, and/or the quality of the velocity samples. It is used to estimate turbulence associated with boundaries, thunderstorms, mesocyclones, and also to locate boundaries (cold front, outflow, lake breeze, etc.) (NWS 2006). Though not conclusive,

spectrum width values of 8-11 knots are often associated with moderate turbulence and values 12 knots or higher may indicate severe turbulence (AFWA TN 98-002, 2005). The spectrum width product can be used to confirm suspected turbulence areas found using other products.

b. Velocity Azimuth Display (VAD)

This product shows the radar derived wind speeds at various heights from 2,000 to 55,000 feet above the ground (NWS 2006). This product can allow the forecaster to examine the current and past vertical wind structure to help identify meteorological conditions associated with atmospheric turbulence evolving over time (e.g., inversions, wind shears, and development of jet streams). Look for areas of sharp turning in the winds with high wind speeds to identify strong local vertical wind shear (AFWA TN 98-002, 2005).

c. Base Velocity

This product displays horizontal wind velocities. Areas of sudden speed or directional shifts are associated with wind shear and atmospheric turbulence. Intense shear regions, such as the top of the thunderstorm associated with storm top divergence, can also be located using base velocity (AFWA TN 98-002, 2005).

d. Vertically Integrated Liquid (VIL)

The VIL is a property computed by the WSR-88D that takes into account the three-dimensional reflectivity of an echo (NWS 2006). The maximum VIL of a storm can be useful in determining the potential for severe convective weather and associated wind shear and turbulence (NWS 2006).

C. TURBULENCE DIAGNOSTICS

As was mentioned earlier, during the 1990's there was a strong advanced towards using automated diagnostics to predict possible turbulent areas. This effort led to the development of the GTG which has now surpassed the individual performance of any one of the diagnostics. However, the diagnostics can still provide useful information as discussed in Section C of Chapter III. In terms of forecasting, the automated diagnostics should be used when possible to help the forecaster understand the underlying causes of the turbulence (i.e., strong vertical wind shear, a jet core through a sharply curved ridge, a strong upper-level front, etc.). Recall, the Ellrod TI2 index (Ellrod and Knapp 1992) is

available through the JAAWIN site and is used by the AFWA for the strategic-level forecast product. The forecaster should utilize these automated diagnostic products for more specific turbulence forecasting. For example, if the Ellrod TI2 index showed that a region was favorable for turbulence, then the forecaster would know that strong vertical wind shear, deformation, and convergence were present for that area. In this sense, the automated diagnostics should not be used as a forecast of turbulence but used as guidance to the forecaster in the turbulence forecast approach.

D. MESOSCALE MODEL DATA

The primary function of the forecast models for turbulence forecasting is to animate those patterns and characteristics recognized as being favorable for turbulent conditions into the future. Again, because of the complex microscale nature of turbulence, turbulence forecasts should generally not be made for much more than 24 hours from forecast time and only mesoscale or smaller models should be considered. If a longer forecast is necessary, the forecaster should relay to the customer the high degree of uncertainty in the forecast and that essentially the forecast would have to be made based on pattern recognition in predicted fields such as the 72 hour forecast 300mb winds. A large scale model such as the GFS or NOGAPS should not be used in forecasting turbulence because of the large horizontal and vertical resolution of those models. The AFWA MM5, the NCEP's RUC-2, and the ETA model, as well as the new WRF model are all mesoscale models that are acceptable for use in the turbulence forecast approach.

Models have become extremely proficient at 24 hour prediction and so they should be utilized by the turbulence forecaster for short-term forecasts. The forecaster should first look for all the patterns and characteristics of the turbulence favorable environment (Section A of this chapter) in the forecast fields. If a pattern, such as a sharply curved trough with a strong jet core, is identified in the analysis the forecaster should pay special attention to how the model develops the pattern over the forecast period and use such guidance in making the final turbulence forecast. If no patterns were recognized in the analysis, the forecaster should look for the development of those patterns during the forecast period.

Not only should model forecast fields be considered, but also post-processed algorithms like the GTG should be utilized. The GTG is run on the RUC-2 model output and is a sum of the best automated diagnostics and weighted by current observations (PIREPs). It has been shown to be quite skillful in turbulence prediction, far superior to any automated diagnostic by itself, and even superior to many subjective human forecasts (Sharman et al. 2006). The GTG can provide grid-scale forecasts, which allow for much more specific horizontal and vertical resolution in the turbulence forecast than can be hand drawn on a 2-dimensional chart. As mentioned previously, the GTG forecast by flight level can be found at http://adds.aviationweather.gov/turbulence/ and is readily accessible to any user with online access. The AWC also offers a Flight Path Tool on this site which can be an extremely valuable tool to the aviation forecaster allowing the user to plot a cross section of any flight route he/she chooses with various variables such as turbulence displayed. Figure 51 shows a cross section with the GTG turbulence forecast plotted for an arbitrary flight path from approximately Offutt Air Force Base (AFB), NE to Shaw AFB, SC with a cruise level at FL300. The light green is predicted light turbulence areas, with the orange being predicted moderate turbulent areas and the black line shows the FL300 elevation line.

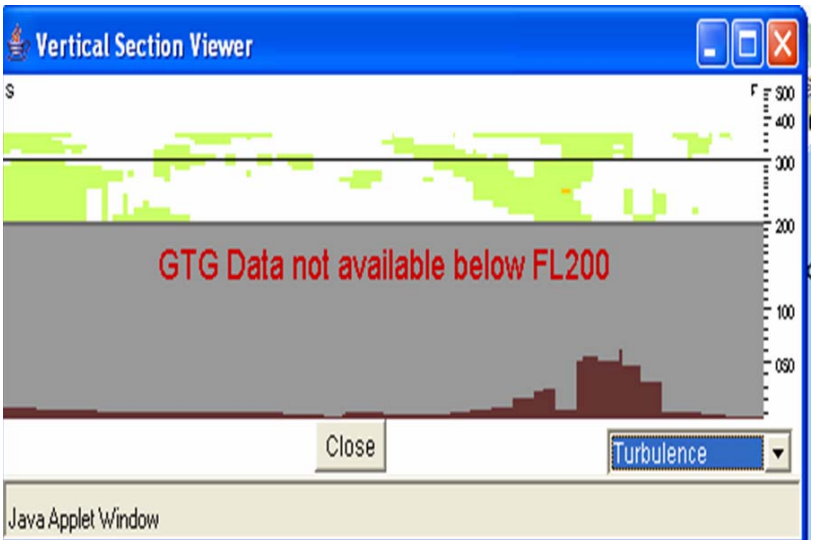

Figure 51. The light green is predicted light turbulence areas, the orange is predicted moderate turbulent areas and the black line shows the FL300 elevation line. Screen capture from http://adds.aviationweather.gov/flight_path/index.php (accessed 2006).

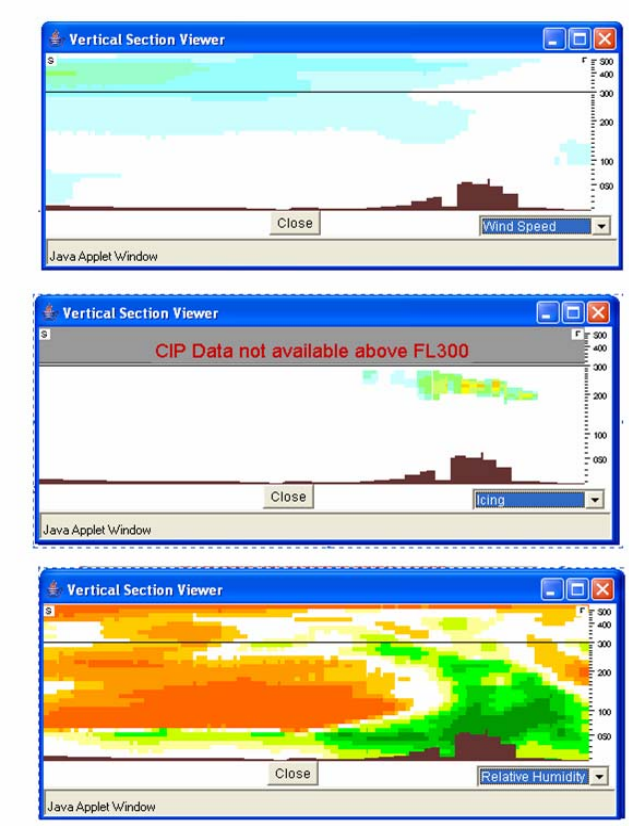

Figure 52. Same as in Figure 51 except with wind speed, icing, and relative humidity shown from top to bottom respectively. Screen capture from http://adds.aviationweather.gov/flight_path/index.php (accessed 2006).

All the GTG products which were used in several figures throughout this thesis were generated through the Flight Path Tool on the AWC turbulence site. On this site users can also overlay the GTG forecast with flight level wind barbs or look at the AWC icing forecast product.

As previously mentioned, the RUC-2 only forecasts to the 12-hour mark, and only covers CONUS. There is an ongoing effort to apply the GTG algorithm to the WRF model which will greatly expand the coverage and capability of the GTG, especially when combined with the ongoing effort to incorporate the EDR observations into the GTG algorithm (Sharman 2006). Until this happens, the GTG can and should still be used by CONUS forecasters to greatly enhance their turbulence forecast.

E. RECOMMENDED APPROACH

As mentioned previously the forecaster must first understand the current and past conditions of the atmosphere, before being able to predict the future state of the

atmosphere. Thus the forecaster should start with a complete analysis of past and current atmospheric conditions. The forecaster should use the patterns and characteristics identified in Section A of this chapter to locate regions with a favorable environment for turbulence. Once the forecaster has thoroughly analyzed and examined the current atmospheric conditions, current observations must be considered. Observations should be used to verify patterns and favorable areas identified in the forecaster's analysis, and to alert the forecaster of all reported turbulent areas. After the forecaster has analyzed and observed the atmosphere, he/she can then animate those patterns and regions into motion via the models and begin to form the forecast. In this process the forecaster should take advantage of automated turbulence diagnostics and models, specifically the GTG, to guide the forecaster to making the best possible turbulence forecast. When forecasters don't have access to automated turbulence diagnostics or the GTG, they should rely on their synoptic analysis, observations, and forecasted fields to form their turbulence forecast. Finally the forecaster should attempt to relay to the customer the uncertainty inherent to turbulence forecasting, and when possible should attempt to relay the uncertainty in each specific turbulence forecast.

THIS PAGE INTENTIONALLY LEFT BLANK

V. CONCLUSION

A. FINAL REMARKS

Turbulence is a significant problem for military and commercial aviation missions. For the years 1983-1997, turbulence contributed to 664 accidents leading to 609 fatalities, 239 serious and 584 minor injuries, for an estimated average annual societal cost of 134 million dollars (Eichenbaum 2000). Forecasting turbulence is difficult due to a lack of observations and due to the fact that turbulence is a microscale phenomenon which NWP models currently can not resolve. Progress in turbulence forecasting has been made with higher resolution models and with the understanding that turbulence is generated by the cascading down of energy from larger scale features resolvable by NWP models. Forecasters are left with examining synoptic features often associated with turbulence and combining those with their experience with automated computer aids to produce comprehensive turbulence analyses and forecasts. The development and implementation of EDR observations offer great potential into a more robust and complete turbulence observation system which could potentially increase model skill in forecasting turbulence. The GTG is currently the superior automated turbulence forecasting algorithm which produces a turbulence forecast for flight levels from 10,000 to 40,000 feet for all of CONUS. Plans are in progress to adapt the GTG algorithm to the new WRF model and to begin ingesting EDR observations into the procedure which could greatly increase its capability and coverage (Sharman 2006).

The guidance currently being used to forecast upper-level turbulence by USAF OWS personnel is AFWA TN 98-002 (2005) and some of the techniques and guidance in that manual are outdated resulting in the over-forecasting of turbulence at USAF OWSs (Schrumpf 2006). The perceived errors in AFWA TN 98-002 propagate through OWS's training curriculums (Schrumpf 2006). For this thesis a review of those techniques was performed along with a review of the most current techniques being used by alternative organizations such as the NOAA/NWS/AWC. New tools and guidance were presented in Chapter IV of this thesis which should allow the forecaster to produce the best possible upper-level turbulence forecast for USAF operations. An updated turbulence forecasting techniques manual based on AFWA TN 98-002 (2005) with the inclusion of the results of

this research was created and can be found in Appendix C. The new manual is designed to be a suggested replacement for the turbulence chapter (Chapter 2) of AFWA TN 98-002 (2005) and to be used as guidance for new USAF forecasters.

B. FUTURE RESEARCH

In the immediate future, research should be focused on developing a GTG type algorithm which the USAF can incorporate into its new WRF model package. EDR observations should be ingested in this algorithm to calibrate and weight the diagnostics. Since there is ongoing research and development in this area in the civilian sector, specifically at NCAR, the researcher would want to work closely with researchers from NCAR who have been developing the use of the GTG with the NWS version of the WRF model, and who have been working to maximize the utility of EDR observations and using them in the GTG.

Recall the two major factors that cause turbulence forecasting difficulty are lack of observations and the small scale (~100m) at which turbulence occurs is irresolvable by current NWP models. Logically, future research should be centered on addressing these two difficulties. There is constant ongoing research in developing higher resolution models and as noted earlier most of the progress in recent years has been in this factor. More research is needed on developing a more robust observing method for upper-level turbulence. EDR observations seem to offer a vast improvement over PIREPs, but still require aircraft to fly directly through the turbulence and still leave much of the atmosphere unobserved.

With the recent development and implementation of Unmanned Aerial Vehicles (UAVs) into USAF operations, research will be needed to study the effects turbulence will have on this generation of aircraft. UAVs are a much smaller and lighter framework than traditional aircraft, and consequently will likely be more sensitive to the effects of turbulence. Research could also consider using the UAVs as an additional tool to observe turbulence.

Finally, the complex nature of turbulence along with the small scale of its occurrence lends itself to being a prime candidate for ensemble type forecasting. The occurrence of turbulence is highly unpredictable and uncertain and this should be relayed

to the user via an ensemble-based forecast which can relay some of that uncertainty. Dutton (1980) finds that forecasts of CAT must be stated in terms of probability if they are to convey the maximum possible information to the user. This argument is made and supported by Cunningham (2006), who concludes ensemble-based probabilistic turbulence forecasts hold a distinct advantage over deterministic turbulence forecasts. An ensemble type turbulence forecast would give the user some idea of the uncertainty in the forecast which would potentially allow the user to make a much more informed decision.

THIS PAGE INTENTIONALLY LEFT BLANK

APPENDIX A: GTG TURBULENCE DIAGNOSTICS

The following lists the current suite of turbulence diagnostic algorithms within GTG taken from the NOAA NWS Aviation Weather Center (AWC). Although all these are or have been computed and evaluated, only a (user selectable) subset is actually included in the GTG combination. Note in some cases the constituent components of a diagnostic are also used as an index.

1. Richardson number and its components (e.g., Endlich 1964, Kronebach 1964, Dutton and Panofsky, 1970, Drazin and Reid, 1981, etc). Theory and observations have shown that at least in some situations clear-air turbulence patches are produced by Kelvin-Helmholtz (KH) instabilities. This occurs when the Richardson number (*Ri*) becomes small. Therefore, theoretically, regions of small Ri should be favored regions of turbulence.

   $Ri = N^2 / S_V^2$,

   where N^2 = Static stability = $g/\theta(\partial\theta/\partial z)$

   and S_V =Vertical wind shear= $| (\partial u/\partial z)^2 + (\partial v/\partial z)^2|^{1/2}$

   where θ is potential temperature, g is the acceleration due to gravity, z is the vertical direction, and u,v are the east-west, north-south velocity components respectively.

2. Colson-Panofsky index (Colson and Panofsky 1965). This index uses simple turbulence energy production and dimensional arguments in a stable atmosphere to derive clear-air turbulence intensities as

   $I_{CP} = \lambda^2 S_V^2 (1 - Ri/Ricrit)$,

   where $\lambda \sim \Delta z$ is a length scale, and Ricrit is an empirical constant (≈ 0.5).

3. Laikthman-AlterZalik index (Laikthman and Al'ter-Zalik 1966, also Vinnichenko, et. al., 1980). This is another tke equation but with a length scale derived from the von Karman formula.

   $\Phi = S_V^2 - \alpha N^2 > 0$, where $\alpha = 1/Pr = K_H/K_M$ = adjustable constant

   $tke = C \Phi^{3/2} / d\Phi/dz$, C is an adjustable constant

4. DTFs (Marroquin 1998). The DTFs (Diagnostic TKE Formulations) use k-ε closure equations (e.g. Stull 1988) and other simplifications to derive diagnostics for tke and/or ε. For DTF3

$$\varepsilon = K_M \left(\frac{c_1}{c_3} S_V^2 - \frac{c_2}{c_3} \frac{N^2}{\mathrm{Pr}}\right)$$

where c_1=1.44, c_2=1.0, c_3=1.92 (Stull, 1988 p. 219) , and K_M and $Pr = K_M / K_H$ are taken as adjustable constants to get best agreement with observations.

5. Eddy dissipation rates estimated from of second-order structure functions (Frehlich and Sharman 2004a, 2004b). The structure function of a variable q is defined as

$$D_q(s) = <[q(x) - q(x+s)]^2>$$

where <> denotes an ensemble average. It is common practice to denote the longitudinal velocity [velocity component parallel to the displacement vector **s**=(*x*,*y*,*z*)] structure function as $D_{LL}(s)$ and the transverse velocity (velocity component normal to **s)** structure function as $D_{NN}(s)$. For 2D or 3D isotropic turbulence $D_{NN}(s)$ is related in a simple way to $D_{LL}(s)$ (e.g., Lindborg 1999), and both are related to turbulence intensity as measured by ε through

$$D_{LL}(s) \propto C_L \, \varepsilon^{2/3} s^{2/3}$$
$$D_{NN}(s) \propto C_N \, \varepsilon^{2/3} s^{2/3}$$

where C_L *and* C_N are universal constants. Longitudinal and transverse structure functions are computed from NWP *u*, *v* and *w* fields and averaged horizontally and over three vertical levels. The values of the average structure functions are then used to derive estimates of $\varepsilon^{1/3}$ on *u* and *v*, and σ_w for the vertical velocity component.

6. Frontogenesis function. Fronts contain regions of low *Ri* and therefore may be conducive to turbulence (e.g., Jacobi et al. 1996) and can also be a source of gravity waves that may be unstable (e.g., Lane et al. 2004). The definition of the frontogenesis function is (e.g., Bluestein, 1992, vol. 2, p. 253)

$$F = \frac{D}{Dt}|\nabla\theta|$$

where $\frac{D}{Dt}$ is the Eulerian time derivative.

This can be rewritten in two dimensions using the thermal wind relation as

$$F \propto \frac{D}{Dt}\left[\left(\frac{\partial u}{\partial\theta}\right)^2 + \left(\frac{\partial v}{\partial\theta}\right)^2\right]^{\frac{1}{2}} = \frac{1}{\left|\frac{\partial\vec{v}}{\partial\theta}\right|}\left[\frac{\partial u}{\partial\theta}\frac{D}{Dt}\left(\frac{\partial u}{\partial\theta}\right) + \frac{\partial v}{\partial\theta}\frac{D}{Dt}\left(\frac{\partial v}{\partial\theta}\right)\right]$$

Expanding on a constant θ surface and invoking continuity gives

(a) $$F_\theta \propto -\left[\frac{\partial u}{\partial\theta}\left(\frac{\partial u}{\partial\theta}\frac{\partial u}{\partial x} + \frac{\partial v}{\partial\theta}\frac{\partial u}{\partial y}\right) + \frac{\partial v}{\partial\theta}\left(\frac{\partial u}{\partial\theta}\frac{\partial v}{\partial x} + \frac{\partial v}{\partial\theta}\frac{\partial v}{\partial y}\right)\right]$$

This is the form used in GTG at upper levels. Note that its formulation is based on an isentropic coordinate system (as used at upper levels in the RUC model), and will not

be valid for other coordinate systems, e.g. a sigma coordinate system. In that case an alternative is to use the second equation cast on constant pressure (p) surfaces as

(b) $$F_p \propto \frac{\partial u}{\partial p}\frac{D}{Dt}\left(\frac{\partial u}{\partial p}\right)+\frac{\partial v}{\partial p}\frac{D}{Dt}\left(\frac{\partial v}{\partial p}\right)$$

This is the form used in GTG at mid-levels.

5. SCATR index, dRi/dt (Roach 1970, Keller 1990). This index is based on attempts by several investigators to forecast turbulence by using a time tendency (i.e. prognostic) equation for the Richardson number. The version used in this study was based on a formulation of this equation in isentropic coordinates by Keller, and termed SCATR (Specific CAT Risk).

   SCATR = $\Phi\ S_V^2$ /24

   with $\Phi = 2/\ S_V^2\ F - \Delta_H$

   Δ_H = horizontal divergence =$(\partial u/\partial x) + (\partial v/\partial y)$

   and F is the frontogenetic function.

6. Brown's index (Brown 1973). This index is a simplification of the Ri tendency equation originally derived by Roach (1970). The simplifications involve use of the thermal wind relation, the gradient wind as an approximation to the horizontal wind and some empiricism. Form (a) is the simplified Ri tendency equation, while form (b) is an extension of (a) to provide a measure of turbulence intensity.

   (a) $$\Phi = (0.3\ \zeta_a^2\ + D_{SH}^2\ + D_{ST}^2\ )^{1/2}$$

   (b) $$\varepsilon = \Phi\ S_V^2\ /24$$

   D_{SH} = shearing deformation = $(\partial v/\partial x) + (\partial u/\partial y)$

   D_{ST} = stretching deformations = $(\partial u/\partial x) - (\partial v/\partial y)$

   ζ_a = absolute vorticity = $\zeta + f$,

   $\zeta = (\partial v/\partial x) - (\partial u/\partial y)$,

   and f is the Coriolis frequency.

7. Ellrod indices (Ellrod and Knapp 1992). This index is derived from simplifications to the frontogenetic function. As such it depends mainly on the magnitudes of the potential temperature horizontal gradient (proportional to S_V through the thermal wind relation) and deformation. Two variants were developed:

   (a) TI1 = S_V DEF

(b) $TI2 = S_V \ (DEF - \Delta_H)$

where $DEF = (D_{SH}^2 + D_{ST}^2)^{1/2}$,

8. Potential vorticity (PV) or horizontal gradient of PV (Shapiro, 1978)

   (a) PV

   (b) $|\nabla PV|$,

   where $PV = -\zeta_a \, \partial\vartheta/\partial p$

9. CCAT index (Vogel and Sampson 1996). The CCAT (Clark's Clear Air Turbulence) index has been used by the US Navy's FNMOC for at least two decades.

$$CCAT = (g/T) \text{ X } (\zeta_a /f) \text{ X } (\mathbf{v} \bullet \nabla |dT/dz|)$$

10. Curvature measures. Tight curvatures in upper level troughs and ridges have been empirically related to turbulence outbreaks (e.g., Lester 1994, Hopkins 1997, Arakawa 1952, and Stone 1997). A measure of curvature is relative vorticity, ζ, with a maximum (positive value) in upper level troughs and a minimum (negative value) in upper level ridges. Therefore $|\zeta|^2$ should be a measure of curvature in both troughs and ridges.

   (a) $$\zeta^2 = |\nabla \times \mathbf{v}_H|^2$$

   Another measure may be related to inertial instability in strongly anticyclonic flows (Arakawa 1952, Stone 1966, Knox 1997)

   (b) $$f[f(1-1/Ri) + \zeta] < 0$$

10. Horizontal temperature gradient. This is a measure of the deformation and also vertical wind shear from the thermal wind relation, and is routinely used by airline forecasters. It was also used in Buldovskij et. al. (1976).

$$|\nabla_H T| = \sqrt{|\partial T/\partial x|^2 + |\partial T/\partial y|^2}$$

11. Dutton's empirical index (Dutton 1980). This index is based on linear regression analyses of a pilot survey of turbulence reports over the N. Atlantic and NW Europe during 1976 and various synoptic scale turbulence indices.

$$E = 1.25 \, S_H + 0.25 \, S_V^2 + 10.5$$

   where the constants are empirically determined by Dutton.

12. Endlich empirical wind index (Endlich, 1964). A limited amount of observations of CAT in jet streams indicated turbulence tended to be associated with both high max winds and directional wind shear, thus

$|\mathbf{v}|\ |d\psi/dz|$, ψ = wind direction

13. MOSS predictors (Reap 1996). These indices are a subset of a suite of turbulence diagnostics used in the NGM-based probability forecasts.

    (a) DEF $|\mathbf{v}|$

    (b) DEF $|dT/dz|$

14. Unbalanced flow diagnostics (McCann 1997, Knox 1997, O'Sullivan and Dunkerton 1995, Koch and Caracena 2002). Flow imbalances due to nongeostrophy will generate inertia-gravity waves (IGWs). The processes by which IGWs may lead to turbulence is an active area of research, but empirically there is some evidence that regions of strong imbalance may be related to turbulence aloft (e.g., Knox 1997; McCann 2001; Koch and Caracena 2002). The UBF diagnostic formulation used within GTG2 is that developed by Koch and Caracena (2002) and McCann (2001). Koch's implementation adds a filter step, which helps performance considerably. In either case the diagnostic is the residual *R* of the nonlinear balance equation

(a) $$R = -\nabla^2\Phi + 2J(u,v) + f\zeta - \beta u$$

where Φ is geopotential, J is the Jacobian operator, and β is the Coriolis frequency gradient.

The Lagrangian Rossby Number (RoL) is another unbalanced flow diagnostic originally suggested by van Tuyl and Young (1982). Following the definition of Ro in Bluestein (1992, eqn. 4.1.93) and evaluating it in isentropic coordinates gives

(b) $$RoL = \frac{|D\vec{v}/Dt|}{|f\,\vec{v}|} \approx \frac{|\vec{v}\bullet\nabla\vec{v}|}{|f\,\vec{v}|} \approx \frac{\left|-\nabla M - f\hat{k}\times\vec{v}\right|}{|f\,\vec{v}|}$$

where M is the Montgomery stream function.

The magnitude of the vertical velocity $|w|$ is also a measure of unbalanced flow. It is computed from the RUC vertical pressure velocity ω,

(c) $$w = -\omega/(\rho g),$$

where ρ is the local atmospheric density.

Other measures developed by McCann (2001) include

(d) $$\text{ABSIA} = |v_i - v_c|^2,$$

where $v_i = |\mathbf{v}\bullet\nabla\mathbf{v}|/f$ and $v_c = K_s|\mathbf{v}|^2/f$,

(e) $$\text{AGI} = \zeta_{curv} + f/2,$$

with $\zeta_{curv} = K_s|\mathbf{v}|$, K_s = streamline curvature

15. North Carolina State University Index (NCSU1) is described in Kaplan et al. (2004), and was developed as a result of several turbulence accident investigations.

$$NCSU1 = MAX\left(u\frac{\partial u}{\partial x} + v\frac{\partial v}{\partial y}, 0 \right) \left| \nabla \zeta \right| / Ri$$

16. Negative vorticity advection (NVA). A rule-of-thumb forecasting approach used by the airlines is to look for regions of large NVA computed as follows (Bluestein, 1992, Vol. 1, p. 335):

$$NVA = MAX\left\{ \left[-u\frac{\partial}{\partial x}(\zeta + f) - v\frac{\partial}{\partial y}(\zeta + f) \right], 0 \right\}$$

APPENDIX B: SYNOPTIC PREDICTOR FIELDS

1. Immediate upstream curvature
2. Entrance/exit region of the jet stream
3. Sign of omega
4. Lapse rate ≥ moist adiabatic
5. Direction of the ageostrophic wind vector
6. Sign of the horizontal temperature advection
7. Sign of the horizontal advection of the total wind velocity shear
8. Vertical variation of the brunt-vaisala frequency > threshold value
9. Flight level absolute vorticity ≤ 10^{-4} s^{-1}
10. Absolute vorticity averaged over two levels ≤ 10^{-4} s^{-1}
11. Flight level relative vorticity ≤ 0 s^{-1}
12. Relative magnitude of isobaric pv terms
13. Vertical total wind shear > threshold value
14. Relative humidity ≥ 50%
15. Sign of horizontal advection of the vertical lapse rate
16. Ageostrophic wind velocity ≥ threshold value
17. Vertical variation of the Richardson number ≥ threshold value
18. Vertical variation of the total wind velocity shear ≥ threshold value
19. Richardson number ≤ threshold value
20. Convective clouds (all bases) < 100 km from accident location
21. Convective clouds (all bases) < 30 km from accident location
22. Ellrod index values (Ellrod and Knapp 1992)
23. NCSU modification of the Ellrod index (Ellrod index/ipv)

(Taken from Table 9 in Kaplan et al. 2002)

THIS PAGE INTENTIONALLY LEFT BLANK

APPENDIX C: FORECASTING TECHNIQUES MANUAL

This appendix is intended to be used as an updated turbulence forecasting techniques manual and is based on AFWA TN 98-002 (2005) with the inclusion of the results of this research. It is the suggested replacement for the turbulence chapter (Chapter 2) of AFWA TN 98-002 (2005). The process of how this manual was developed was described throughout this thesis. The manual is designed for operational use and will not include such discussions.

The guidance provided by AFWA TN 98-002 is not entirely outdated. Much of the material in the turbulence chapter of this manual is still quite accurate and true. The definition, description, categories, intensities, and aircraft dependence are described particularly well by AFWA TN 98-002 (2005). Therefore, those sections which are still current (wake turbulence, intensity categories, aircraft dependence) have been merged together with those sections which were revised and added. The updating of this manual mainly applied to the forecasting guidance and rules of thumb given in AFWA TN 98-002 (2005) as well as focusing on the major causes of clear-air turbulence (CAT) associated with the jet stream and replacing the emphasis on 500mb and surface analyses with an emphasis on upper-level (200-300mb) analyses. There were a few organizational changes as well. This new manual starts with a definition and description of turbulence, followed by a discussion of turbulence intensities, aircraft sensitivities, forecasting difficulties, observations, dynamics and associated synoptic conditions, automated diagnostics, the Graphical Turbulence Guidance (GTG) system, and finally the suggested turbulence forecast approach. This new organization is intended to provide a more fluent flow and increased clarity and understanding.

I. TURBULENCE

A. DEFINITION AND DESCRIPTION

Turbulence is the gustiness superimposed on the mean wind. These rapid, turbulent fluctuations in vertical velocity, horizontal velocity, temperature, humidity, and pressure about their mean values are random. Therefore, we cannot hope to forecast clear-air turbulence (CAT) exactly. Instead, the forecaster is limited to a statistical description of CAT (Lee et al. 1984). The unexpected air movement associated with turbulence can cause serious damage to aircraft and potentially injure aircrew members and passengers.

Turbulence is created by abrupt, irregular movements of air that create sharp, quick updrafts and/or downdrafts acting to dissipate gradients of kinetic energy. These updrafts and downdrafts occur in combinations and move aircraft unexpectedly. There are two basic atmospheric conditions that cause turbulence: thermal conditions (surface heating) and mechanical mixing.

1. Thermal Conditions

Surface heating can generate turbulent conditions. As solar radiation heats the surface, the air above it is warmed by contact. Warmer air is less dense, and "bubbles" of warm air rise upward as updrafts. Uneven surface heating, and the cooling of rising air, allows for areas of downdrafts as well. These vertical motions may be restricted to low levels, or may generate cumulus clouds that can grow to great heights as thunderstorms. When these vertical motions are restricted to the boundary layer and lower levels, they can create seemingly random areas of turbulence commonly referred to as boundary layer turbulence. When and if these vertical motions do break through the boundary layer they can generate cumulus clouds that can grow to great heights as thunderstorms. Within these thunderstorms, intense updrafts can exist alongside intense downdrafts. This is another prime area for turbulence, appropriately referred to as convective turbulence. Convective turbulence is often found in and around thunderstorms, especially strong and severe storms where deep convection is persistent.

2. Mechanical Mixing

Mechanical turbulence is caused by horizontal and vertical wind shear and is the result of pressure gradient differences, terrain obstructions, and/or frontal zone shear. The jet stream and upper-level fronts are most commonly associated with this type of turbulence. In both regions, strong horizontal and vertical wind shear is likely and can lead to the generation of turbulence.

Figure 53 shows a major form of shear turbulence which develops in a flow changing speed so rapidly in a given direction that smooth flow is no longer dynamically possible.

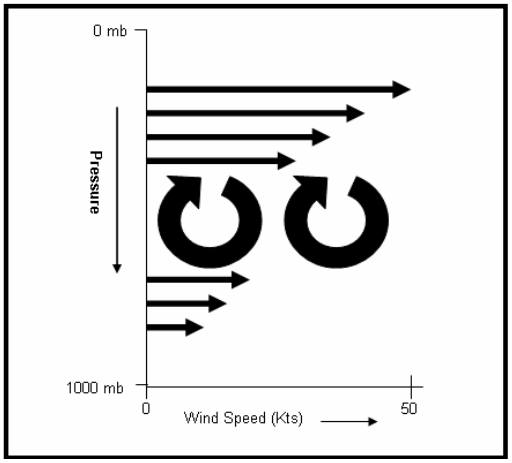

Figure 53. Example of turbulence generated by vertical wind shear. The great vertical variation in the speed of the flow turns smooth flow into turbulent eddies.

This shearing can occur in both the vertical, and the horizontal, and can occur due to both directional and speed changes in the wind. In operational forecasting, vertical speed shear is predominantly the major challenge and of the most importance (Holcomb 1976). This type of turbulence is commonly referred to as clear-air turbulence (CAT), because it often occurs in the upper troposphere in the absence of any clouds, and commonly in the presence of the jet stream, or upper-level fronts. Vertical speed shear in jet-stream flow can be found both below and above the jet maximum, where wind speed decreases rapidly in the vertical away from the jet core. Most turbulence forecasts made above 10,000 feet are for areas where intense shear is present, and therefore CAT is likely.

Strong vertical wind shear within a stable layer can lead to the development of Kelvin-Helmholtz waves, a phenomenon that resembles a breaking ocean wave. The breaking of these waves can be a principal mechanism responsible for CAT. The presence of these waves is often marked by “billow” wave-cloud formations (Ludlam 1967) which can be observed in satellite imagery or radar (Ellrod and Knapp 1992).

Mountain wave turbulence is another form of mechanical turbulence caused by terrain obstructions, which force flow around the terrain and can cause wave like patterns (turbulence) to develop in the flow as shown in Figure 54. Local terrain can magnify gradient winds to cause strong winds and turbulence near the surface, which creates eddy currents that can make flight operations hazardous. Strong turbulence is often associated with irregular and mountainous terrain. The greater the irregularity of the terrain and the sharper the slope of the mountains, the greater the intensity and vertical extent of the turbulence will be.

Figure 54. Example of turbulence induced by terrain (UCAR, 2005a).

3. Wake Turbulence

A final form of turbulence not really associated with thermal or mechanical turbulence is wake turbulence. Although neither forecasted nor recorded in a Terminal Aerodrome Forecast (TAF), wake turbulence is a problem with the increased use of heavy aircraft. The forecaster should be aware of how wake turbulence forms and be aware of its effects.

a. Characteristics

Every aircraft generates two counter-rotating wingtip vortices. Wake turbulence results when an aircraft encounters vortices from another aircraft. Vortex generation begins when the nose wheel lifts off the ground and ends when the nose touches back down again during landings. A vortex forms at each wingtip as air circulates outward, upward, and around the wingtip. The diameter of the vortex core varies with the size and weight of the aircraft.

These vortices can be 25 to 50 feet in diameter with a much larger area of turbulence. They usually stay fairly close together (about 3/4 of the wing span) until dissipation. They sink at a rate of 400 to 500 feet per minute and stabilize about 900 feet below the flight path, where they begin to dissipate. Vortex size is reduced by the use of winglets, smaller “wings” that curve upward from aircraft wing tips.

b. Dissipation

Atmospheric turbulence increases the dissipation of wake turbulence while ground effect and surface winds alter the low-level vortex characteristics only slightly. As the vortex sinks into the boundary layer, it begins to move laterally at about 5 knots. A crosswind will decrease the lateral movement of a vortex moving toward the wind and increase the movement of a vortex moving with the wind. This could hold one of the vortices over the runway for an extended period or allow one to drift onto a parallel runway. Vortices persist longer during inversions. Listed below are some rules for avoiding wake turbulence from the Federal Aviation Administration (FAA) Aeronautical Information Manual:

• Stable conditions combined with a crosswind of about 5 knots may keep the upwind vortex over the runway for periods of up to 15 minutes.

• Vortex generation begins with lift-off and lasts until touchdown. Therefore, aircraft should avoid flying below the flight path of a recent arrival or departure.

• If two aircraft fly in the same direction within 15 minutes of each other, the second should maintain an altitude equal to or higher than the first. If required to fly slightly below the first, the second aircraft should fly upwind of the first.

4. Gravity Waves and Stratospheric Turbulence

Stratospheric CAT and tropospheric CAT are fundamentally different. Tropospheric CAT is primarily caused by deformations in the horizontal wind field and vertical wind shears. "Breaking" of gravity or buoyancy waves causes stratospheric CAT. A gravity wave is generated when an air parcel at equilibrium with its environment is rapidly displaced vertically and then continues to oscillate in an up-and-down motion as the parcel tries to get back to its equilibrium state. This can happen over mountain ranges for example and result in mountain waves (gravity waves caused by the complex terrain of mountain ranges). Severe weather events, convection, and jet streams also generate gravity waves. Some general rules of thumb regarding gravity waves are:

- Gravity waves that propagate into the stratosphere grow in amplitude due to decreasing air densities.
- Organized deep convection can generate gravity waves that break in the stratosphere and generate turbulence.
- Stratospheric-breaking mountain waves on the order of 10 to 100 km wavelength typically generate turbulence felt by aircraft.
- Typical wavelengths of gravity waves are: 5 to 5000 km horizontally and .1 to 5 km vertically and they can last anywhere from 5 minutes to over a day.

B. INTENSITIES

There is currently no standardized method of categorizing turbulence intensities. Different agencies use slightly different categorization methods. The Air Force currently uses the following intensity definitions where the levels of turbulence intensity are based on the impact to aircraft flying through the area of concern:

1. Light Turbulence

The aircraft experiences slight, erratic changes in attitude and/or altitude, caused by a slight variation in airspeed of 5 to 14 knots with a vertical gust velocity of 5 to 19 feet per second. Light turbulence may be found in many areas, such as:

• At low altitudes in rough terrain when winds exceed 15 knots.

• In mountainous areas, even with light winds.

• In and near cumulus clouds.

• Near the tropopause.

2. Moderate Turbulence

The aircraft experiences moderate changes in attitude and/or altitude, but the pilot remains in positive control at all times. The aircraft encounters small variations in

airspeed of 15 to 24 knots; vertical gust velocity is 20 to 35 feet per second. Moderate turbulence may be found:

- In towering cumuliform clouds and thunderstorms.
- Within 100 nm of the jet stream on the cold air side.
- At low altitudes in rough terrain when the surface winds exceed 25 knots.
- In mountain waves (up to 300 miles leeward of Ridge), winds perpendicular to the Ridge exceed 50 knots.
- In mountain waves as far as 150 miles leeward of the Ridge and 5,000 feet above the tropopause when wind perpendicular to the Ridge is 25 to 50 knots.

3. Severe Turbulence

The aircraft experiences abrupt changes in attitude and/or altitude and may be out of the pilot's control for short periods. The aircraft encounters large variations in airspeed greater than or equal to 25 knots and the vertical gust velocity is 36 to 49 feet per second. Severe turbulence occurs:

- In and near mature thunderstorms.
- Near jet stream altitude and about 50 to 100 miles on the cold-air side of the jet core.
- In mountain waves (up to 50 miles leeward of Ridge), winds perpendicular to Ridge are 25 to 50 knots.
- Up to 150 nm leeward of the Ridge and within 5,000 feet of the tropopause when a mountain wave exists and winds perpendicular to the Ridge exceed 50 knots.

4. Extreme Turbulence

The aircraft is violently tossed about and is practically impossible to control. Structural damage may occur. Rapid fluctuations in airspeed are the same as severe turbulence (greater than or equal to 25 knots) and the vertical gust velocity is greater than or equal to 50 feet per second. Though extreme turbulence is rarely encountered, it is usually found in the strongest forms of convection and wind shear. The two most frequent locations of extreme turbulence are:

- In mountain waves in or near the rotor cloud.
- In severe thunderstorms, especially in organized squall lines.

C. AIRCRAFT TURBULENCE SENSITIVITIES

Another complexity with observing and forecasting turbulence arises from the wide variation in aircraft the USAF and commercial airlines operate. Because there are so many different aircraft, each with large differences in weight, structural design, and capabilities, each type of aircraft will experience turbulence in different ways.

Table 6 lists the categories for most military fixed-wing and rotary-wing aircraft at their typical flight configurations. Turbulence forecasts in TAFs are specified for Category II aircraft. Modify the local turbulence forecast for the type of aircraft supported. Use caution, however; an aircraft's sensitivity varies considerably with its weight (amount of fuel, cargo, munitions, etc.), air density, wing surface area, wing sweep angle, airspeed, and aircraft flight "attitude."

Since aircraft sensitivity to turbulence varies considerably, use caution when applying forecast turbulence (Category II) to a specific aircraft type, configuration, and

mission profile. Table 7 is a guide to convert turbulence intensities for the different categories of aircraft.

Table 6. Aircraft category type from Table 2.7 in AFWA TN 98-002 (2005).

Category	Aircraft Type			
I	OH-58	UH-1	AH-1	
II	C-141	C-9	RAH-66	C-12
	C-21	F-106	C-20	C-5A
	E-4A	F-15	AH-64	B-52
	C-130	C-17	F-117	F-16
	KC-135	C-23	CH-47	U-21
	OV-1	CH-3	UH-60	CH-53
	CH-54	VC-137	T-38	
III	OV-10	KC-10	T-37	A-10
IV	A-7	F-4	B-1B	F-111*

* At 50 degree wing configuration.

Table 7. Turbulence intensities for different categories of aircraft based on Table 6 and taken from Table 2.8 in AFWA TN 98-002 (2005). For example, what a Category I aircraft might report as Moderate turbulence may only be Occasional Light turbulence for a Category IV aircraft.

	I	II	III	IV
	N	N	N	N
	(L)	N	N	N
	L	(L)	N	N
	L-(M)	L	(L)	N
Turbulence	M	L-(M)	L	(L)
Reported As	M-(S)	M	L-(M)	L
	S	M-(S)	M	L-(M)
	S-(X)	S	M-(S)	M
	X	S-(X)	S	M-(S)
	X	X	S-(X)	S
	X	X	X	S-(X)
	X	X	X	X

N = None ( ) = Occasional (less than 1/3 of the time)
L = Light M = Moderate S = Severe X = Extreme

Note: Use caution when converting extreme turbulence reports between various aircraft types. Extreme turbulence causes a range of effects from a minimum threshold (rapid airspeed fluctuations greater than 25 knots) to a maximum threshold (structural damage). Even though the table considers this, the design is more for the sake of "completeness" rather than observational or scientific evidence.

1. Fixed Wing Aircraft

Generally, the effects of turbulence for fixed-wing aircraft are increased with:

- Non-level flight.
- Increased airspeed.
- Increased wing surface area.
- Decreased weight of the aircraft.
- Decreased air density (increased altitude).
- Decreased wing sweep angle (wings more perpendicular to fuselage).

2. Rotary Wing Aircraft

Generally, the effects of turbulence for rotary-wing aircraft are increased with:

- Increased airspeed.
- Decreased weight of the aircraft.
- Decreased lift velocity (the faster the lift-off, the less the turbulence).
- Increased arc of the rotor blade (the longer the blade, the greater the turbulence).

D. FORECASTING DIFFICULTIES

Problems encountered in forecasting turbulence include the large temporal and spatial scales of the observation network, the reliability of pilot reports, and the short-lived, random nature of turbulence. Turbulence is a microscale phenomenon in an atmosphere where existing observations are made at the mesoscale at best (Lee et al. 1984). CAT forecasters are left with examining synoptic features often associated with CAT and combining those with their experience with automated computer aids to produce comprehensive CAT analyses and forecasts (Lee et al. 1984).

There are essentially two main factors which make forecasting turbulence difficult: (1) lack of observational turbulence data and (2) turbulent eddies at the scales which affect aircraft (~100m) are a microscale phenomenon and numerical weather prediction (NWP) models cannot resolve that scale (Abernethy and Sharman 2006).

Over the past half-century most of the progress made in turbulence forecasting has been in increased model resolution and improved eddy simulation and understanding. These improvements are predicated on the idea that most of the energy associated with turbulent eddies at aircraft scales cascades down from larger scales of atmospheric motion (Dutton and Panofsky 1970; Abernathy and Sharman 2006). Upon this realization, the effort was focused on linking large-scale features, easily resolvable by NWP models, to the formation of turbulent microscale eddies. In this process a vast assortment of diagnostics or empirical based rules of thumb (also referred to as algorithms, indexes, etc.) have been created to describe and predict turbulence. The skill of each of these diagnostics' ability to forecast upper-level turbulence is highly variable. None of the diagnostics offer a completely satisfactory method of forecasting turbulence, but rather reflect the imperfect understanding of the atmospheric processes involved.

In recent years there has been a focused effort on developing an automated turbulence forecasting system. The first major development came in 2000 with the Integrated Turbulence Forecasting Algorithm, developed by the Turbulence Product Development Team (TPDT) under sponsorship from the FAA/AWRP, NCAR/RAL, and NOAA's Forecast Systems Laboratory (NOAA/FSL). There were automated turbulence forecasting systems before this, but they were mainly just an automated calculation of one of the common diagnostics. For example, the Air Force Weather Agency uses the

MM5 model to produce a turbulence forecast by calculating the Ellrod II diagnostic (Ellrod and Knapp 1992) using the model output data and displaying a map of where the Ellrod diagnostic predicts turbulence. The Ellrod index is simply defined as the wind shear times the sum of the horizontal deformation and convergence. But the ITFA took into consideration several of the diagnostics. Soon after the ITFA was developed, it was implemented, and became known as the Graphical Turbulence Guidance (GTG) forecasting product. The diagnostics currently being used in the GTG can be found in Sharman et al. (2006), and the GTG will be discussed in more detail later.

E. OBSERVATION ISSUES

Turbulence which affects flight operations most often occurs as a microscale phenomenon making it very difficult to observe. There is no current observing system with the horizontal and vertical resolution to accurately observe turbulence. Such a system would require, at the very least, less than a kilometer resolution.

1. PIREPs

"Currently, the best available real-time information concerning turbulence comes from pilot reports (PIREPs)." (Takacs 2006) The reports include the date and time, latitude and longitude, altitude, and severity, as determined by the pilot, of the turbulence encounter. Unfortunately, there is no consistent objective measurement technique allowing for regular observations of turbulence. Airplanes encountering turbulence are the only source of observations available to weather personnel. Because of the irregular time and spatial distribution of airplane routes, the observations are just as irregular, providing a less than reliable observation system with intense coverage over certain regions and very poor coverage over other regions.

Furthermore, the objectivity and accuracy of the observations are to be questioned. PIREPs of turbulence are made by the pilots themselves, as they are requested to log turbulence encounters and identify intensity based on their own experience or impressions. What may be a "severe" encounter with turbulence for one pilot may be a "light-moderate" turbulence for another pilot (Tebaldi 2002). The lack of null reports or smooth reports from pilots is unfortunate. The majority of PIREPs are made for light turbulence or greater. In areas where there are huge data gaps, the forecaster then has to guess whether there were no flights in this area to report turbulence, or whether the pilot did not experience any turbulence and made no report. In either case, the forecaster cannot conclude whether there is turbulence in the area or not. The majority of pilots are trying to avoid turbulence as much as possible in order to have as smooth as flight as possible. For these reasons it is important for the forecaster to understand the distribution of PIREPs is not a true representative of the state of the atmosphere because most non-turbulent areas are not reported and many turbulent areas may go unreported. It is equally important for the forecaster to understand PIREPs can be utilized to identify regions where turbulence has been occurring and can provide a subjective assessment of how intense the turbulence was for the area (as shown in Figure 55.)

Despite the disadvantages of using PIREPs for the verification of turbulence forecasting techniques, few other better options are currently available to researchers and operational meteorologists. Automated turbulence observations, however, from aircraft will enhance the available PIREP database (Cunningham 2006).

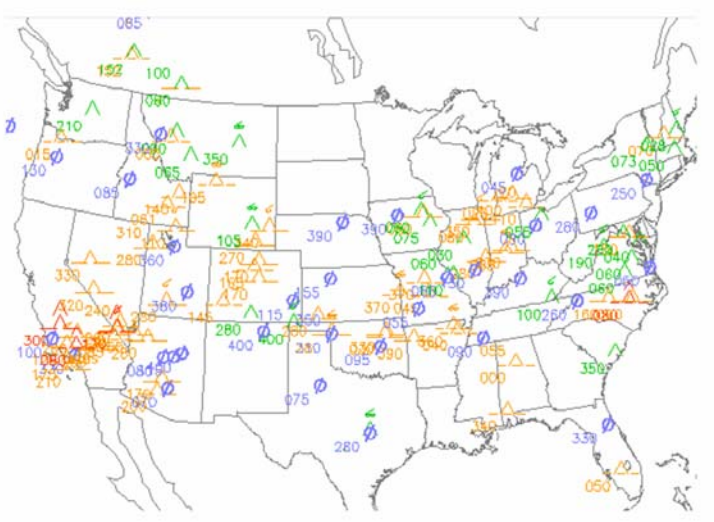

Figure 55. Example PIREPs observation display from the AWC for 1800 GMT, 14 April 2006.

In the last decade, a more objective form of observing turbulence has been developed in the form of automated turbulence measurements taken from aircraft every minute of their flight from take off to landing.

2. In-situ

The automated turbulence measurements by aircraft are estimates of a form of the eddy dissipation rate, ε, which is MacCready's (1964) proposed universal turbulence standardization technique. It is quantitatively based on atmospheric turbulence, as opposed to the qualitative and aircraft-dependent turbulence a pilot may "feel." MacCready (1964) defines the eddy dissipation rate (EDR) as "the rate at which the turbulence energy is converted into heat for steady turbulence." He stated that an EDR can be measured independently of aircraft type or speed. Eddy dissipation rate can be measured by detecting "…the small longitudinal (or lateral) velocity turbulent fluctuation…" (MacCready 1964).

The EDR is a quantitative, state-of-the-atmosphere turbulence metric unlike the subjective turbulence PIREPs. The EDR reports were intended to augment the PIREPs, and were designed to address the deficiencies of the PIREPs. Because EDR measurements provide a routine, quantitative measurement of the atmospheric turbulence, they also include much needed null reports. This allows forecasters to clearly identify regions of smooth flying and make the appropriate adjustments to their forecasts.

Two main algorithms have been developed to measure the EDR from on-board data: (1) Vertical accelerations and (2) Vertical wind component. The first algorithm uses vertical accelerations and a mathematical model of the aircraft response to turbulence in order to estimate EDR values. The second uses a calculation of the vertical wind component. A detailed description of these methods and the associated quality control methods can be found in Cornman (1995, 2004).

3. EDR Reporting

With both EDR estimation methods, a time series of EDR values is produced over a one-minute cruise-mode reporting interval. Two values are sent in the EDR report which can be thought of as the median value for the minute and the maximum value for the minute. This gives some indication of whether the turbulence is relatively continuous or discrete for the minute time period. For example, if the maximum value is vastly different from the median value for a given minute, it can be deducted that the turbulence event was a discrete event (Cornman 2004). Both the peak and the median EDR values are binned into categories before they are downloaded from the aircraft. The minimum EDR category is 0.05. The categories then increment by 0.10 to the maximum of 0.85. Studies have shown the 0.05 EDR category is reported over 90% of the time, while EDR categories above 0.65 are extremely rare (less than 0.01%) (Takacs 2006). An EDR report of 0.05 is considered to be a null report of turbulence.

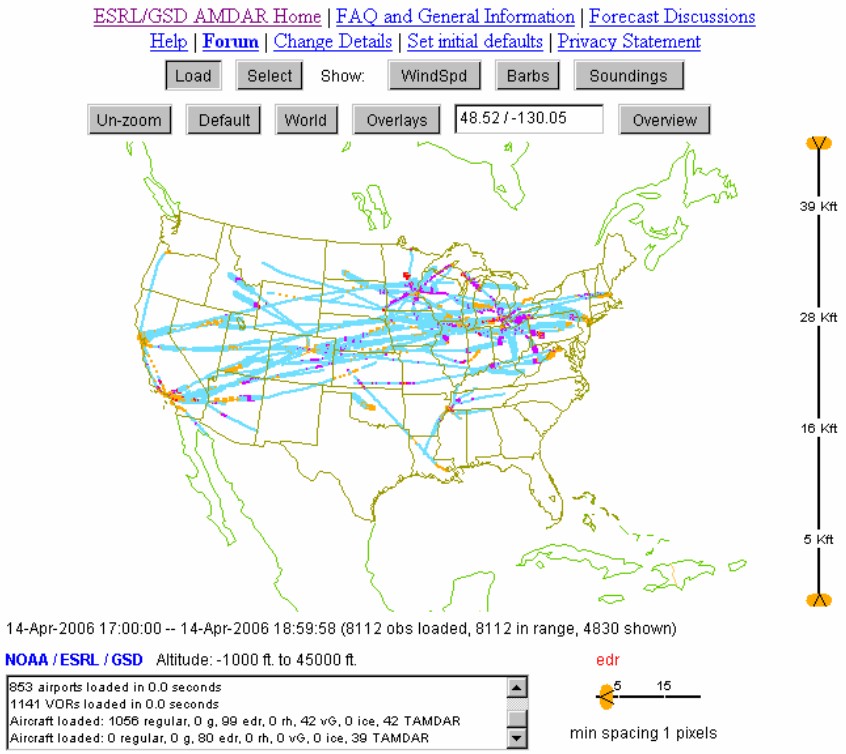

Figure 56. Example EDR observations plot from ESRL/GSD (2006) for 1700 thru 1900 GMT, 14 April 2006. Refer to section A of Chapter III for more details.

A primary advantage of the EDR reports is that they are aircraft-independent measures of turbulence (Cornman 2004). Through careful testing and verification, Cornman (2004) shows EDR reports can be used as a universal, aircraft-independent metric for communicating turbulence information between users and if a user desires an aircraft-dependent measure it can be estimated via a relation derived in Cornman (2004).

Currently, about 400 combined United Airlines and Delta aircraft are equipped with EDR reporting capability. The Global Systems Division of the Earth System Research Laboratory (ESRL/GSD), formerly Forecast Systems Laboratory (FSL), has

taken a lead role in providing automated meteorological reports from commercial aircraft to atmospheric researchers and to government operational forecasters. Recently, ESRL/GSD added automated turbulence data to the other weather data on their unofficial (not operational) website http://acweb.fsl.noaa.gov/ (ESRL/GSD 2006). It may be possible for the EDR to be directly ingested into NWP models, which suggests a future possibility of forecasting EDR directly (AMS 2003). If a pilot is provided EDR data directly, he/she may be able to relate the information to an aircraft-dependent chart (particular to their aircraft flight characteristics, as well and make a determination on how to continue their flight (Cunningham 2006).

F. DYNAMICS AND ASSOCIATED SYNOPTIC CONDITIONS

With each type of turbulence there are different physical causes and conditions which are responsible for creating the turbulence. Understanding these different physical (or dynamical) causes is critical to being able to effectively forecast turbulence. A detailed discussion of these physical causes for the various types of turbulence is given in the following subsections starting with thermal turbulence, then CAT, and finishing with mountain wave turbulence.

1. Thermal Turbulence

Thermal turbulence, also called boundary layer or convective turbulence, is associated with static instability. An excellent measure of the static stability of air is the potential lapse rate, Γ: $\Gamma = \Delta\theta/\Delta Z$, where $\Delta\theta$ is the change in potential temperature over a layer of thickness ΔZ (Lee et al. 1984). For dry air, when Γ is positive the air is considered to be statically stable. When Γ is negative the air is statically unstable, and when Γ is 0 neutral stability occurs. Thermal turbulence starts in statically unstable air (Lee et al. 1984). Typically, this turbulence occurs in the boundary layer as it warms on a hot, sunny day. This leads to a negative Γ in the boundary layer or just above it, as the surface is much warmer than the air above. When the air is statically unstable it can break down into rising/descending parcels of hot/cold turbulent air. Some of these thermals can rise far enough to cause clouds. Many other thermals are trapped below the cloud base by the temperature inversion just below the cloud base. It is important to note although thermal turbulence is most commonly found near the earth's surface, it can occur in the upper troposphere where radiational cooling or horizontal advection lowers the lapse rate, such as near cirrus clouds (Lee et al. 1984).

2. Clear-Air Turbulence

Unlike thermal turbulence, CAT is created in statically stable air. CAT occurs when the wind shear is particularly strong. When the wind shear is strong enough to create CAT the air is considered to be dynamically unstable (Lee et al. 1984). It has been shown dynamic CAT can occur only when the wind shear is strong enough to overpower the stability. The Richardson number (Kronebach 1964) is a ratio that compares the relative strength of the static stability versus the wind shear:

$$\text{Richardson number} = \text{Ri} = \frac{g\left(\frac{\Delta\theta}{\Delta z}\right)}{\left(\frac{\Delta v}{\Delta z}\right)^2}$$

where g is the acceleration due to gravity and Δ V/ΔZ is the vector wind shear occurring over the vertical distance ΔZ (Kronebach 1964).

The Ri indicates while the wind shear tends to produce turbulent kinetic energy, stability tends to damp this energy. This means Ri must be less than one for turbulence to have a chance to occur. However, theory and experiment have shown dynamic turbulence can only occur when the Ri is less than or equal to 0.25, or when the shear is four times greater than the stability. When air has a RI less than 0.25 it is considered to be dynamically unstable. Additionally, statically unstable air (Γ<0) is automatically dynamically unstable because the Ri is negative in that case due to the negative lapse rate. It has been shown (Miles and Howard 1964) when Ri is near 0.25, Kelvin-Helmholtz waves often occur.

CAT often occurs near the jet stream at the tropopause as shown in Figure 57. These occurrences of CAT peak during winter months and reach a minimum in the summer. The root of this CAT is often strong vertical wind shear (speed and/or direction) and strong horizontal wind shear in this region associated with the jet combined with the static stability which often exists near the tropopause. The jet is usually stronger during the winter months when strong thermal gradients are enhanced, especially over CONUS. Strong shears can first generate Kelvin-Helmholtz waves. These waves amplify, roll-up, and break similar to ocean waves (Lee et al. 1984).

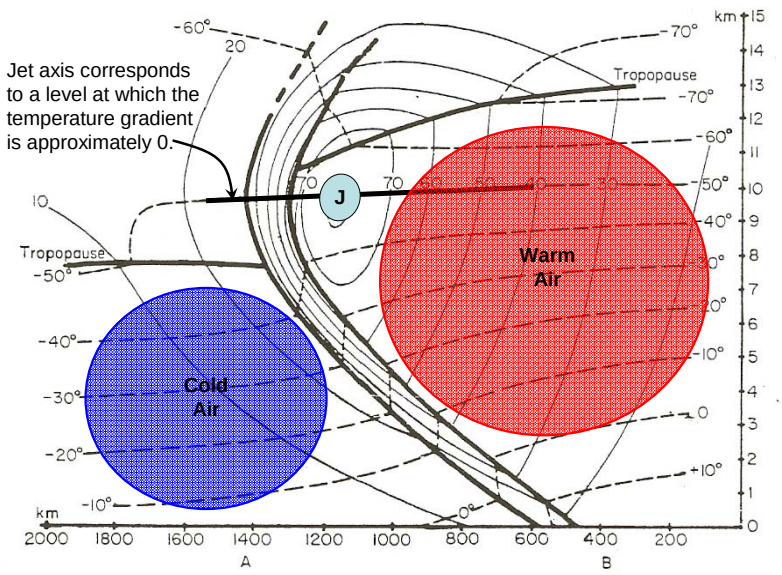

Figure 57. Typical jet stream and upper level front set up. Pale blue circle with "J" marks the jet max. Solid lines are isotachs. Dashed lines are isotherms.

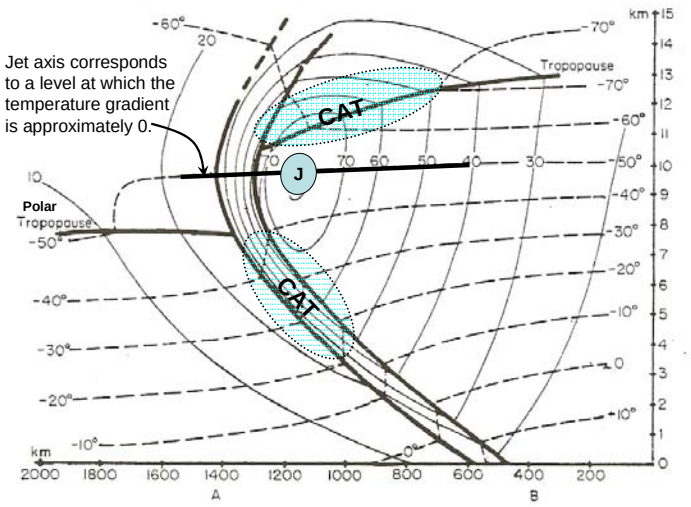

Figure 58. Same as in Figure 57 except typical location of CAT is shown in bright blue areas.

In the 1950s and 1960s early attempts to forecast CAT at the operational level involved the determination of synoptic or mesoscale conditions which are conducive to turbulence, since numerical models could not come close to resolving CAT. One of the approaches was to empirically relate forecast synoptic flow patterns to the occurrence of CAT (Rammer 1973). From these types of studies, it was shown curved segments of the jet stream associated with troughs, ridges, and closed upper lows were more likely areas to contain CAT than straight jet segments (Ellrod and Knapp 1992). Mesoscale conditions were also studied using aircraft and radiosondes. Regions favorable for significant CAT were determined to have the following characteristics:

- Strong vertical wind shear (speed and directional)
- Strong horizontal shear
- Significant convergence
- Significant horizontal deformation
- Lapse-rate discontinuities
- Strong horizontal thermal gradients

(Ellrod and Knapp1992)

Note all of these characteristics are consistent with the characteristics of sloping upper-level frontal zones. Numerical techniques to forecast turbulence have mainly focused on predictions of vertical and horizontal wind shear, which can be relatively easily calculated from model output fields.

In a 2002 study led by NASA on characterizing the severe turbulence environments associated with commercial aviation accidents, an effort was made to determine the most prevalent synoptic scale atmospheric configuration associated with severe turbulence reports (Kaplan et al. 2002). The synoptic predictor fields represent standard derived quantities often associated with turbulence in recent studies (e.g., Keller

1990; Ellrod and Knapp 1992; Knox 1997). In the NASA study these predictor fields were calculated and the magnitudes were compared to location, elevation, and time of accident. The most useful and least useful predictor fields were then determined for when and where severe accident-producing turbulence should be occurring. Table 8 shows the most useful predictors from all 44 of the NASA case studies.

Table 8. Best Predictors for 44 Accident Case Studies (% of 44) (Kaplan et al. 2002).

1. Immediate upstream curvature	(98%)
2. Convective clouds (all bases) < 100 km away	(86%)
3. Upward vertical motion	(82%)
4. Layer-averaged absolute vorticity $\leq 10^{-4}$ s^{-1}	(80%)
5. Jet entrance region	(77%)
6. Higher vertical shear advection	(77%)
7. Lapse rate ≥ moist adiabatic	(77%)
8. Absolute vorticity at flight level $\leq 10^{-4}$ s^{-1}	(75%)
9. Convective clouds (all bases) < 30 km away	(74%)
10. Horizontal cold advection	(73%)
11. Flight level relative vorticity $\leq$ 0 s^{-1}	(68%)
12. Leftward-directed $v_{ageostrophic}$ flow	(64%)

It was concluded from this study the most persistent synoptic predictors of severe turbulence are a ridge or trough axis where a region of changing flow curvature is occurring, convection, upward vertical motion, low relative vorticity, and the entrance region of a jet stream (Kaplan et al. 2002). For the case studies, there was a great deal of uncertainty concerning what processes accompanying the jet entrance regions consistently organized the environment which created turbulence of greater than moderate intensity. It was found that buoyancy-based forcing, shear-based forcing, kinematics-based forcing, and complex combinations thereof can be related to characterizing the environment that organizes turbulence but may or may not be a discriminating condition for the development of severe accident-producing turbulence (Kaplan et al. 2003). Consequently, trying to discriminate when and where the environment will develop microscale severe turbulence is an unsolved problem which will continue to challenge meteorologists.

3. Mountain Wave

Mountain waves are a form of internal gravity wave, where the wave disturbance is forced by a terrain feature. This disturbance occurs when the mean atmospheric flow encounters mountainous terrain and instead of being able to continue on its present course, it is forced vertically, transporting momentum and potential energy with it. Once displaced, this air can respond in several ways, primarily depending on the stability of the surrounding atmosphere and the general shape, height and width of the mountain range. In an unstable environment, the displaced air will continue to rise until it reaches thermal equilibrium. Once thermal equilibrium is reached, this displaced air will follow the environmental flow, which has minimal vertical motion. Thus an unstable environment is not conducive to wave propagation. If the environment is stable, the displaced air

becomes colder and denser than its surroundings. The rate of ascent then slows and ultimately reverses directions so that it may reach thermal equilibrium. As the air descends it gains kinetic energy, thus, once reaching thermal equilibrium the air is not able to stop. It continues to descend, warming dry adiabatically, becoming warmer than its surroundings. This warmer, more buoyant air, slowly stops descending and begins to ascend back to its equilibrium level. This oscillating process continues until kinetic energy dissipates, damping the amplitude of the wave (Coughlin 2005).

It is critical the forecaster accurately diagnose the atmospheric conditions and understand the small variations which can change laminar flow into turbulent flow. There are two primary types of mountain induced waves to be concerned with: trapped lee waves, and vertically propagating mountain waves.

a. Trapped Lee Waves

Trapped lee waves are waves that propagate horizontally due to strong vertical wind shear or large stability changes just above ridge top level, either of which can act as a vertical propagation barrier (Coughlin 2005). This barrier interface allows wave energy to oscillate vertically below it. Typically, the scenario leading to a trapped lee wave response has an inversion just above the mountain ridge top level with less stable stratification above the inversion. A trapped lee wave response can excite an oscillation which can lead to the development of cloud bands like those shown in Figure 59 that have equidistant horizontal spacing as they oscillate and are parallel to that of the ridge axis. If the atmospheric conditions are favorable these cloud bands can extend dozens of times for hundreds of kilometers (Coughlin 2005).

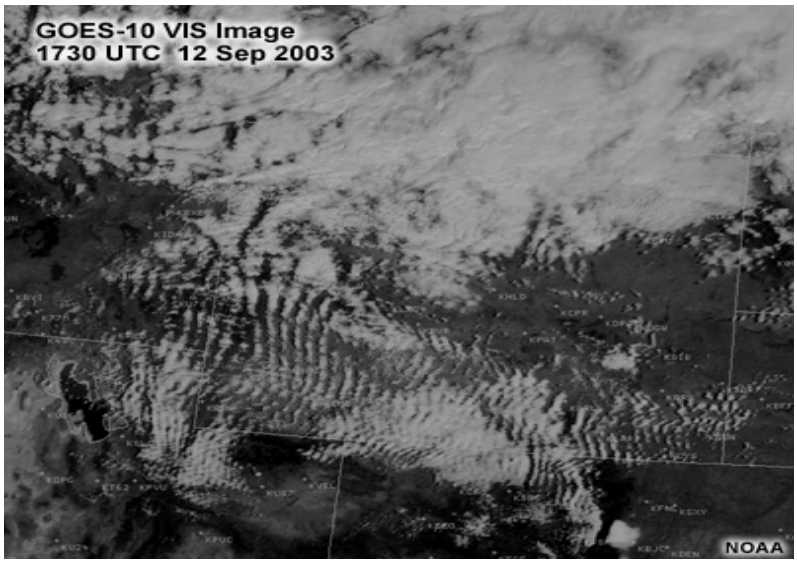

Figure 59. A trapped lee wave response formed across Wyoming on 12 September 2003. The width of the wave train exceeds 700 km. The combination of strong wind shear and an inversion located just above the ridge top created nearly ideal conditions for trapped waves (UCAR 2005a).

Trapped lee waves are very common and significant effects to aircraft can be felt even downstream of hills with as little as 300-500m elevation gain above the background elevation (Queney et al. 1960). Turbulence associated with trapped waves

can be moderate to severe, especially in a rotor zone. However, the flow associated with trapped waves is thought to be primarily laminar (especially above ridge top level) due to the stunted vertical propagation. Therefore, turbulence is relatively nominal, especially for smaller and narrow mountains (Coughlin 2005).

b. Vertically Propagating Waves (VPWs)

As one might expect, VPWs are waves that propagate vertically. Uniform stability and minimal background vertical wind shear allows for these waves to extend to great altitudes, thus disturbing flow in the troposphere and stratosphere. Unlike trapped lee waves, which have multiple cloud crests, VPWs almost always have one wave crest with some less severe events having a second or third wave crest of lesser vertical prominence (Durran 1986). A large cloud shield, almost always present, develops just downstream and sharply parallel to the axis of the mountain barrier. This cloud shield remains quasi-stationary (especially the leading edge) for the duration of the event and can have IR temps of -40° to -60° Celsius. Because VPWs are just a single wave, it is difficult to determine their exact wavelength; however, VPWs generally have wavelengths 30km or greater (Durran 1986). Unlike trapped wave responses, VPWs have a longer wavelength response that is easily discernable on both high resolution and low resolution imagery. Typically, it is larger mountain ranges like the Alps, Pyrenees, Rockies and Sierra Nevada that excite VPWs. Much like that of an ocean wave, the greater the amplitude of the wave the more likely the wave will break, thus causing severe to extreme turbulence. The large amplitude response of a VPW, thus, has a higher propensity to break than do trapped lee waves (Coughlin 2005).

G. DIAGNOSTICS

There have been a large number of aviation turbulence diagnostics (or indices) developed to help diagnose and forecast the occurrence of turbulence, especially CAT. These forecast techniques are usually based on parameters derived from upper air numerical weather prediction (NWP) data such as vertical wind shear, scalar wind speed, horizontal wind shear, deformation, and the non-dimensional Richardson number. The diagnostics have been developed based on the well understood dynamics and forcing which cause turbulence and the well observed synoptic conditions which favor turbulent conditions. The objective of these diagnostics is to take the conditions which have been known to cause turbulence, such as strong wind shear, and use models to forecast specifically these conditions. Usually, a model like AFWA's MM5 is run, and then through post-processing, a diagnostic is computed using the model predicted fields. This diagnostic is then mapped like any other model output and areas where the diagnostic predicts strong turbulence will occur are noted. Every diagnostic is model dependent since the diagnostic is computed after the model has run. This means that a diagnostic applied to one model output with a certain grid resolution may look totally different applied to another model with a different grid resolution. Thus, results will not only vary between the different diagnostics, but also will vary for any single diagnostic applied to different models.

Each diagnostic has different thresholds, and extensive research and testing has to be done to determine what those thresholds are and how they might change for different synoptic conditions. However, none of these diagnostics have been shown to capture all of the turbulence forecasting problems. The NWP diagnostics were designed to attempt

to capture grid scale processes that produce the mesoscale (10-100 km) meteorological conditions conducive to sub-grid scale turbulence. Thus, they cannot explicitly forecast turbulence on the scales sensed by aircraft (10-100 m) (Knox et al. 1997). No single diagnostic should be used as a sole source for forecasting turbulence. Forecast skills of these diagnostics depend on the forecaster and how the forecaster interprets and uses the information the diagnostic provides. The diagnostics' skills reflect researchers' imperfect understanding of the atmospheric processes involved (Abernathy and Sharman 2006). Three diagnostics are analyzed below and illustrate how the diagnostics help to predict turbulence. The choice of diagnostics has no significance as Tebaldi et al. (2002) show that no one diagnostic is superior to another. Notice that the three diagnostics are not entirely unique to one another (i.e., each of the three below use VWS).

1. Ri (Kronebach 1964)

Turbulence can occur in statically stable air if the wind shear is strong enough. The air is considered to be dynamically unstable when this happens. The Richardson number has been commonly used as a measure for possible turbulent conditions since it relates shear and stability. Recall that theory and experiment have shown that dynamic turbulence can only occur when Ri is less than or equal to 0.25. The Ri diagnostic then simply automates the calculation of Ri. Post-processed model fields are used to calculate the Ri as defined above, and every grid point in the model atmosphere will have a forecasted Ri value. The forecaster will then be alerted to areas in the atmosphere where the model predicts the Ri to be less than 0.25. If the forecaster were to simply forecast turbulence for every area that the Ri is less than 0.25, an extreme amount of over-forecasting would result. Recall that the Ri does not explicitly forecast turbulence; the mere fact Ri is less than 0.25 does not necessitate turbulence will exist, only that conditions are very favorable for turbulence. Furthermore, there is currently an inability to accurately measure vertical wind shear at the resolution necessary to detect areas prime for turbulence. For these reasons, the Ri diagnostic cannot be relied upon as a sole source for turbulence forecasts, but rather should be used only as guidance to the forecaster.

2. Ellrod (Ellrod and Knapp 1992)

One diagnostic frequently used by AWC forecasters is the Ellrod index (Ellrod and Knapp 1992). The Ellrod index is defined as the vertical wind shear (VWS) times the sum of the horizontal deformation (DEF) and convergence (CVG). All three of the above components of the Ellrod index are known to increase frontogenesis, which increases the likelihood of CAT occurrence (Ellrod and Knapp 1992). The first two components, VWS and DEF, are easily calculated by using u and v wind-component forecasts. Ellrod and Knapp (1992) define VWS as:

$$VWS = \frac{(\Delta u^2 + \Delta v^2)^{1/2}}{\Delta z}$$

The vertical layer thickness is given by Δz. Ellrod and Knapp (1992) define deformation as:

$$DEF = (DST^2 + DSH^2)^{1/2}$$

where DST is the stretching deformation and DSH is the shearing deformation and are defined as:

$$DST = \frac{\partial u}{\partial x} - \frac{\partial v}{\partial y}$$

$$\text{DSH} = \frac{\partial v}{\partial x} - \frac{\partial u}{\partial y}$$

The final component, CVG, is defined as:

$$CVG = -\left(\frac{\partial u}{\partial x} - \frac{\partial v}{\partial y} \right)$$

AFWA uses the Ellrod TI2 index to produce their strategic level turbulence forecast. The Ellrod TI2 index is defined as:

TI2 = VWS X [DEF + CVG]

Ellrod index guidance displays are generated for all NCEP models and are utilized by both military and civilian forecasters. The Ellrod index over the US from the NCEP's North American Model (NAM) is available at http://aviationweather.gov/exp/ellrod/eta. The Ellrod index has been found to be quite skillful in determining the existence of turbulent conditions. However, both the original paper and case studies have shown the index to be limited in skill in determining the intensity of the turbulence, so the Ellrod index is frequently used in conjunction with other indices. Like the other diagnostics, the Ellrod index does not directly calculate the phenomenon that is turbulence, but only attempts to calculate its cause.

3. Dutton (Dutton 1980)

Dutton (1980) performed a study on different indices on data collected during the 1976 Turbulence Survey. Data from over 4500 flights over the North Atlantic and north-west Europe were collected. The goal of the study was to assess the potential, as predictors of CAT, from various synoptic-scale meteorological indices computed by an automated NWP model. Dutton (1980) found that an index combining the predictive abilities of vertical and horizontal wind shear significantly out-performed concurrent conventional CAT forecasts.

The empirical index Dutton (1980) claimed as the best predictor of CAT is:

Dutton = 1.5 x HWS + 0.25 x VWS + 10.5

where HWS represents horizontal wind shear and VWS represents vertical wind shear. It is not surprising that vertical and horizontal wind shear were the best indicators of CAT in Dutton's study, since it is known that these two physical processes create CAT. So formulating an automated index which is calculated based upon the HWS and VWS would logically be a good indicator of areas favorable for turbulence. When diagnostics like Dutton's and Ellrod's are combined with other diagnostics a more complete representation of the synoptic conditions which generate turbulence are automated and can result in a better forecast as shown by Tebaldi (2002) and Sharman et al. (2006).

E. GRAPHICAL TURBULENCE GUIDANCE

To best utilize the various turbulence indices, the NCAR has developed the Integrated Turbulence Forecast Algorithm (ITFA). The ITFA has recently become an operational NWS product generated at the AWC and has been renamed the Graphical Turbulence Guidance (GTG). The GTG generates up to 31 different turbulence diagnostics from the Rapid Update Cycle (RUC) numerical model data, normalizes the various diagnostics into a turbulence potential, scores their current skill as compared to current pilot reports, and then weights the various diagnostics into a combined index. This dynamic weighting of turbulence indices is repeated hourly for the analysis of turbulence and every 3 hours for the forecast so as to capture the best possible guidance for turbulence over the CONUS. The GTG is only generated from RUC data so it is only available over the CONUS for up to a 12-hour forecast. The GTG also is limited to flight levels above 10,000 ft.

The GTG process starts by automatically ingesting gridded NWP, which should accurately represent the large-scale features of the atmosphere that may be related to aircraft-scale turbulence. In principle, any high resolution NWP model could be used, but the National Centers for Environmental Prediction's (NCEP's) RUC model was chosen because of the higher effective vertical resolution provided by the isentropic vertical coordinate system at upper levels in the model (Benjamin et al. 2004). The main task of the GTG forecasting method is to integrate a combination of several separate turbulence diagnostics, and to weight each diagnostic so as to get the best agreement with available observations (i.e., PIREPs). When a sufficient number of PIREPs are available in real time the weights are determined dynamically and updated with every RUC model update. When there is an insufficient number of PIREPs available (i.e., at night when commercial flights are significantly reduced), a set of climatologically derived static weights are used (Sharman et al. 2006). The GTG process involves a six-step procedure which is explained in Sharman et al. (2006).

Currently, the entire cycle repeats with every major NWP update; for RUC-2 this is every 3 hours. The process is performed separately for middle and upper levels, and the results are merged at the flight level 20,000 foot boundary. When using weights based on climatology, steps 3 and 4 are bypassed and a constant set of weights are used for the analysis time and all forecast times. The procedure for deriving these climatology-based or default weights, along with their current values is given in Sharman et al. (2006). The GTG product is available at:

(a) http://adds.aviationweather.gov/turbulence/ or,

(b) http://aviationweather.gov/exp/gtg/mdt.shtml.

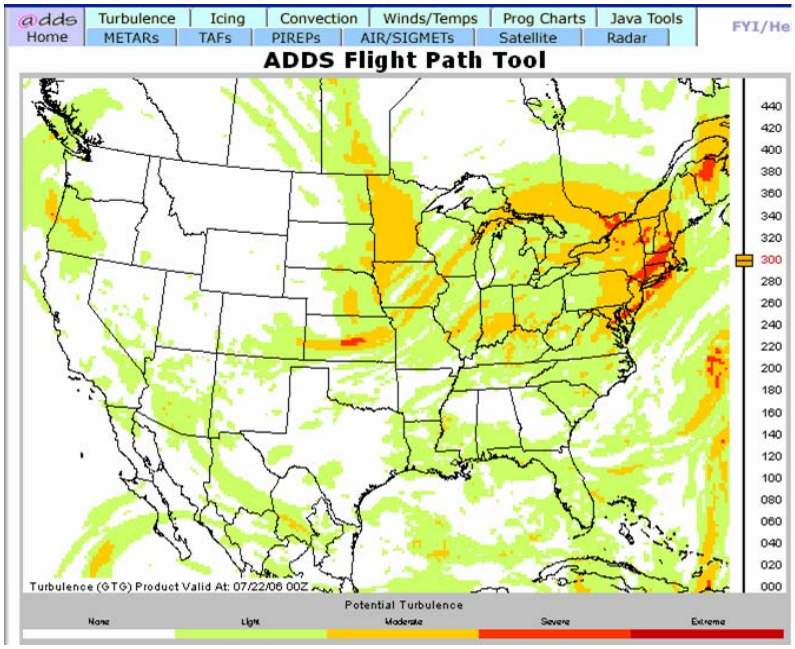

Figure 60. Example of the GTG product from the AWC website for FL 3000 ft valid 0000 GMT, 22 July 2006 and produced at 1800 GMT, 21 July 2006.

Sharman et al. (2006) describes some of the rigorous testing and verification done on the GTG recently and found the overall performance of the GTG "to be skillful enough to provide useful information to meteorologists and dispatchers for strategic planning for turbulence avoidance." Sharman et al. (2006) also concludes the GTG combination provides superior guidance than any single turbulence diagnostic in detecting CAT.

II. TURBULENCE FORECAST APPROACH

What follows is a suggested forecast approach for AFWA OWS turbulence forecasters or any newly trained turbulence forecaster. As is the case with all forecasting, a good forecast starts with a good analysis. The forecaster must first understand the current and past conditions of the atmosphere before being able to predict the future state of the atmosphere. A complete synoptic analysis which includes recognizing distinct synoptic patterns and features which favor turbulent conditions is presented in Section A for each of the types of turbulence. Observations, discussed in Section B, should be used to verify patterns and favorable areas identified in the forecaster's analysis, and to alert the forecaster of all reported turbulent areas. Section C discusses the turbulence diagnostics and how they should be used in the turbulence forecast process. The use of models and the GTG will be discussed in Section D. Finally, Section E will summarize the overall suggested turbulence forecast approach.

A. SYNOPTIC ANALYSIS

Three types of turbulence have been defined; thermal turbulence, CAT, and mountain wave turbulence. Recall that atmospheric turbulence was classified into the above categories because each type of turbulence is caused by different physical processes. Bearing this in mind, the following subsections are broken down by the type of turbulence, similar to the approach the forecaster should take. That is, the forecaster should start with an analysis of thermal turbulence, then CAT, and finally mountain wave turbulence.

1. Thermal Turbulence

Recall that surface heating can generate turbulent conditions. As solar radiation heats the surface, the air above it is warmed by contact. Warmer air is less dense, and "bubbles" of warm air rise upward as updrafts. Uneven surface heating, and the cooling of rising air, allows for areas of downdrafts as well. Characteristics of boundary layer turbulence include:

- The maximum occurrence is between late morning and late afternoon.
- The impact on flight operations is greatest during terminal approach and departure and during low-level flights.
- Moderate turbulence may occur in hot, arid regions, as the result of irregular convective currents from intense surface heating (AFWA TN 98-002, 2005).

Within thunderstorms, intense updrafts can exist alongside intense downdrafts. This is conducive for turbulence to exist, specifically convective turbulence. Convective turbulence is often found in and around thunderstorms, especially strong and severe storms where deep convection is persistent. The stronger the convection becomes, the stronger the turbulence will be. While moderate or severe turbulence can be found anywhere within the storm, including the clear air along its outer edges, the highest probability of turbulence is found in the storm core (AFWA TN 98-002, 2005).

The early morning sounding from Davenport, Iowa for 1200 GMT, 10 August 2006 shown in Figure 61 exemplifies a convective regime sounding which should alert the forecaster to possible convective turbulence. The high value of the Convective Available Potential Energy (CAPE) as well as the low value of the Lifted Index indicates the weak atmospheric stability in which strong updrafts and downdrafts can occur and

cause turbulence. A stronger CAPE will result in more energy being available to support stronger updrafts and potentially violent convection and thunderstorms. The sounding reveals an important low-level inversion which will temporarily inhibit convection. But as the day progresses and the surface is heated by solar energy the inversion can will dissipate in which case all of the built up CAPE can be realized and intense convection can develop. Therefore, a strong low-level inversion can allow the CAPE to build up creating a greater potential for strong convection, but at the same time if the inversion becomes too strong, the boundary layer may never warm enough throughout the day to "break" the inversion and realize the CAPE. EDR observations over Iowa for this day in August confirm that turbulence was present over the Davenport region and surrounding areas. Radar data also showed convective activity in this region.

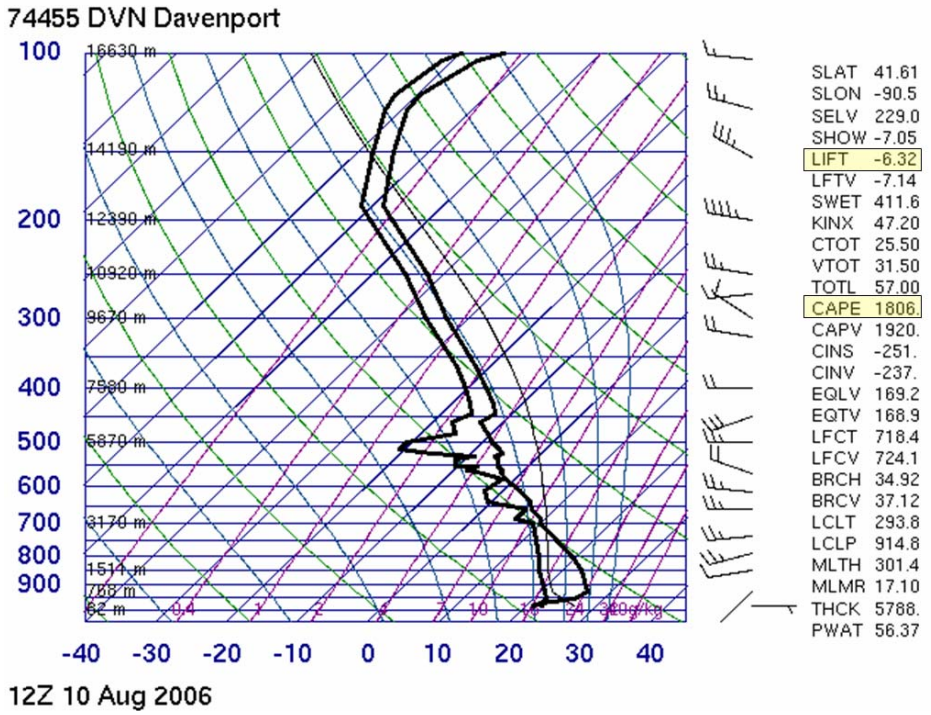

Figure 61. Atmospheric sounding for Davenport, Iowa on at 1200 GMT, 10 August 2006. The sounding has a CAPE of 1806 J/kg and a Lifted Index of -6, indicating conditions are favorable for significant convection to develop.

Significant downdrafts will also exist beneath the cloud base, usually associated with areas of heavy rain and generally areas of highest water concentration are the areas of heaviest turbulence (AWS TR/105-39, 1949). Thus, the forecaster should expect significant turbulence where the most intense rain columns are seen on the radar (AWS TR/105-39, 1949). Potentially hazardous turbulence is present in all thunderstorms, and a severe thunderstorm can severely damage an aircraft (AWS FM/83-002, 1983). Turbulence has been encountered several thousand feet above and 20 miles laterally from a severe storm (AWS FM/83-002, 1983). A low-level turbulent area is often associated with the shear zone in the gust front of a strong thunderstorm. A roll cloud on the leading edge of a storm marks the top of the eddies in this shear and it signifies an extremely turbulent zone as shown in Figure 62. Gust fronts extend 10 to 20 miles away from the

thunderstorm with extreme turbulence-causing wind shears existing behind and across the gust front (AWS FM/83-002, 1983).

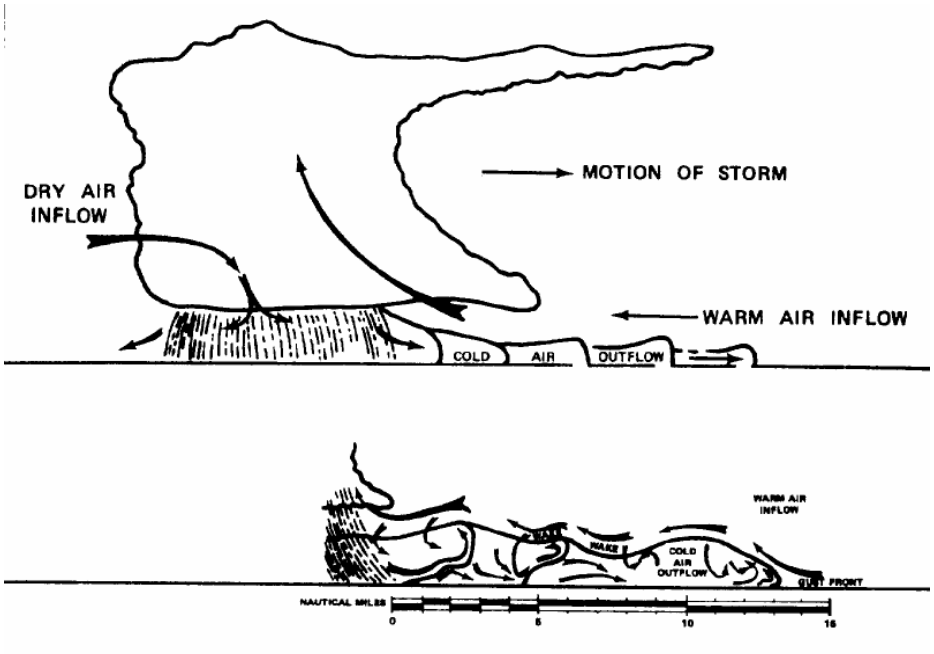

Figure 62. Typical thunderstorm with up/downdrafts and outflow shown, taken from (AWS FM/83-002, 1983). The eddies shown in the outflow region signify an extremely turbulent zone.

A common feature of a capped boundary layer where a strong inversion exists aloft is significant low-level wind shear (LLWS). In a capped boundary layer turbulence may not exist at the surface and boundary layer where the atmosphere is stable, but as aviators cross the interface from the boundary layer to the free atmosphere through the inversion, they will likely experience LLWS which is very similar to turbulence and can have the same damaging effects.

Turbulence forecasters should expect turbulence to exist in and surrounding any significant convective regions and should utilize tools like the radar, visible and IR satellite imagery, and atmospheric soundings to identify areas of strong convection. For more guidance on convective weather see Chapter 3 of AFWA TN 98-002 (2005).

2. CAT

a. Jet identification

When performing an analysis for CAT the suggested starting point is an upper-level chart such as the 200mb, 250mb, or 300mb chart. Jet streams can almost always be identified in these upper-level charts. Normally the polar jet stream is found on the 300mb chart (most prominent in the winter for midlatitude regions), while the subtropical jet can best be seen in the 200mb chart (most prominent in the summer for midlatitude regions). When forecasting for tropical regions, the 200mb chart is preferred and similarly, for polar regions the 300mb chart is preferred. Figure 63 is a typical 300mb chart for 1800 GMT, 9 March 2006 showing 300mb heights and isotachs. On this day there was a very strong jet located over the eastern Midwest region making the jet

identification quite simple. Figure 64 shows the EDR turbulence observations over a period of 2 hours (1700-1900 GMT) on top of the same chart as in Figure 63.

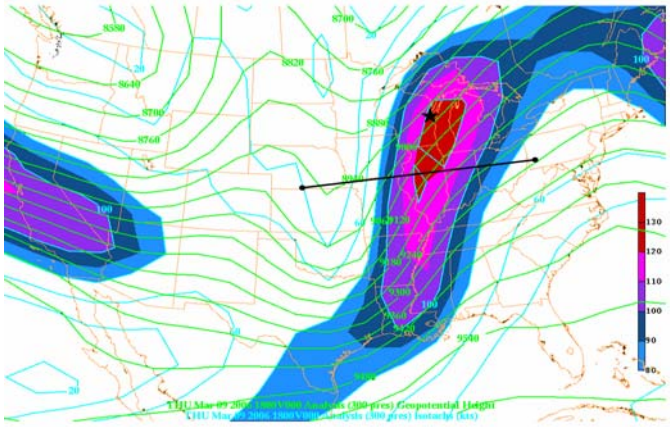

Figure 63. 300mb heights (m; green solid lines) and isotachs (kts; blue solid lines) are shown here for 1800 GMT, 9 March 2006. Isotachs greater than 80 are filled according to color scale in bottom right corner. A strong north-south oriented jet exists from the Great Lakes down to Louisiana. The black line shows the area used for the cross-section figures in this section and the black star indicates the location of the sounding shown in Figure 66.

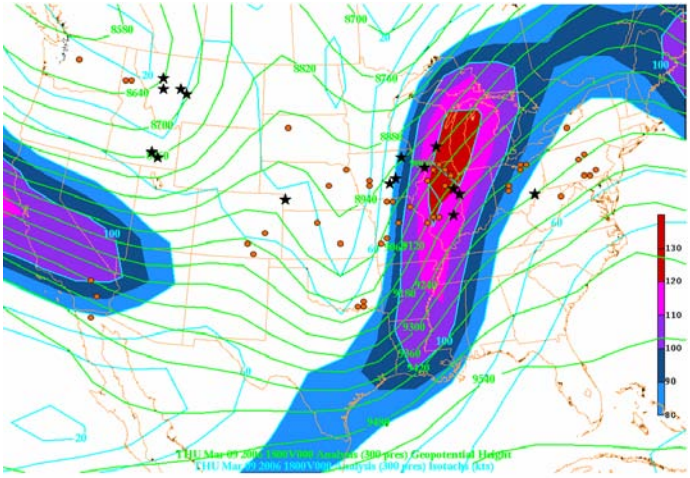

Figure 64. Same as in Figure 63 except with EDR observations shown for 1700-1900 GMT, 9 March 2006. The black stars are observations of moderate turbulence (0.25 EDR category), and the orange circles are observations of light-moderate turbulence (0.15 median/0.25 peak EDR category). The height of the moderate turbulence observations in the jet region range from 32,000 ft (275mb) to 39,000 ft (197mb) while all observations shown above are between 20,000 and 40,000 feet.

The CAT analysis begins with jet identification because the jet stream exhibits nearly all of the factors (i.e., strong thermal gradients, strong vertical wind shear, and strong horizontal wind shear) that have been associated with turbulence and that have been discussed in the previous chapters of this thesis. Additionally, the stronger the jet,

the more likely turbulence will exist in its proximity. Jet entrance regions and exit regions are particularly conducive for turbulence as well as confluent jet streams. When two jet streams are within 300 nm of each other there is a high probability of CAT in the confluent zone between the jets (Lee et al. 1984). The northern jet stream is accompanied by colder temperatures and thus is usually at a lower altitude than the southern jet stream and will cut underneath the southern jet stream. This will cause an increase in static stability and strong vertical directional and speed shears in the confluent zone and a rapid backing of the wind with height between the levels of the two jets. The result is a very favorable environment for moderate or greater CAT.

b. Jet core

Jet cores are very favorable areas for CAT and should be investigated next. The environment accompanying the jet core includes very strong winds with weaker surrounding winds in the vertical and horizontal, and consequently is a prime location for strong vertical and horizontal wind shear. Figure 65 shows the jet core from a cross-section view of the jet in Figure 63 and comes from the global GFS model analysis with one-degree resolution. Cross sections from mesoscale models with enhanced horizontal and vertical resolution can also depict the intense shears associated with the CAT environment. It is suggested that the forecaster identify jet cores after identifying the upper-level flow and jet streams. The position of the jet core is also very important, especially with respect to curvature which will be discussed later (Section d.).

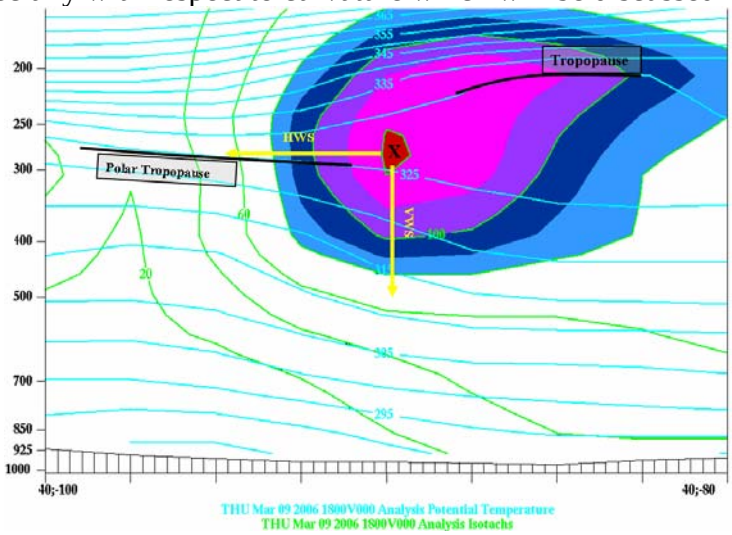

Figure 65. Cross-section from Iowa to Ohio across the jet showing isotachs (kts; solid green lines) and potential temperature (˚K; solid light blue lines) for 1800 GMT, 9 March 2006. The jet is shown with the filled-in isotachs and the jet core (130 kts) is indicated by the "X". Note the strong horizontal and vertical wind shear through the jet region as shown by the yellow arrows.

c. VWS & HWS

The cross-section in Figure 65 is a good example of how vertical wind shear (VWS) can be identified as well as horizontal wind shear (HWS). Cross-sections are an extremely valuable tool for forecasting turbulence and for aviation forecasting in general, especially when using high resolution mesoscale models. Drawing a horizontal

line out from the jet core to the west (left) as shown by the HWS yellow arrow in Figure 65, the forecaster can see that there is significant horizontal speed shear in the upper troposphere in this region. Drawing a vertical line straight down form the jet core as shown by the VWS yellow arrow in Figure 65, the forecaster can quickly see that for that location, approximately 40˚N; 89.8˚W, there is significant vertical speed shear also. Another useful tool for identifying vertical wind shear (speed and directional), as well as convective turbulence, is the atmospheric sounding. Figure 66 below is the sounding for Green Bay, WI (shown as the black star in Figure 63) and illustrates how vertical wind shear can be identified using a sounding. It is important to note the smoothing associated with automated products such as the GFS analysis shown in Figure 65. This smoothing, which occurs with all models, can tend to reduce intense shears and features associated with the CAT environment and the forecaster should be aware the actual shears, temperature gradients, and atmospheric processes may be more intense than the model can resolve. Therefore, atmospheric soundings generated from rawinsonde observations can give higher vertical resolution without model smoothing and can give a more detailed picture of the vertical CAT environment which can supplement model cross sections.

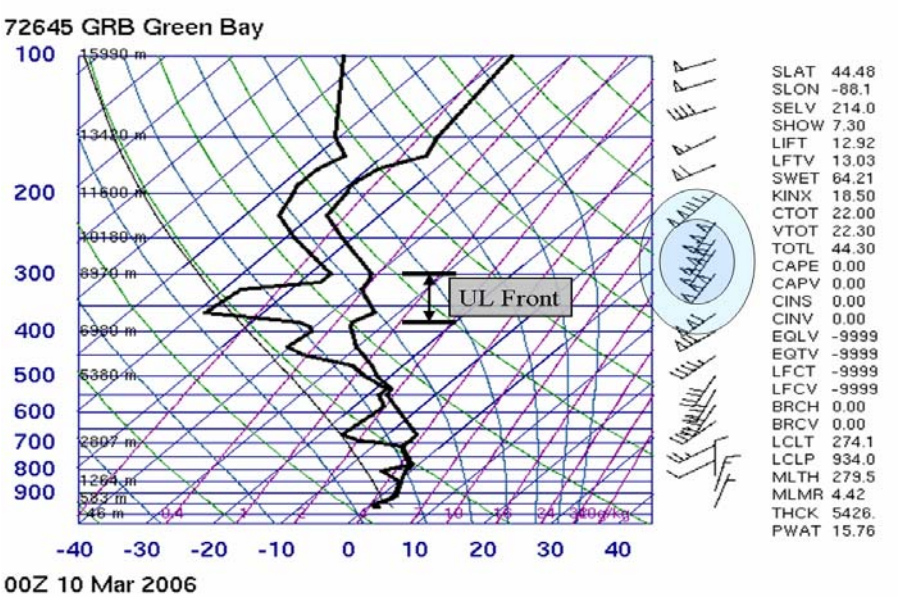

Figure 66. Sounding for Green Bay, WI for 000 GMT (6 hours after above figures), 10 March 2006. Note the vertical wind barbs to the right of the sounding, which show significant VWS near the UL front as expected, going from 70 kts at 400mb to 110 kts at 375mb and 150 kts at 300mb. Winds near the surface are 5 knots, while aloft they reach 160 knots. The blue ovals indicate the jet level, with the darker inside blue oval indicating the approximate jet core. The upper-level front is also visible in this sounding.

A difficult question for forecasters and researchers to answer is how much shear is necessary for turbulence? Because of the very nature and complexity of turbulence it is extremely difficult to define a certain amount of shear will always result in turbulence or will never result in turbulence. As has been shown, there are several other factors which can inhibit or create turbulence so a certain amount of VWS may be associated

with turbulence in one region but not another. However, there have been several efforts to try to quantify the amount of shear necessary for turbulence with the understanding that the quantifications are not definitive, but rather provide general guidance to probable turbulent conditions. Table 9 below is one such attempt from AFWA TN 98-002 (2005) which the forecaster should use to understand how much shear to look for during the analysis and forecast process. Again, the forecaster must be aware of model smoothing when considering actual amounts of shear and should use either a high resolution mesoscale model or a sounding to identify vertical shear amounts for Table 9 and similarly, a high resolution human analysis or model to identify horizontal shear.

Table 9. Wind shear critical values from Table 2-12 in AFWA TN 98-002 (2005).

	Turbulence Intensity			
	Light	**Moderate**	**Severe**	**Extreme**
Horizontal Shear		25-49 kt/90 NM	50-89 kt/90 NM	$\geq$ 90 kt/90 NM
Vertical Shear	3-5 kt/1,000 ft	6-9 kt/1,000 ft	10-15 kt/1,000 ft	> 15 kt/1,000 ft

d. Upper-level fronts

Upper-tropospheric fronts above and below jets are preferred regions for turbulence (Carlson 1998). Closely associated with upper-level fronts is tropopause folding. Tropopause folding constitutes an intense phase of upper-tropospheric frontal development and is closely associated with strong upper-tropospheric jet streaks. Turbulence is commonly found near the tropopause fold where the vertical and horizontal wind shear is very sharp and narrow. Furthermore, low Richardson numbers are an inherent property of upper-tropospheric fronts and their accompanying jets (Carlson 1998). Recall that low Richardson numbers mean the atmosphere is in a favorable state for turbulence to exist as the restoring effect of buoyancy is unable to overcome the VWS. Generally, a stronger jet is characterized by a strong upper-level front which is supported by vertical and horizontal wind shear and intense thermal gradients. This results in an environment prime for CAT. Figure 67 shows first a common cross sectional view of the upper-level front structure along with a tropopause fold and the resulting favorable areas of CAT and second, the same GFS analysis from Figure 65 with the upper-level front structure, tropopause folding, and favorable CAT areas all highlighted.

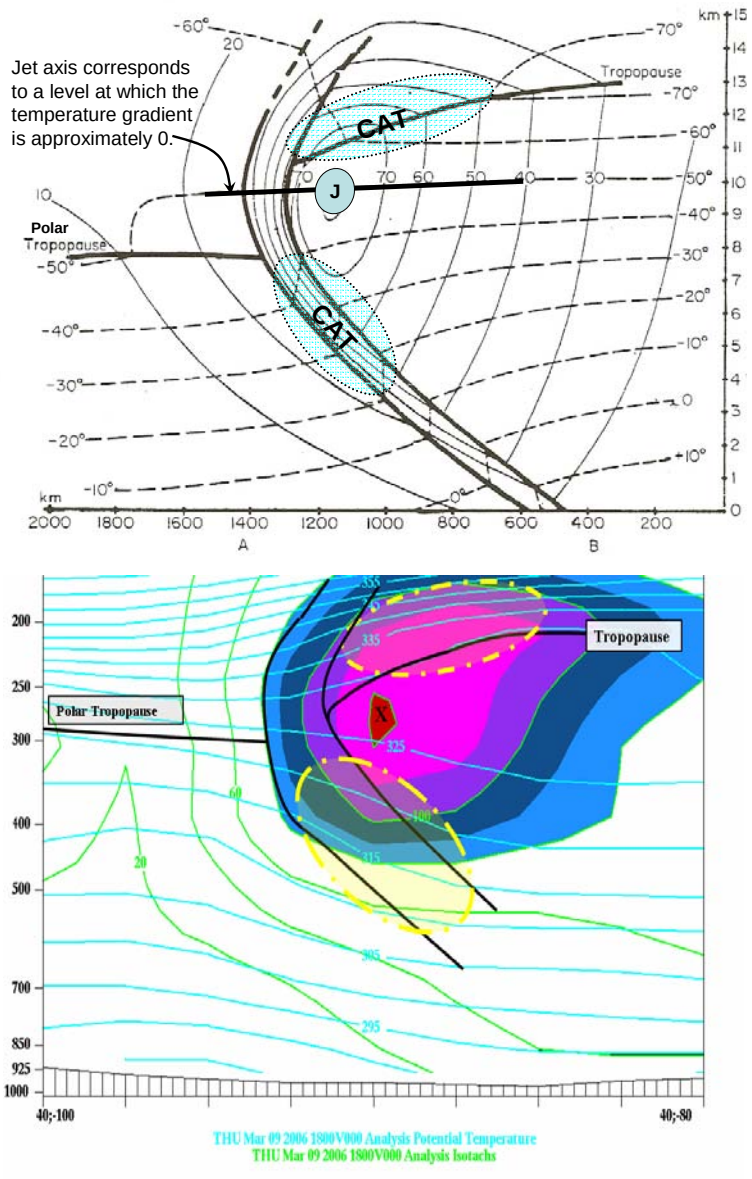

Figure 67. On top is the typical upper-level front structure along with a tropopause fold and favorable areas of CAT (blue ovals). The bottom chart is the analysis from 1800 GMT, 9 March 2006 (Figure 65) with the favorable CAT areas (dashed yellow ovals) and upper-level front shown

e. Curvature

Sharp curvature in the upper-level flow indicates areas where large HWS occurs, particularly at the region of strongest curvature (such as a trough or ridge) where the direction of flow changes most rapidly. These conditions are conducive to the formation of the shallow stable layers and coincident layers of wind shear associated with CAT (Lee et al. 1984). It is difficult to quantify how much curvature is needed for favorable turbulent conditions, however, there are some guidelines established by Lee et al. (1984) which are useful:

- Moderate turbulence is expected when wind speeds are between 60 and 120 knots with a wind shift greater than 120 degrees (within a 200 nm area)
- Severe turbulence is expected when winds exceed 120 knots with a wind shift of 90 degrees or greater (within a 200 nm area)

Note that with increasing wind speeds, turbulence intensity increases and less wind directional shift is necessary to sustain the turbulence. The requirement that the wind shift occur within a 200 nm area ensures that the curvature is sharp and confined.

As Kaplan et al. (2002) found, upper-level curvature is a key pattern in identifying CAT. Curvature should be identified in the upper-level charts, and should be associated with jet analysis. Areas of sharp curvature are important regions to consider for CAT potential, but more important than just the curvature is where the jet stream or core is located with respect to the curvature. When strong winds exist in the curvature turbulence is likely, and the stronger winds result in an increase in turbulence intensity and probability. When there is a strong jet core in the point of maximum curvature, like shown in Figure 68, moderate or greater CAT potential is high. Figure 68 shows an anticyclonic curved ridge, but the same would apply for a sharply curved cyclonic trough as can be seen in Figure 69. Figure 70 shows the PIREPs for the example in Figure 69 which verify that turbulence does exist associated with the sharp trough and jet core.

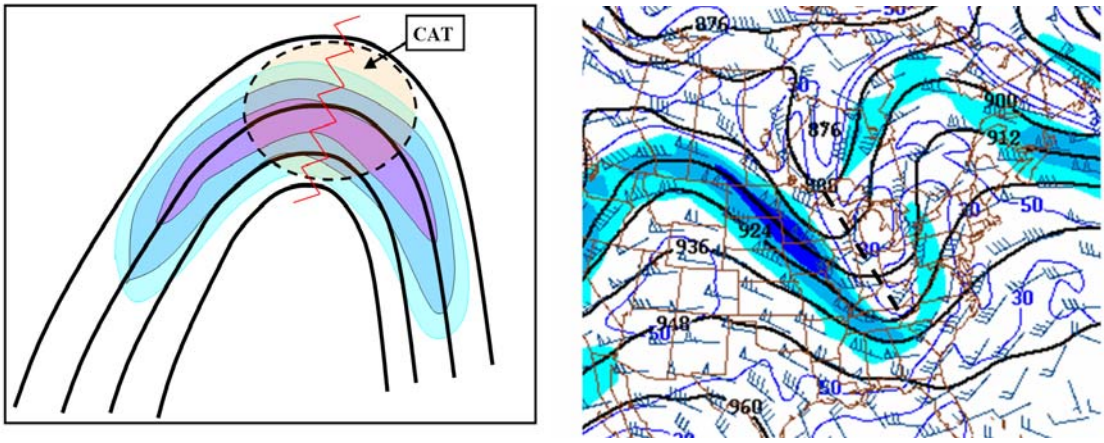

Figure 68. (a) Example of a jet core inside peak anticyclonic curvature. 300mb heights (solid black lines), 300mb jet shown in color filled isotachs with purple indicating jet core, and potential CAT area shown in shaded orange dashed oval. (b) Sharp cyclonic curvature can be seen over the Great Lakes and Midwest with a jet located inside the curvature although not exactly at the peak, CAT is still likely for 1800 GMT, 3 April 2006.

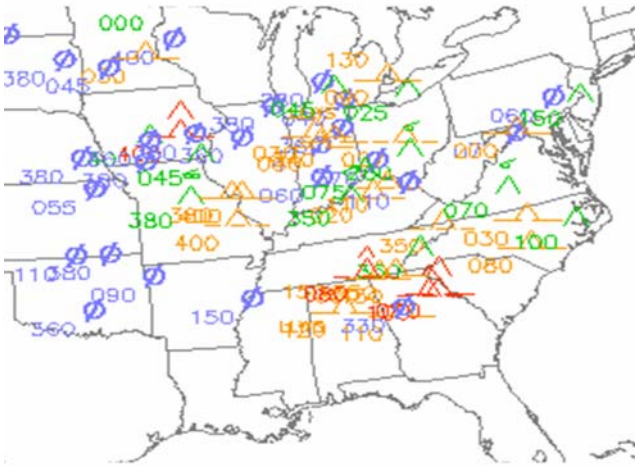

Figure 69. PIREPs for 1800 GMT, 3 April 2006. CAT reports are frequent in the area of maximum curvature from Iowa (maximum winds) to the Southwest US at the bottom of the trough (minimum winds).

f. Upward Vertical Motion

Recall from Table 8 that Kaplan et al. (2002) found that upward vertical motion was number three on their list of best predictors for CAT. When possible, vertical motion should be a part of the analysis process. The cross section is a useful way to view vertical motion as shown below in Figure 70 which goes back to the earlier example from 1800 GMT, 9 March 2006 and shows vertical motion on the cross-section plot. With the maximum upward vertical motion occurring underneath the jet core and in an area of significant vertical and horizontal wind shear, moderate or greater turbulence is very likely in this area.

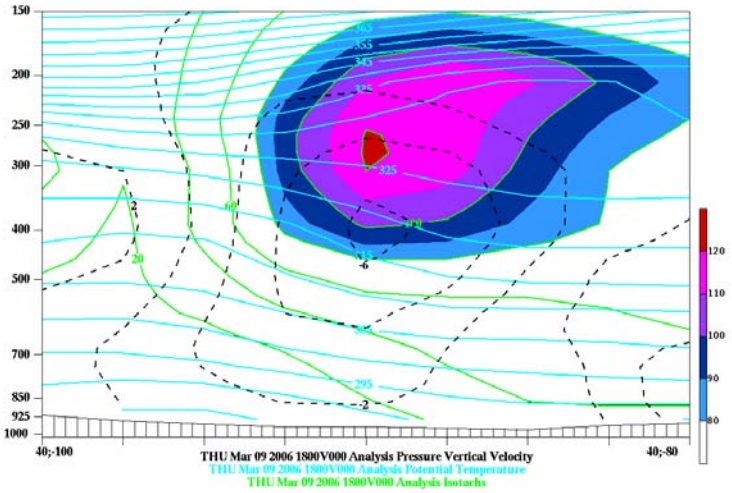

Figure 70. Pressure vertical velocity (mb/s; black dashed lines) is plotted for 1800 GMT, 9 March 2006 on this cross-section along with the isotachs (kts; green, color filled lines), and potential temperature (˚K; light blue lines). Negative values of vertical velocity indicate upward vertical motion. Maximum upward vertical motion occurs underneath the jet core around 400mb in the vicinity of the upper-level front.

g. Horizontal Deformation

Deformation zone CAT is common and found in the region where the atmosphere is undergoing contraction in one direction and elongation or stretching in the perpendicular direction, relative to the motion of the air stream (as in Figure 71) (AFWA TN 98-002). Recall Ellrod and Knapp (1992) also found horizontal deformation to be a significant factor in forming the CAT environment. A cloud border is often located near and parallel to the stretching axis. In Figure 71 a visible satellite image shows a typical deformation zone which can be favorable for the CAT environment.

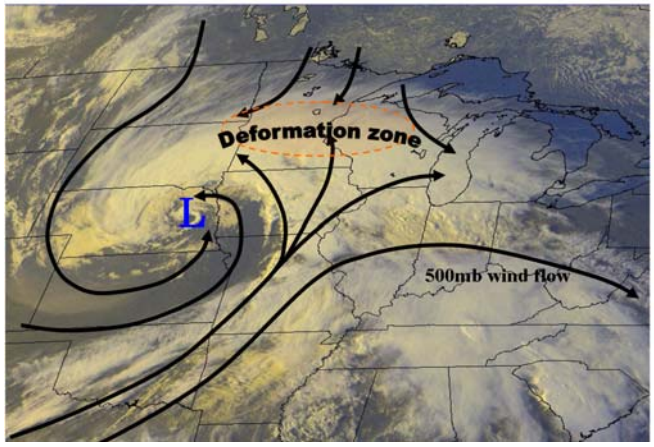

Figure 71. CAT in the deformation zone associated with the classic comma cloud pattern. Favorable CAT area shown in orange shaded region. Black stream lines represent general 500mb flow pattern. Adapted from AF 15th OWS SOP-3 (2006). Also shows how use of satellite imagery can help identify areas of CAT.

h. Horizontal cold air advection

The 500 mb chart is a very common and useful weather analysis chart. Horizontal cold air advection at 500mb as well as significant positive vorticity, which is related to strong vertical motion, are often found associated with a mobile upper-level front near the jet stream. CAT frequently occurs in regions of increasing thermal gradients and increasing vertical wind shear. Consequently, using the 500mb chart to identify regions of significant cold air advection and positive vorticity can be useful in predicting favorable regions of CAT. Figure 72 below shows 500mb heights, isotherms, and absolute vorticity for 1800 GMT, 9 March 2006. Note the significant cold air advection and vorticity over northeastern Montana. In the 300mb chart this was an area of curvature, specifically it appeared to be at the bottom of a sharp, tilted 300mb trough. However winds were not significant and no jet was in the area and so the forecaster might dismiss this area as not likely for turbulence. But this 500mb chart should give the forecaster some further indication that turbulence may exist in this area due to the horizontal cold air advection, vorticity, and likely significant shear that is developing over northeastern Montana. Over the Southern Plains there is significant positive vorticity in the isotherm trough as well as some temperature advection. This area corresponds to the entrance region of the 300mb jet core that was shown in Figures 63 and 64. The observed moderate or greater CAT was mostly downstream of the maximum vorticity over Illinois, Wisconsin, and Iowa.

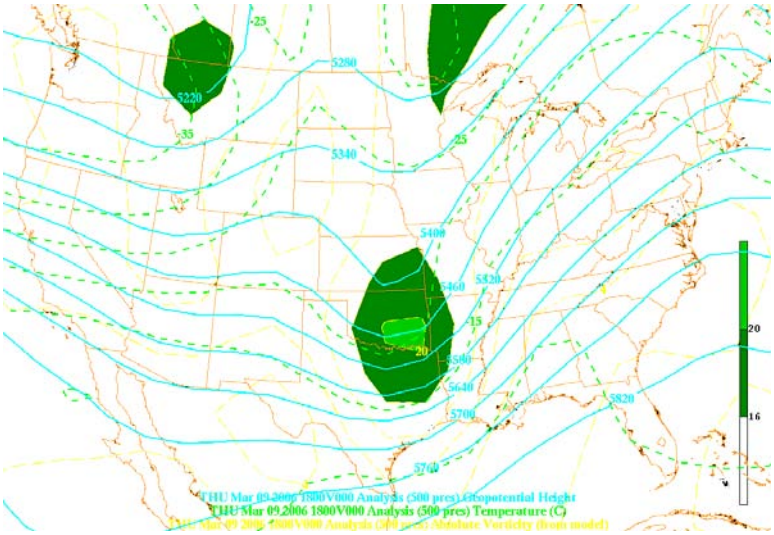

Figure 72. 500mb analysis chart for 1800 GMT, 9 March 2006 with heights (m; blue solid lines), isotherms (˚C; green dashed lines), and absolute vorticity (s^{-1}; yellow dashed and color filled) shown.

3. Mountain Wave

Mountain wave turbulence can be a significant hazard to aircraft and is most common near large, distinct mountain ranges. Mountain wave systems can occur whenever strong flow in a stable environment encounters a topographic barrier. Forecasting mountain wave turbulence has been fairly well studied, and perhaps the most useful and reliable approach is identifying where mountain waves exist by cloud identification, by eye or by satellite imagery. AFWA TN 98-002 (2005) lists the following cloud features that are indicators of mountain wave activity:

> There are specific clouds associated with mountain wave turbulence. These are cap (foehn wall), roll (rotor), lenticular, and "mother-of-pearl" clouds. Figure 73 illustrates the structure of a strong mountain wave and associated cloud patterns. The lines and arrows depict windflow.

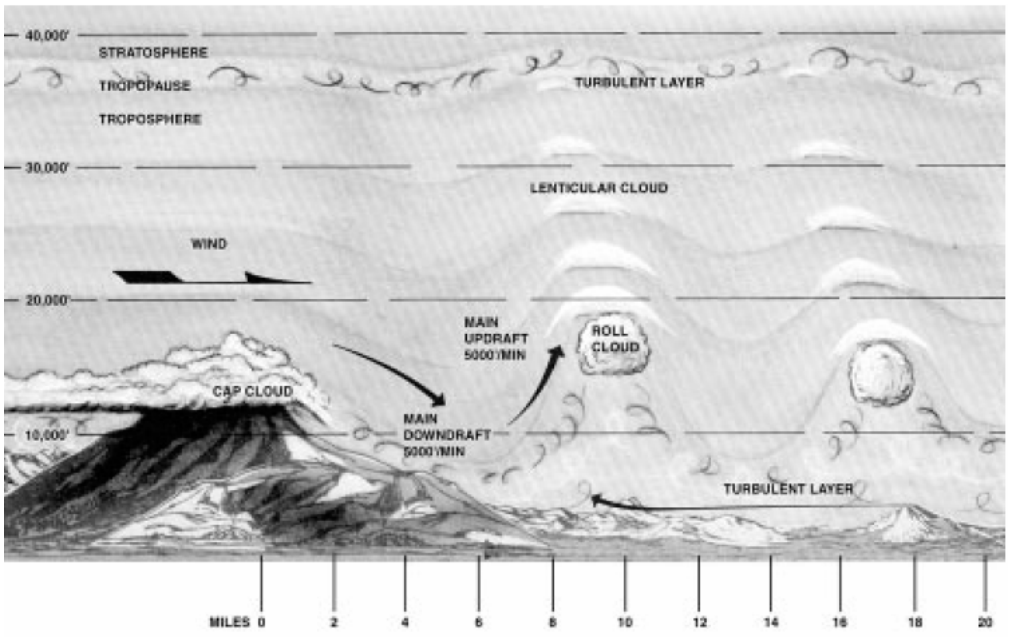

Figure 73. Mountain-wave cloud structure. The figure illustrates the structure of a strong mountain wave and associated cloud patterns. The lines and arrows depict windflow. (Figure 2-49 in AFWA TN 98-002).

Cap Cloud. The cap cloud hugs the tops of mountains and flows down the leeward side with the appearance of a waterfall. This cloud is dangerous because it hides the mountain and has strong downdrafts associated with it. The downdrafts can be as strong as 5,000 to 8,000 feet per minute.

Roll Cloud. The roll cloud, also called a rotor cloud, looks like a line of cumulus clouds parallel to the ridge line. It forms on the lee side and has its base near the height of the mountain peak and top near twice the height of the peak. The roll cloud often merges with the lenticular clouds above, forming a solid cloud mass to the tropopause. The roll cloud is dangerously turbulent with strong updrafts (5,000 feet per minute) on the windward side and dangerous downdrafts (5,000 feet per minute) on its leeward edge. This cloud may form immediately on the lee of the mountain or it may be a distance of 10 miles downwind – depending on wind speed.

Lenticular Clouds. Lenticular clouds are relatively thin, lens-shaped clouds with bases above the roll cloud. Their tops extend to the tropopause. These clouds have a tiered or stacked look due to atmosphere stability above the mountain ridge. All lenticular clouds are associated with turbulence. In polar regions, lenticular clouds can appear in the stratosphere as high as 80,000 feet. These clouds are called “mother-of pearl” (nacreous) clouds.

Another important feature to look for when identifying mountain wave activity is the foehn gap which indicates turbulent lee waves are present. The gap is located between the cirrus clouds and mountain range on the leeward side of the range as shown in Figure 74.

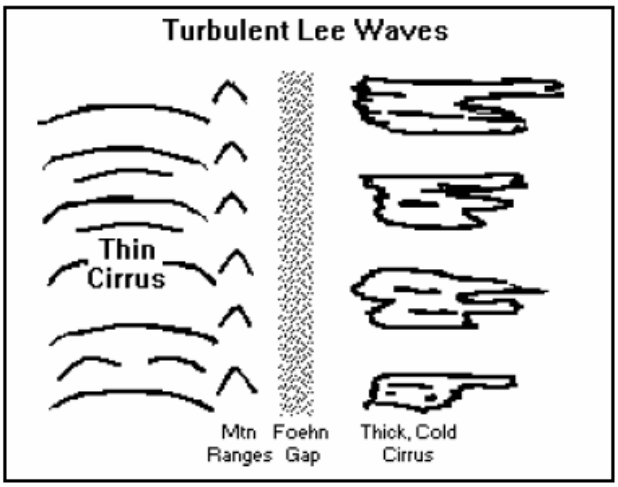

Figure 74. A foehn gap shown here with the typical mountain-wave clouds indicates turbulent waves are present (AFWA TN 98-002, 2005).

Mountain wave intensity depends on several factors, but generally is proportional to turbulence intensity. Mountain wave intensity factors include: wind speed, height and slope of the mountain (highest, steepest mountain produces most intense wave and turbulence), stability above and to the lee of the mountain (very stable air above and to the lee of the mountain produces most intense turbulence) (AFWA TN 98-002, 2005). Some necessary ingredients for significant mountain wave development are as follows:

- A minimum wind component of 25 knots perpendicular to the mountain ridge at the height of the ridge.
- Wind profile should show very little change of wind direction with height and increasing wind speeds with altitude high into the troposphere.

Table 10 and Figure 75 (used together), provide guidance in forecasting mountain wave turbulence.

Table 10. Low-level mountain wave turbulence. (Lee et al. 1984).

Low-Level Mountain-Wave Turbulence (Surface To 5,000 Ft Above Ridge Line)			
Low-Level Feature Wind Component Normal to Mountain Range at Mountain Top and > 24 kt **and**	**Turbulence Intensity**		
	Light	**Moderate**	**Severe**
dP Across Mountain at Surface is	See Figure 2-48	See Figure 2-48	See Figure 2-48
|dT| Across Mountain at 850 mb is	< 6°C	6°C - 9°C	> 9°C
|dT/dX| Along Mountain Range at 850 mb is	<4°C/60 NM	4-6°C/60 NM	>6°C/60 NM
Lee-Side Surface Gusts	< 25 kt	25 - 50 kt	> 50 kt
Winds Below 500 mb > 50 kt	Increase the Turbulence found by one degree of intensity (i.e., Moderate to Severe)		

Notes: (1) dP is the change in surface pressure across the range.
(2) |dT| is the absolute value of the 850-mb temperature difference across the range.
(3) |dT/dX| is the absolute value of the 850-mb temperature gradient along mountain range.
(4) Turbulence category forecast is the worst category obtained from each of the four parameters.

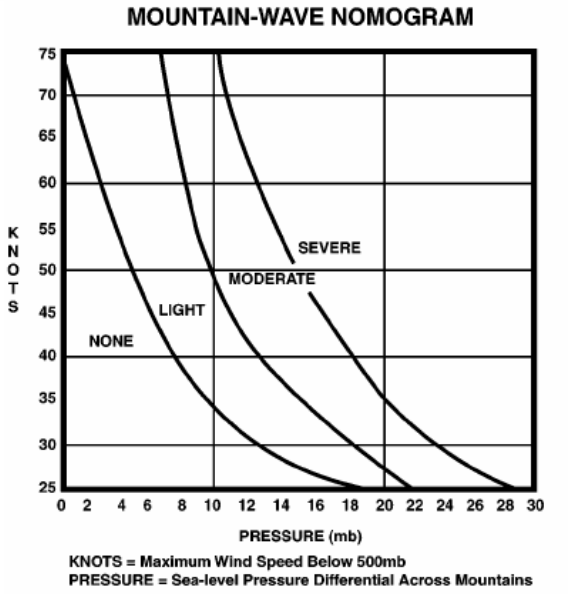

Figure 75. Mountain-wave nomogram to be used to predict mountain wave intensity (Lee et al. 1984

a. Trapped Lee Waves

Trapped lee waves are often found downstream of the rotor zone, although a weak rotor may exist under each lee wave. These waves are typically at an altitude within a few thousand feet of the mountain ridge crest and turbulence is generally restricted to altitudes below 25,000 feet. Strong turbulence can develop between the bases of associated lenticular clouds and the ground. Lenticular clouds form near the crests of mountain waves (UCAR 2005a). A deep, stable layer with smooth, horizontal flow that increases with height above the barrier will result in a series of shallow trapped lee waves. A general rule of thumb, called the "1.6 rule," is useful: if the wind speed at 2000 m above ridge-top level is more than 1.6 times the ridge-top wind speed, then you should expect a trapped lee wave regime (UCAR 2005a).

The sounding in Figure 76 shows that while winds near the surface are light, winds at ridge-top level are 25-35 knots. The sounding also reveals an incredibly strong inversion immediately above ridge-top level. Under these conditions, the forecaster should expect a significant wave response. In Figure 76, wind speeds increase from 25 knots at 650 hPa to 55 knots at 550 hPa, which clearly exceeds the 1.6 rule-of-

thumb. On this day significant trapped lee waves were observed and there were several EDR reports of light and moderate turbulence near Riverton, WY ranging in elevation from 697mb to 496mb. Thus, rawinsonde observations can be used to evaluate the vertical structure of wind and atmospheric stability. The limitation is the availability of observations at proper locations. Ideally, they should be positioned upstream of the mountain barrier where ambient atmospheric conditions can be assessed (UCAR 2005a).

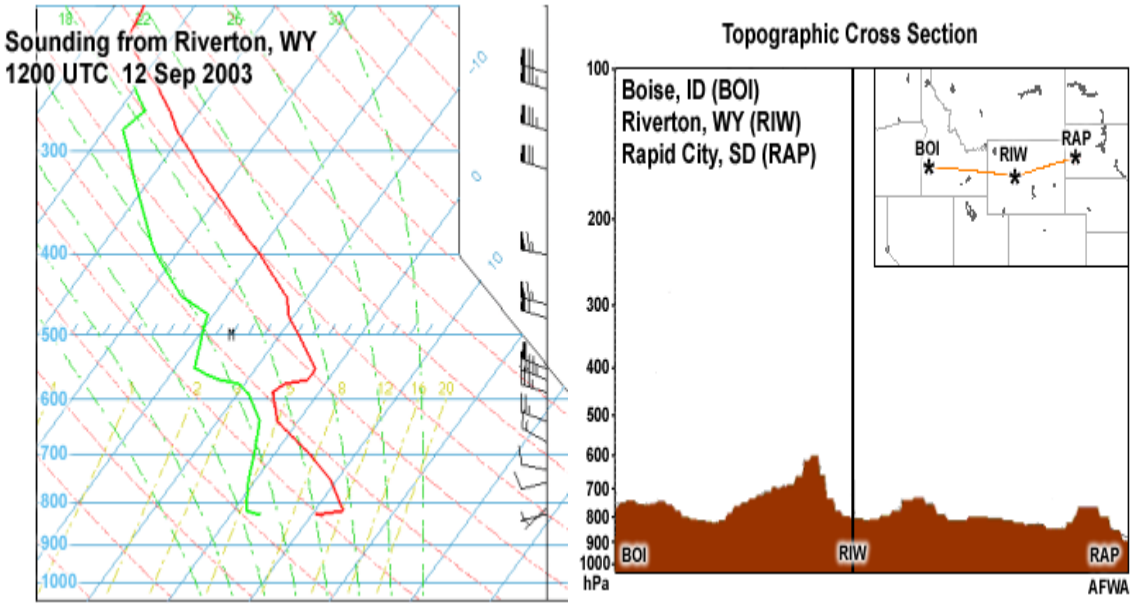

Figure 76. On the left is a sounding from Riverton, Wyoming at 1200 UTC on 12 September 2003. On the right is a vertical cross section of topography which shows that the Rocky Mountains lie immediately to the west of Riverton. The mountains are oriented north-south and ridge-top level is approximately 600 hPa (UCAR 2005a).

b. Vertically Propagating Waves (VPWs)

VPW develop on the leeside of large-scale mountain ranges like the Rockies, and much like trapped lee waves, occur when upstream synoptic-scale flow becomes perpendicular to the mountain ridge axis. They can also develop to the lee of much smaller, isolated terrain causing additional complexity. What distinguishes a trapped lee wave response from a VPW is the atmospheric stability and shear. While increasing stability favors a trapped lee wave, it is detrimental to a VPW. Specifically, a mountain top inversion like that shown in the Figure 76 sounding will not allow a VPW to exist. However, the atmosphere must be stable in order for a mountain wave to exist, so some stability is required for a VPW. Vertical wind shear is also detrimental to a VPW while wind greatly increasing with height is favorable for a trapped wave. To excite a VPW, having a wind profile with little change in speed or direction at and above the mountain (i.e., no jet max aloft) is necessary. The 1.6 rule-of-thumb mentioned above for trapped lee waves can still be utilized for VPWs, but with VPWs the mountain top wind speed should be less than 1.6 times the wind speed 2000 m above mountain top

to allow vertical propagation (Coughlin 2005). For further information on VPWs the reader/forecaster is referred to Coughlin (2005) and to UCAR (2005a) which offers a very useful online module on mountain waves.

B. TURBULENCE DATA AND REPORTS

Observations should be used to verify patterns and favorable areas identified in the forecaster's analysis, and to alert the forecaster of all reported turbulent areas. PIREPs are the traditional and most widely used method, and still the only method being used outside of CONUS, although they are highly subjective and pilot dependent. EDR observations offer a more objective approach, with potentially greater coverage capability but the majority of current aircraft are unequipped with the technology capable of reporting EDR values, resulting in limited spatial coverage to the 100 or so aircraft routes that do have EDR capability. Both types of observations offer the only insight available into the true turbulent atmosphere and should be utilized by the forecaster. Satellite imagery and radar data should also be used to help identify regions of turbulence and will be discussed in more detail later. Because turbulence is such a brief, microscale phenomena it can be dangerous to simply forecast persistence. That is, if a PIREP is reported in a region of interest, the forecaster should not automatically forecast turbulence for that region over the next 12 to 24 hours, or even in the region downstream of that PIREP. Rather the forecaster should attempt to understand what is causing the turbulence (i.e., strong vertical wind shear, a jet core through a sharply curved ridge, a strong upper-level front, etc.). Once the forecaster has some idea of what caused the turbulence the forecast should be made based on whether those conditions will continue to exist or not.

An effective way to use EDR and PIREPs observations is to overlay them on a 300mb (or an alternative upper-level) chart as done in Figure 77. In Figure 77 only the EDR observations are shown and the forecaster can quickly see that there is moderate turbulence being reported (via EDR observations) associated with the strong north-south jet core located over the southern Great Lakes region. The forecaster can also quickly see that there is moderate turbulence being reported over Montana and Idaho not associated with any jet and as such may require further investigation by the forecaster. Upon further investigation the forecaster will find that these observations are at 39,980 ft (188mb) near the tropopause or in the stratosphere. A weaker and narrow wind maximum of about 60 knots extended down through Montana and Nevada and a cross-section through Montana reveals this maximum occurs at about 250mb with sharply decreasing winds above the maximum and to the east and west which would be conducive for the CAT environment. The EDR observations over California and Nevada seem to indicate a lack of moderate-or-greater turbulence associated with the jet streak off of the Pacific Coast, however, there were three PIREPs of moderate turbulence during this time period over southwest Nevada and southeast California. Recall that the coverage of EDR observations is currently limited and thus, PIREPs can often provide very useful information where EDR observations can not.

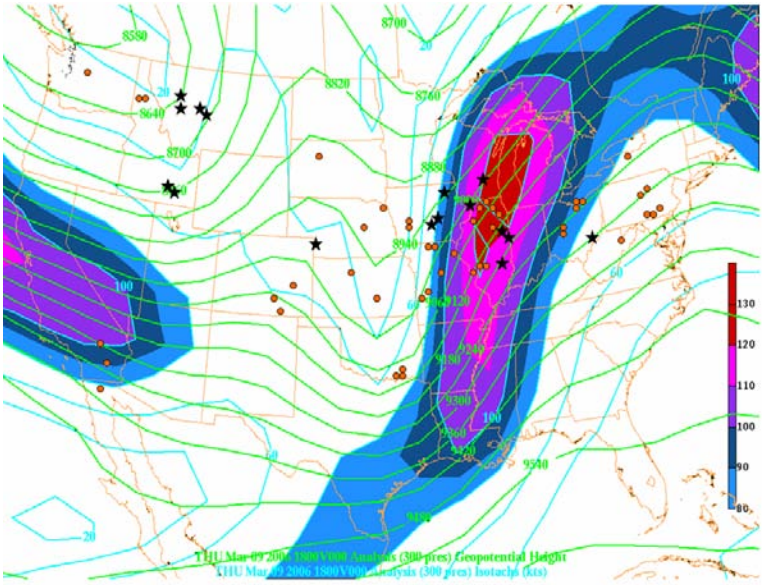

Figure 77. Same as Figure 64. The figure illustrates how EDR observations can be used to help identify and alert the forecaster as to where CAT is occurring and thereby validate forecaster's first guess at the turbulent state of the atmosphere from the synoptic analysis.

1. Accessing EDR observations

EDR observations currently are only available via the NOAA/ESRL/GSD aircraft data web. Current EDR data is only available to NOAA sites and users with a login and password account. The term ACARS is used to designate automated weather reports from commercial aircraft and stands for Aircraft Communications Addressing and Reporting System. Because the ACARS data is proprietary to the airlines providing the data, certain restrictions may apply to accessing the data. ACARS data can be received in several ways: Web-based graphical displays, either java-based or not, web-based access to binary data in netCDF format , or LDM access to binary data in netCDF format. The web-based graphical display using java is very useful and shown below in Figure 78. It can be accessed at http://acweb.fsl.noaa.gov/java/. The default load page is shown in Figure 78a. For the java display the forecaster can view EDR information to include the EDR category, aircraft number, and elevation of each EDR observation. The forecaster can also right click on the observation and bring up a window like that shown in Figure 78c which shows every observation that aircraft has made on that flight route. Additionally, the forecaster can slide the tabs on the ruler to right of the map in Figure 78b up and down to display observations for certain altitudes only. For example, if the forecaster wanted to focus in on CAT only, then he/she could bring the bottom tab up to 20,000 feet and EDR observations for 20,000 feet to 40,000 feet would be displayed which might rid the map of some clutter from lower altitude observations.

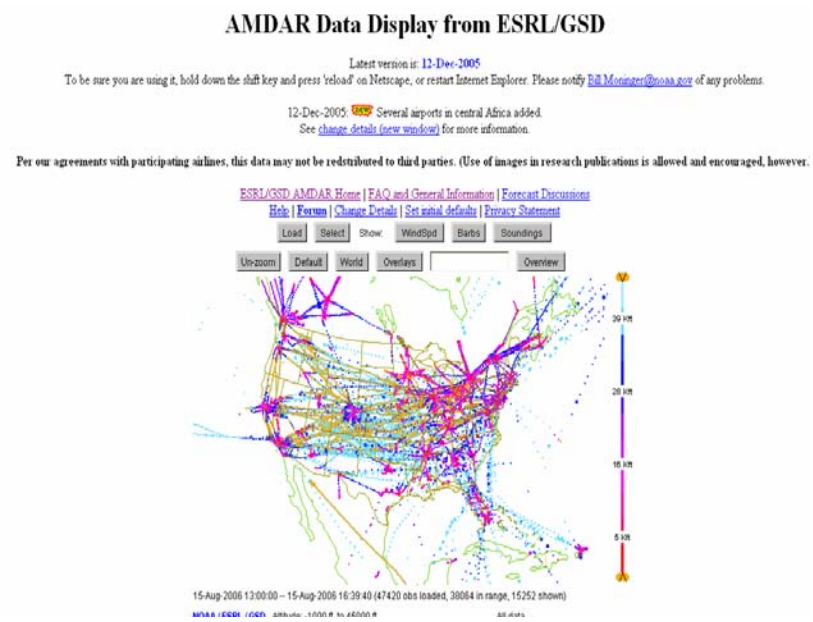
AMDAR Data Display from ESRL/GSD
Latest version is: 12-Dec-2005
To be sure you are using it, hold down the shift key and press 'reload' on Netscape, or restart Internet Explorer. Please notify Bill.Moninger@noaa.gov of any problems.
12-Dec-2005: NEW! Several airports in central Africa added.
See change details (new window) for more information.
Per our agreements with participating airlines, this data may not be redistributed to third parties. (Use of images in research publications is allowed and encouraged, however.
ESRL/GSD AMDAR Home | FAQ and General Information | Forecast Discussions
Help | Forum | Change Details | Set initial defaults | Privacy Statement
Load Select Show: WindSpd Barbs Soundings
Un-zoom Default World Overlays Overview
39 Kft
28 Kft
16 Kft
5 Kft
15-Aug-2006 13:00:00 – 15-Aug-2006 16:39:40 (47420 obs loaded, 38084 in range, 15252 shown)

(a)

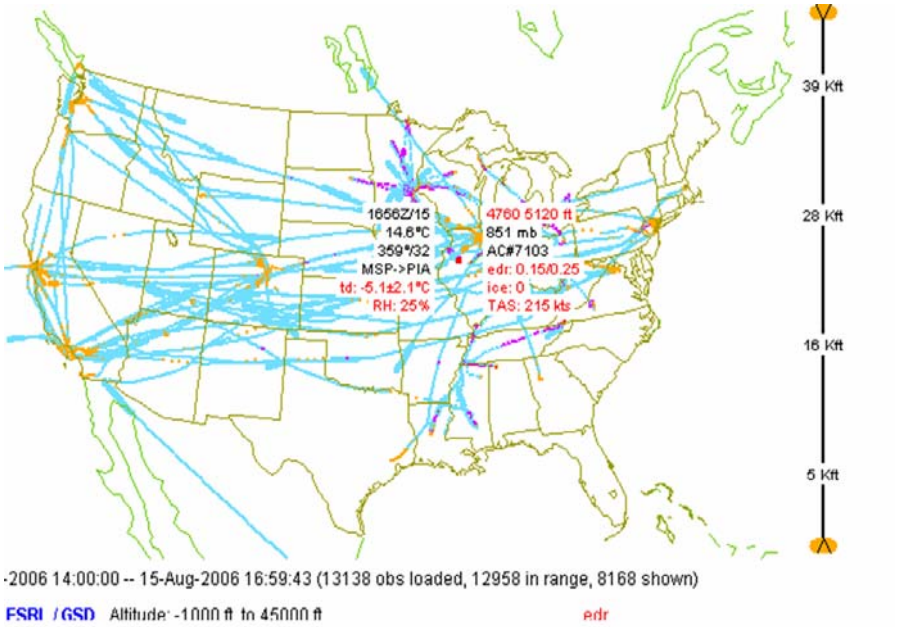
1656Z/15
14.6°C
359°/32
MSP->PIA
td: -5.1±2.1°C
RH: 25%
4760 5120 ft
851 mb
AC#7103
edr: 0.15/0.25
ice: 0
TAS: 215 kts
39 Kft
28 Kft
16 Kft
5 Kft
-2006 14:00:00 -- 15-Aug-2006 16:59:43 (13138 obs loaded, 12958 in range, 8168 shown)
ESRL/GSD Altitude: -1000 ft to 45000 ft
edr

(b)

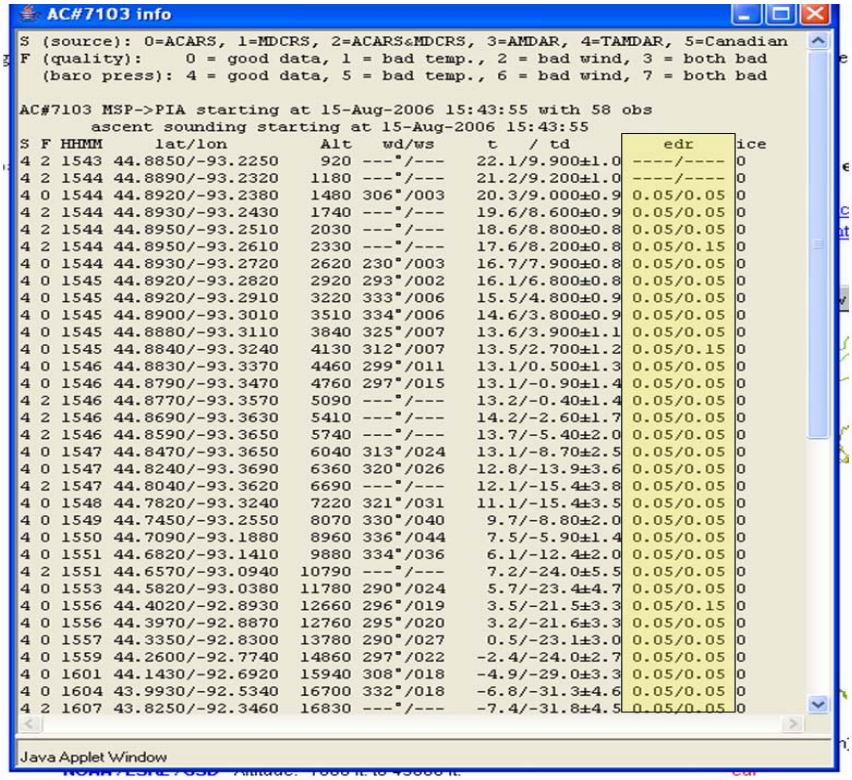

(c)

Figure 78. (a) Web-based java display default load page (http://acweb.fsl.noaa.gov/java/) (b) forecaster can move cursor over any EDR observation and that observation information will be displayed. (c) if forecaster right clicks on an EDR observation, a list of every EDR observation of that particular aircraft for that flight will be displayed along with it's elevation and lat/long position (EDR column is highlighted for clarity).

2. Accessing PIREPs

It is assumed that the forecaster already has some knowledge of using PIREPs and where to access them. PIREPs are available from a wide variety of platforms and sources, but they all share the same basic form that has been shown throughout this chapter and all have been taken from the NOAA/NWS AWC turbulence website; http://adds.aviationweather.gov/turbulence/. Most PIREPs displays are shown as images and are not java-based displays like the EDR observations shown previously. This can make some PIREPs displays difficult to read, particularly the elevation of PIREPs when there are a large number of PIREPs in a small region. While not as glamorous as the EDR display shown in Figure 78, the vital information (location, elevation, and intensity of turbulence) is relayed to the forecaster.

3. Satellite Imagery

a. IR/VIS

Turbulence can sometimes be detected in infrared (IR) or visible (VIS) satellite imagery. There are two distinctive features which the forecaster should look for in IR/VIS images; transverse bands and billows. Transverse bands are defined as

irregular, wavelike cirrus cloud patterns that form nearly perpendicular to the upper flow (AFWA TN 98-002, 2005) and can be seen in Figure 79 in VIS and IR images. These bands are usually associated with the low latitude subtropical jet stream and indicate large vertical and possibly horizontal wind shears. The additional presence of thermal instability commonly causes severe turbulence in the wider, thicker transverse bands and these bands often have a carrot-shaped appearance, similar to cumulonimbus anvils. Cloud bands, in general, tend to be aligned with the cloud layer shear vector. For this reason, the presence of cirrus bands which differ in orientation from the prevailing wind direction (transverse to the flow) indicate directional shear with height (AFWA TN 98-002, 2005).

Billows are wave cloud patterns in cirrus, or middle-level clouds which are regularly spaced, narrow, and oriented to the upper flow (AFWA TN 98-002, 2005). Billows are commonly visible when a strong jet intersects either a frontal cloud system or a line of cumulonimbus clouds at a large crossing angle. The anvil debris of convective clouds in these situations extends well downstream from its source. The individual wave clouds dissipate quickly (i.e., less than 30 minutes), however, new waves can reform nearby when favorable conditions exist. Turbulence intensity does seem to correlate well with the wavelength of the billows; the longer the wavelength of the billows, the better the chance for significant turbulence (AFWA TN 98-002, 2005).

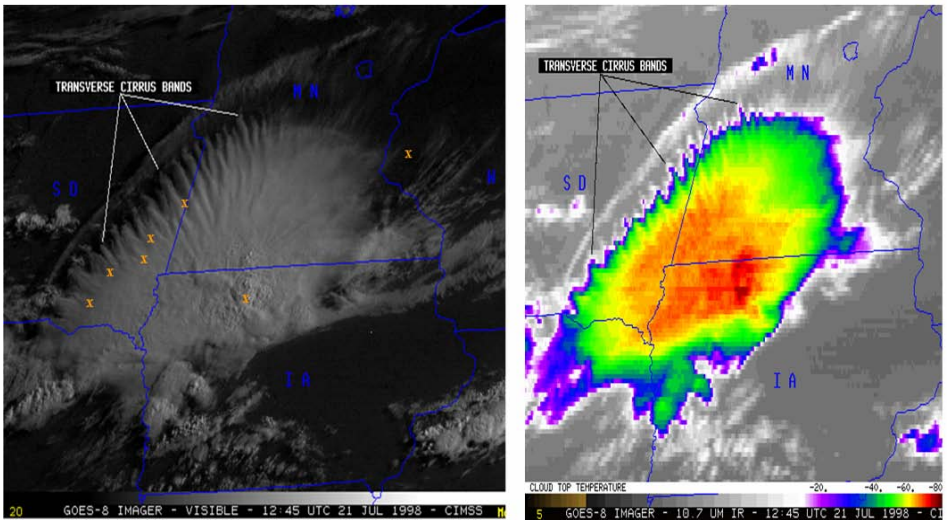

(a) (b)

Figure 79. A series of transverse cirrus bands are distinctly visible in the (a) NOAA GOES-8 VIS image and (b) NOAA GOES-8 IR image from 1245 GMT, 21 July 1998. Such transverse bands are often satellite signatures of high-altitude turbulence and can form along the northern periphery of convective storms (CIMSS 2006). Several reports of moderate turbulence (orange 'x's in (a)) were received from aircraft flying between 33,000 and 39,000 feet across eastern South Dakota, southern Minnesota, and western Wisconsin from 1000 GMT to 1500 GMT. The moderate turbulence over northern Iowa is likely the result of convective turbulence.

b. Water Vapor

Water vapor imagery can also be very useful for identifying turbulence. The forecaster should look for water vapor darkening; elongated bands, or large oval-shaped gray regions that become darker in successive images (AFWA TN 98-002, 2005). Cold advection and convergence in the middle and upper troposphere result in compensating sinking through a deep layer. Cross sections of such features reveal sloping baroclinic zones and/or tropopause folds indicating stratospheric air may be descending into the upper troposphere and creating a very favorable environment for turbulence. Moderate or greater turbulence occurs 80 percent of the time when water vapor darkening occurs, especially if the darkening persists for at least three hours (AFWA TN 98-002, 2005) as it does in Figure 80. Mountain waves or trapped lee waves can also often be detected in satellite imagery. Figure 80 illustrates mountain waves in water vapor imagery.

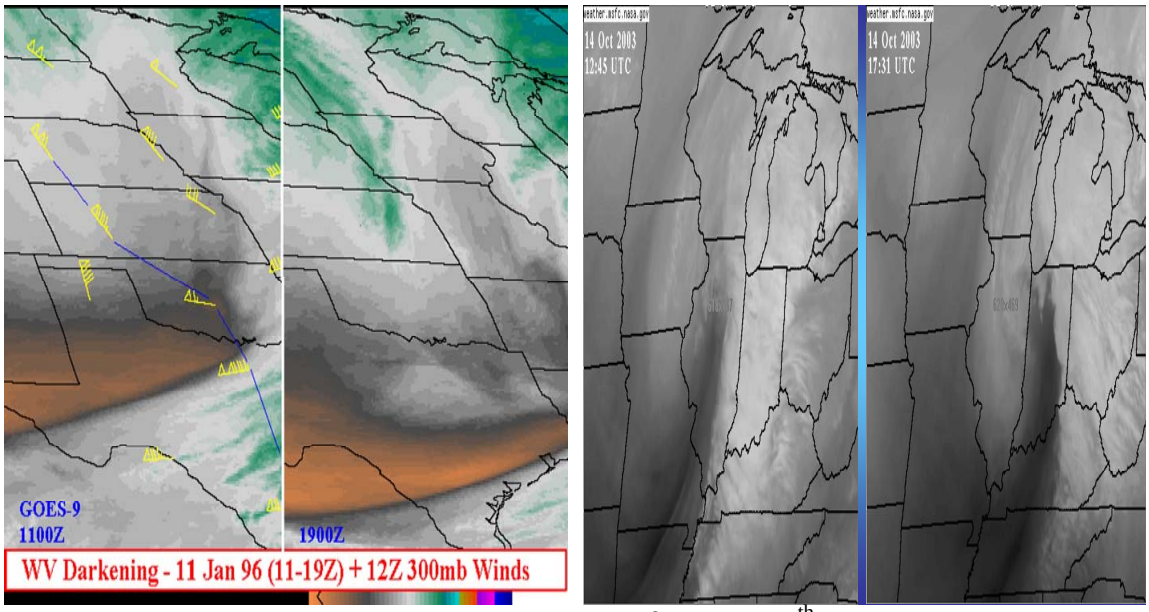

Figure 80. Water vapor darkening examples from AF 15th OWS SOP-3 (2006). Darkening exists in both of the GOES-9 water vapor images. On the left the darkening occurs over an 8 hour period, and on the right it occurs over a 5 hour period. Moderate or greater turbulence occurs 80 percent of the time in such areas of darkening (AF 15th OWS SOP-3 2006).

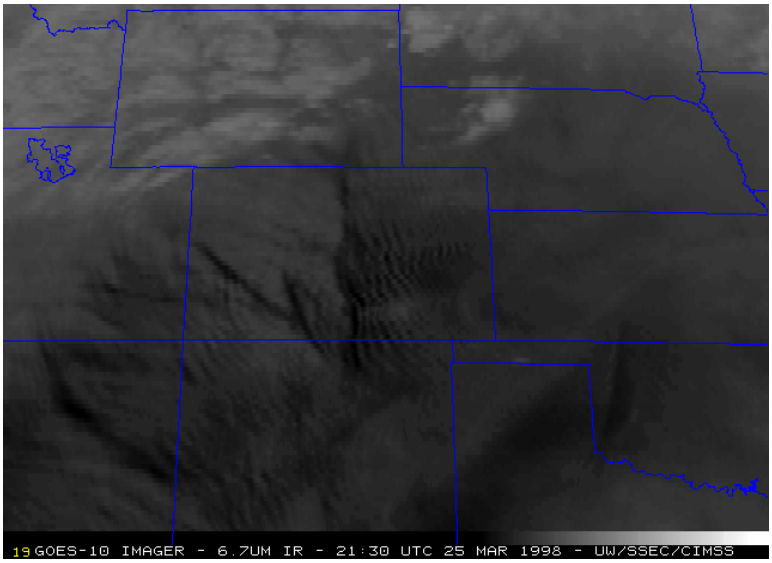

Figure 81. GOES-10 water vapor imagery shows widespread mountain waves over Colorado and New Mexico at 2130 GMT, 25 March 1998. Such a signature on water vapor imagery can often indicate turbulence (CIMSS 2006).

4. Radar

Although the radar is not commonly associated with turbulence, it can be quite useful in identifying convective turbulent regimes. The radar's ability to display convection is of great value to the forecaster. A quick look at the current radar can highlight regions where convection is taking place, and consequently the forecaster should focus in on these areas as favorable for convective turbulence. The radar can also account for the intensity of the convection which is proportional to the intensity of convective turbulence. Figure 82 is a national composite radar image from the NWS for 1858 GMT, 10 August 2006.

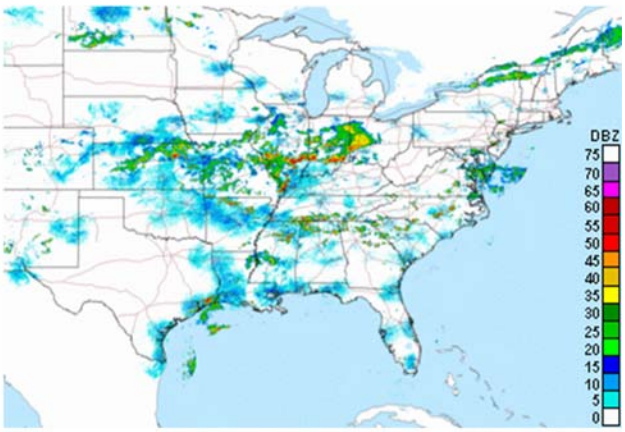

Figure 82. NWS composite radar image for 1858 GMT, 10 August 2006. Most intense convection is shown by red colors located over northeastern Kansas, southern Illinois and Indiana, and western Ohio. These are areas the forecaster should then further look for turbulence.

The intense convection over northeastern Kansas, southern Illinois and Indiana, and western Ohio should alert the forecaster that convective turbulence is likely in these areas and requires further investigation. By considering the current EDR observations, shown in Figure 83, the forecaster can see that turbulence is present in these convective areas. The forecaster can overlay the EDR or PIREPs observations onto the radar or even satellite imagery in much the same way that was done with the 300mb chart.

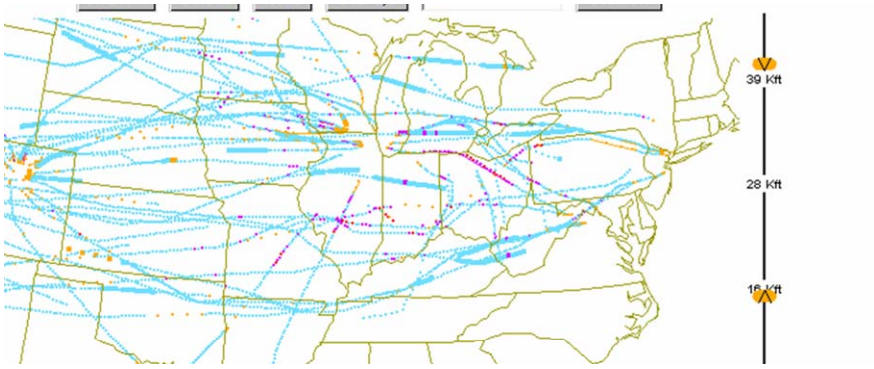

Figure 83. EDR observations from ESRL/GSD confirm the presence of turbulence in the convective areas shown in Figure 83.

The WSR-88D radar has additional functionality which can help in identifying turbulence favorable environments. This radar can provide unique, near real-time capabilities to detect and display turbulence indicators such as frontal boundaries, low-level jets, gust fronts, and upper-level wind shear (AFWA TN 98-002, 2005). Some of the WSR-88D products useful in turbulence forecasting are described here:

a. Spectrum Width

This WSR-88D radar product depicts a full 360 degree sweep of spectrum width data indicating a measure of velocity dispersion within the radar sample volume and is available for every elevation angle sampled (NWS 2006). The spectrum width provides a measure of the variability of the mean radial velocity estimates due to wind shear, turbulence, and/or the quality of the velocity samples. It is used to estimate turbulence associated with boundaries, thunderstorms, and mesocyclones, and also to locate boundaries (cold front, outflow, lake breeze, etc.) (NWS 2006). Though not conclusive, spectrum width values of 8-11 knots are often associated with moderate turbulence and values 12 knots or higher may indicate severe turbulence (AFWA TN 98-002, 2005). The spectrum width product can be used to confirm suspected turbulence areas found using other products.

b. Velocity Azimuth Display (VAD)

This product shows the radar derived wind speeds at various heights from 2,000 to 55,000 feet above the ground (NWS 2006). This product can allow the forecaster to examine the current and past vertical wind structure to help identify meteorological conditions associated with atmospheric turbulence evolving over time (e.g., inversions, wind shears, and development of jet streams). Look for areas of sharp turning in the winds with high wind speeds to identify strong local vertical wind shear (AFWA TN 98-002, 2005).

c. Base Velocity

This product displays horizontal wind velocities. Areas of sudden speed or directional shifts are associated with wind shear and atmospheric turbulence. Intense shear regions, such as the top of the thunderstorm associated with storm top divergence, can also be located using base velocity (AFWA TN 98-002, 2005).

d. Vertically Integrated Liquid (VIL)

The VIL is a property computed by the WSR-88D that takes into account the three-dimensional reflectivity of an echo (NWS 2006). The maximum VIL of a storm can be useful in determining the potential for severe convective weather and associated wind shear and turbulence (NWS 2006).

C. TURBULENCE DIAGNOSTICS

During the 1990's there was a strong advance towards using automated diagnostics to predict possible turbulent areas. This effort led to the development of the GTG which has now surpassed the individual performance of any one of the diagnostics. However, the diagnostics can still provide useful information as discussed previously. In terms of forecasting, the automated diagnostics should be used when possible to help the forecaster understand the underlying causes of the turbulence (i.e., strong vertical wind shear, a jet core through a sharply curved ridge, a strong upper-level front, etc.). Recall, the Ellrod TI2 index (Ellrod and Knapp 1992) is available through the JAAWIN site and is used by the AFWA for the strategic-level forecast product. The forecaster should utilize these automated diagnostic products for more specific turbulence forecasting. For example, if the Ellrod TI2 index showed that a region was favorable for turbulence, then the forecaster would know that strong vertical wind shear, deformation, and convergence were present for that area. In this sense, the automated diagnostics should not be used as a forecast of turbulence but used as guidance to the forecaster in the turbulence forecast approach.

D. MESOSCALE MODEL DATA

The primary function of the forecast models for turbulence forecasting is to animate those patterns and characteristics recognized as being favorable for turbulent conditions into the future. Again, because of the complex microscale nature of turbulence, turbulence forecasts should generally not be made for much more than 24 hours from forecast time and only mesoscale or smaller models should be considered. If a longer forecast is necessary, the forecaster should relay to the customer the high degree of uncertainty in the forecast and that essentially the forecast would have to be made based on pattern recognition in predicted fields such as the 72 hour forecast 300mb winds. A large scale model such as the GFS or NOGAPS should not be used in forecasting turbulence because of the large horizontal and vertical resolution of those models. The AFWA MM5, the NCEP's RUC-2, and the ETA model, as well as the new WRF model are all mesoscale models that are acceptable for use in the turbulence forecast approach.

Models have become extremely proficient at 24 prediction and so they should be utilized by the turbulence forecaster for short-term forecasts. The forecaster should first look for all the patterns and characteristics of the turbulence favorable environment (Section A of this chapter) in the forecast fields. If a pattern, such as a sharply curved

trough with a strong jet core, is identified in the analysis the forecaster should pay special attention to how the model develops the pattern over the forecast period and use such guidance in making the final turbulence forecast. If no patterns were recognized in the analysis, the forecaster should look for the development of those patterns during the forecast period.

Not only should model forecast fields be considered, but also post-processed algorithms like the GTG should be utilized. The GTG is run on the RUC-2 model output and is a sum of the best automated diagnostics and weighted by current observations (PIREPs). It has been shown to be quite skillful in turbulence prediction, far superior to any automated diagnostic by itself, and even superior to many subjective human forecasts (Sharman et al. 2006). The GTG can provide grid-scale forecasts, which allow for much more specific horizontal and vertical resolution in the turbulence forecast than can be hand drawn on a 2-dimensional chart. The GTG forecast by flight level can be found at http://adds.aviationweather.gov/turbulence/ and is readily accessible to any user with online access. The AWC also offers a Flight Path Tool on this site which can be an extremely valuable tool to the aviation forecaster allowing the user to plot a cross section of any flight route he/she chooses with various variables such as turbulence displayed. Figure 84 shows a cross section with the GTG turbulence forecast plotted for an arbitrary flight path from approximately Offutt Air Force Base (AFB), NE to Shaw AFB, SC with a cruise level at FL300. The light green is predicted light turbulence areas, with the orange being predicted moderate turbulent areas and the black line shows the FL300 elevation line.

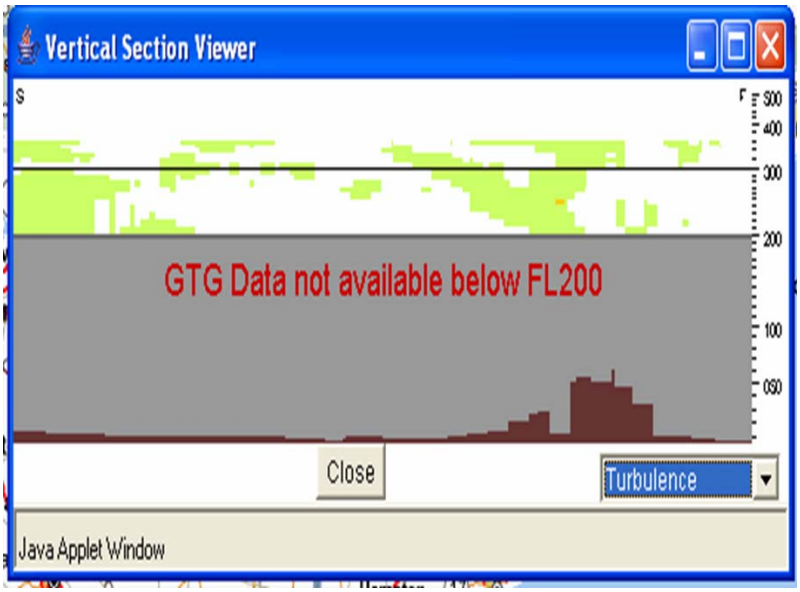

Figure 84. The light green is predicted light turbulence areas, the orange is predicted moderate turbulent areas and the black line shows the FL300 elevation line. Screen capture from http://adds.aviationweather.gov/flight_path/index.php (accessed 2006).

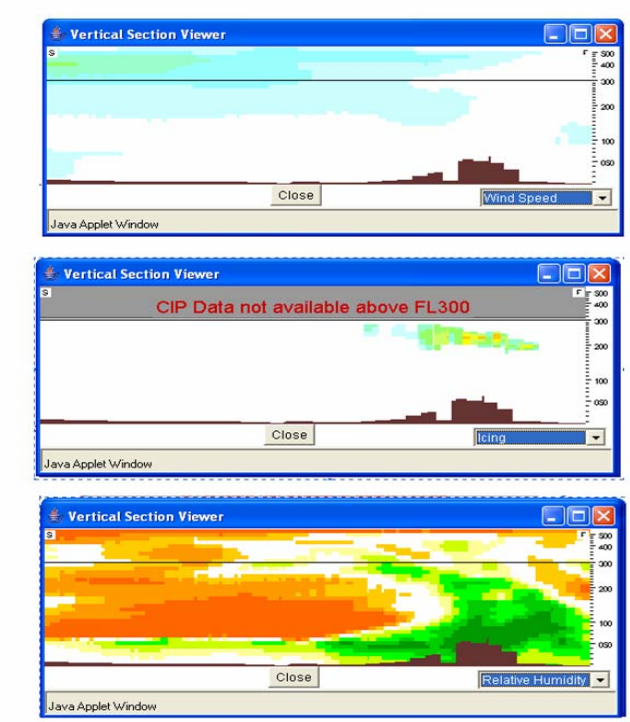

Figure 85. Same as in Figure 84 except with wind speed, icing, and relative humidity are shown from top to bottom respectively. Screen capture from http://adds.aviationweather.gov/flight_path/index.php (accessed 2006).

All the GTG products which were used in several figures throughout this thesis were generated through the Flight Path Tool on the AWC turbulence site. On this site users can also overlay the GTG forecast with flight level wind barbs or look at the AWC icing forecast product.

As previously mentioned, the RUC-2 only forecasts to the 12-hour mark, and only covers CONUS. There is an ongoing effort to apply the GTG algorithm to the WRF model which will greatly expand the coverage and capability of the GTG, especially when combined with the ongoing effort to incorporate the EDR observations into the GTG algorithm (Sharman 2006). Until this happens, the GTG can and should still be used by CONUS forecasters to greatly enhance their turbulence forecast.

E. RECOMMENDED APPROACH

As mentioned previously the forecaster must first understand the current and past conditions of the atmosphere, before being able to predict the future state of the atmosphere. Thus the forecaster should start with a complete analysis of past and current atmospheric conditions. The forecaster should use the patterns and characteristics identified in Section A of this chapter to locate regions with a favorable environment for turbulence. Once the forecaster has thoroughly analyzed and examined the current atmospheric conditions, current observations must be considered. Observations should be used to verify patterns and favorable areas identified in the forecaster's analysis, and

to alert the forecaster of all reported turbulent areas. After the forecaster has analyzed and observed the atmosphere, he/she can then animate those patterns and regions into motion via the models and begin to form the forecast. In this process the forecaster should take advantage of automated turbulence diagnostics and models, specifically the GTG, to guide the forecaster to making the best possible turbulence forecast. When forecasters don't have access to automated turbulence diagnostics or the GTG, they should rely on their synoptic analysis, observations, and forecasted fields to form their turbulence forecast. Finally the forecaster should attempt to relay to the customer the uncertainty inherent to turbulence forecasting, and when possible should attempt to relay the uncertainty in each specific turbulence forecast.

THIS PAGE LEFT INTENTIONALLY BLANK

LIST OF REFERENCES

AMS, 2003: Support for automated observations from U.S. commercial aircraft. *Bulletin of the American Meteorological Society*, **84**, 515-517.

Abernathy, J., and R. Sharman, 2006: Clear-air turbulence nowcasting and forecasting using in-situ turbulence data. 12th Conference on Aviation Range and Aerospace Meteorology. Poster session 1.5, extended abstract, 11pp.

Air Force Weather Agency Technical Note 98-002 (AFWA TN 98-002), cited 2005: Meteorological Techniques. [Available online at: https://wwwmil.offutt.af.mil/afwadnt/doctrace.asp?file=TN_98002_Complete.zip&tag=TN 98-002], (Accessed January 28, 2006), 242 pp.

Air Force Instruction 15-128 (AFI 15-128), cited 2005: Air and Space Weather Operations Roles and Responsibilities. [Available online at http://www.e-publishing.af.mil/pubfiles/af/15/afi15-128/afi15-128.pdf], (Accessed April 15, 2006).

Air Force 15th Operational Weather Squadron Standard Operating Procedures (AF 15th OWS SOP-3), 2006: Creating global graphic products. Available from AF 15th OWS, 21 pp.

Air Weather Service Forecaster Memo 83-002 (AWS FM/83-002), 1983: Thunderstorms. [Available online at https://notus2.afccc.af.mil/SCIS/afwtl/AFWA TECHCAT-NIPRNET.pdf], (Accessed August 30, 2006), 8pp.

Air Weather Service Technical Report 105-39 (AWS TR/105-39), 1949: Further Studies of thunderstorm conditions affecting flight operations: Turbulence. [Available online at https://notus2.afccc.af.mil/SCIS/afwtl/AFWATECHCAT-NIPRNET.pdf], (Accessed August 30, 2006), 36pp.

Benjamin, S.G., G.A. Grell, J.M. Brown, T.G. Smirnova, and R. Bleck, 2004: Mesoscale weather prediction with the RUC hybrid isentropic-terrain-following coordinate model. *Mon. Wea. Rev*., **132**, 473-494.

Brown, R., 1973: New indices to locate clear-air turbulence. *Meteor*. *Mag*., **102**, 347–360.

Brown, B.G., J.L. Mahoney, R. Sharman, J. Vogt, and J. Henderson, 2000: Use of automated observations for verification of turbulence forecasts. Report to the FAA. Available from B.G. Brown (bgb@ucar.edu).

Carlson, T. N., 1998: Mid-Latitude Weather Systems. American Meteorological Society, Boston, MA, 507pp.

Clark, T. L., J. R. Scoggins, and R. E. Cox, 1975: Distinguishing between CAT and non-CAT areas by use of discriminant functional analysis. *Mon. Wea. Rev*., **103**, 514–520.

Colson, D. and H. A. Panofsky, 1965: An index of clear-air turbulence. *Quart. J.Roy. Meteor. Soc.*, **91,** 507-513.

Cooperative Institute for Meteorological Satellite Studies (CIMSS), 2006: GOES Gallery. University of Wisconsin-Madison Space Science and Engineering Center. [Available online at http://cimss.ssec.wisc.edu/goes/misc/], (Accessed August 2, 2006).

Cornman, L. B., C. S. Morse, and G. Cunning, 1995: Real-time estimation of atmospheric turbulence severity from in-situ aircraft measurements. J. Aircraft, 32, 171–177.

——, G. Meymaris, and M. Limber, 2004: An update on the FAA Aviation Weather Research Program's in situ turbulence measurement and reporting system. Preprints, 11th Conf. on Aviation, Range, and Aerospace Meteorology, Hyannis, MA, Amer. Meteor. Soc., CD-ROM, P4.3.

Coughlin, J. D., 2005: Forecasting the onset and intensity of vertically propagating mountain waves over the Alps. Thesis completed at Naval Postgraduate School, Monterey, CA, 79 pp.

Cunningham, J. G, 2006: Applying Ensemble Prediction Systems to Department of Defense Operations. Thesis completed at Naval Postgraduate School, Monterey, CA, 149 pp.

Durran, D. R., 1986: Mountain Waves. Mesoscale Meteorology and Forecasting, P.S. Ray, Ed., American Meteorological Society, 472-492.

Dutton, J., and H. A. Panofsky, 1970: Clear air turbulence: A mystery may be unfolding. *Science*, **167**, 937–944.

Dutton, J., 1980: Probability forecasts of clear-air turbulence based on numerical model output. *Meterol. Mag*., **109**, 293-310.

Eichenbaum, H., 2000: Historical overview of turbulence accidents. MCR Federal, Inc. report TR-7100/023-1.

Ellrod, G. P., and D. L. Knapp, 1992: An objective clear-air turbulence forecasting technique: Verification and operational use. *Wea. Forecasting*, **7**, 150–165.

ESRL/GSD, cited 2006: FSL Aircraft Data (ACARS/AMDAR) Information. [Available online at http://amdar.noaa.gov/.], (Accessed July 20, 2006).

Frehlich R. and R. Sharman. 2004: Estimates of Turbulence from Numerical Weather Prediction Model Output with Applications to Turbulence Diagnosis and Data Assimilation. *Monthly Weather Review*, **132**, 2308–2324.

Holcomb, M. C., 1976: Jet-stream analysis and turbulence forecasting. Air Force Global Weather Center Tech. Manual AFGWC TM 76-1, 101 pp.

Hooke, W.H., 1986: Gravity Waves. Mesoscale Meteorology and Forecasting. P. S. Ray, Ed., American Meteorological Society, 272-288.

Kaplan, M.L, A.W. Huffman, and K.M. Lux, 2002: Characterizing the severe turbulence environments associated with commercial aviation accidents, Part I: Cases study synoptic observational analyses. NASA Contractor Report, NASA/CR-2002-211918, 57 pp.

_____, _____, _____, and J. D. Cetola, 2003: Characterizing the severe turbulence environments associated with commercial aviation accidents, Part II: Hydrostatic mesobeta scale numerical simulations of supergradient wind flow and streamwise ageostrophic frontogenesis. NASA Contractor Report, NASA/CR-2003-212138, 45 pp.

Kaplan, M. L., and Coauthors, 2004: Characterizing the severe turbulence environments associated with commercial aviation accidents. A real-time turbulence model (RTTM) designed for the operational prediction of hazardous aviation turbulence environments. NASA Contractor Report, NASA/CR-2004-213025, 54 pp.

Keller, J. L., 1990: Clear-air turbulence as a response to meso- and synoptic-scale dynamical processes. *Mon. Wea. Rev.*, **118,** 2228-2242.

Knox, J. A., 1997: Possible Mechanisms of clear-air turbulence in strongly anticyclonic flows. *Mon. Wea. Rev.*, **125,** 1251-1259.

Kronebach, G. W., 1964: An automated procedure for forecasting clear-air turbulence. *J. Appl. Meteor.*, **3,** 119-125.

Lane, T. P., J. D. Doyle, R. Plougonven, M. A. Shapiro, and R. D. Sharman, 2004: Observations and numerical simulations of inertia–gravity waves and shearing instabilities in the vicinity of a jet stream. *J. Atmos. Sci*., **61**, 2692–2706.

——, R. Sharman, H.-M. Hsu, W. D. Hall, M. A. Shapiro, R. Plougonven, and J. J. Murray, 2005: Numerical simulations of gravity waves and turbulence during the ATReC campaign. 43d AIAA Aerospace Science and Exhibit, Reno, NV, American Institute of Aeronautics and Astronautics, AIAA-2005-262.

Lee, D. R., R. S. Stull, and W. S. Irvine, 1984: Clear air turbulence forecasting techniques. Air Force Global Weather Center Tech. Note AFGWC TN-79/001, 87 pp.

Ludlam, F. H., 1967: Characteristics of billow clouds and their relation to clear-air turbulence. *Quart. J. Roy. Meteorol. Soc*., **93**, 419-435.

MacCready Jr., P. B., 1964: Standardization of gustiness values from aircraft. *Journal of Applied Meteorology*, **3**, 439–449.

Mahoney, J. L., and B. G. Brown, 2000: Forecaster assessment of turbulence algorithms: A summary of results for the winter 2000 study. Report, submitted to the FAA Weather Research Program Turbulence Development Team, 20 pp.

Mahoney, J. L., J. Braid, B. G. Brown, T. Fowler, and J. Wolff, 2001: A forecaster evaluation of turbulence algorithms: A summary of results of the winter 2001 study. Report, submitted to the FAA Weather Research Program Turbulence Development Team, 42 pp.

Mahoney, J. L., J. Braid, B. G. Brown, C. Fischer, T. Fowler, M. Kay, and J. Wolf: 2002: Forecaster assessment of turbulence algorithms: A summary of results for the winter 2002 study. Report, submitted to the FAA Weather Research Program Turbulence Development Team, 29 pp.

Mahoney, J. L., C. Fischer, and M. Kelsch, 2003: Forecasters' evaluation of the integrated turbulence forecast algorithm, winter 2003. Report, submitted to the FAA Weather Research Program Turbulence Development Team, 4 pp.

Miles, J. W. and Howard, L.N, 1964: Note on a heterogeneous shear flow. *J. Fluid Mech.*, **20**, 331-40.

National Weather Service, cited 2006: National Weather Service Glossary. National Oceanic and Atmospheric Administration's National Weather Service. [Available online at: http://www.weather.gov/glossary/], (Accessed August 31, 2006).

Queney , P., G. Corby, N. Gerbier, H. Koschmieder, and J. Zierep, 1960: The airflow over mountains. WMO Tech Note 34, 135 pp.

Rammer, W. A., 1973: Model relationships of CAT to upper wind flow patterns. National Meteorological Center Aviation Weather Forecast Branch Note, 14 pp.

Schrumpf, B.Q., 2006: Personal communication on December 12, 2005. USAF 15th Operational Weather Squadron, Assistant Director of Operations.

Schwartz, B., S. G. Benjamin, S. M. Green, and M. R. Jardin, 2000: Accuracy of RUC-1 and RUC-2 wind and aircraft trajectory forecasts by comparison with ACARS observations. *Wea. Forecasting*, **15,** 313-326.

Sharman, R., 2006: Personal communication on May 24, 2006. National Center for Atmospheric Research (NCAR), Boulder, Colorado.

Sharman, R., C. Tebaldi, G. Wiener, and J. Wolff, 2006: An integrated approach to mid- and upper-level turbulence forecasting. *Wea*. *Forecasting*, submitted.

Takacs, A., L. Holland, R. Hueftle, B. Brown, and A. Holmes, 2006: Using in situ eddy dissipation rate (EDR) observations for turbulence forecast verificiation.

Tebaldi, C., D. Nychka, B. G. Brown, and R. Sharman, 2002: Flexible discriminant techniques for forecasting clear-air turbulence. *Environmetrics*, **13**, 859–878.

UCAR, cited 2005a: Mountain waves and downslope winds. COMET MetEd Website. [Available online at: http://meted.ucar.edu/mesoprim/mtnwave/], (Accessed May 10, 2005).

UCAR, cited 2005b: RAP annual report 2003. UCAR Website. [Available online at: http://www.rap.ucar.edu/asr2003/atmospheric-turbulence.html], (Accessed August 15, 2005).

THIS PAGE LEFT INTENTIONALLY BLANK

INITIAL DISTRIBUTION LIST

1. Defense Technical Information Center
   Ft. Belvoir, Virginia

2. Dudley Knox Library
   Naval Postgraduate School
   Monterey, California

3. Air Force Weather Technical Library
   Air Force Combat Climatology Center
   Asheville, North Carolina

4. Dr. Chuck Wash
   Naval Postgraduate School
   Monterey, California

5. Lt Col Karl Pfeiffer, USAF
   Naval Postgraduate School
   Monterey, California

6. Dr. Philip Durkee
   Naval Postgraduate School
   Monterey, California

7. Captain Scott Lisko, USAF
   15th Operational Weather Squadron
   Scott AFB, Illinois

8. Captain Jeffrey Cunningham, USAF
   Operational Ensembles Modeler
   HQ AFWA/DNXM
   Offutt AFB, Nebraska